

**Development of New Technology for Design of
Solar Support Structures**

(太陽光発電用基礎設計における新技術開発に関する研究)

**A thesis submitted in partial fulfillment of the
requirements for the degree of**

Master of Science

In

Environmental Science and Technology

By

OWINO ALEX OTIENO

Department of Environmental Science and Technology

Graduate School of Bioresources

Mie University, Japan

March, 2019

Development of New Technology for Design of Solar Support Structures

A thesis submitted in partial fulfillment of the requirements for the degree of

Master of Science
In
Environmental Science and Technology

By

OWINO ALEX OTIENO

Examined and approved as to style and contents by

Prof. Dr. Zakaria Hossain
Chairman of the Examination Committee

Prof. Dr. Toshinori Sakai

Co-chair of the Committee

Prof. Dr. Kajisa Takamitsu

Co-chair of the Committee

**Department of Environmental Science and Technology
Graduate School of Bioresources
Mie University, Japan
March, 2019**

Development of New Technology for Design of Solar Support Structures

**A thesis submitted in partial fulfillment of the requirements for the degree of
Master of Science
In
Environmental Science and Technology**

**Graduate School of Bioresources
Mie University, Japan**

By

OWINO ALEX OTIENO

March, 2019

**SPECIAL DEDICATIONS TO
MY BELOVED PARENTS**

**WITH LOTS OF GRATITUDE TO
MY SUPERVISORS:
PROF. ZAKARIA HOSSAIN
DR. JIM SHIAU**

ACKNOWLEDGEMENTS

All praises and thanks to the Almighty God who enabled me to start and complete my Masters Research.

The completion of this research work would not been possible without the whole-hearted assistance and support of many people, whom I would like to thank. First of all, I would like to express my sincere thanks and appreciation to my research advisor, Prof. Dr. Zakaria Hossain, for his wholehearted guidance and suggestions throughout this research program. Sincere thanks are extended to Dr. Jim Shiau, University of Southern Queensland, Australia for the earnest support and mentorship in the whole period of my research. I also would like to thank Prof. Dr. Kajisa Takamitsu, Prof. Dr. Toshinori Sakai, Prof. Dr. Ishiguru Satoro, Prof. Dr. Ohno, Prof. Dr. Kenji Okajima, Prof. Dr. Narioka Hajime, Prof. Dr. Nobuo Toride, and other members of the thesis review and proof reading committee for carefully reviewing and providing with useful suggestions. More thanks and special regards to my friends of the Laboratory of International Environment Conservation, Faculty of Bioresource, Mie University. I gratefully acknowledge Cosmowinds Company Ltd., Nagoya, Aichi, Japan and Beppu Construction Company Ltd., Yokkaichi, Japan for helping me in the research experiment execution process.

Special thanks are due to the Japan International Cooperation Agency (JICA) and Japan Federation of International Cooperation Centers (JICE) for providing me with the social support, tangible(financial) support and information support for my study and living in this beautiful country, Japan through, the Africa Business Education Initiative (ABE) scholarship program, I remain indebted to them.

Special thanks to the continued support of my parents throughout my research period.

ABSTRACT

The rising queries on climate change and other environmental issues have demanded sustainable developments in recent year. Increasing demand for clean energy is pushing for more economical means of constructing such structures with maximum evaluation focused on the cost of installation and the ultimate strength of the fully loaded structure hence composite single piles come into place. Composite single-piles are one of the major components of a foundation as they act as the primary component in the transmission of the weights above the structure into the ground for stability to be attained. Most research being done today in solar energy are mostly related to the development of various types of solar cells and the reduction in the size of solar panels while improving the operation and energy tapping efficiency. Many engineering structures both above ground and under the ground surface are subject to forces that create overturning moments upon them. In this study, the structure under consideration is the composite single pile foundation of solar panels as very little research has been conducted on the safety of foundation for solar panels. This thesis focuses on the design and testing of a composite single pile foundation taking into account the strength factor, bearing capacity and foundation safety factor. The foundation consists of a hollow steel pipe bonded to the ground by a thin layer of cement and sand mortar. As studied in this research the design of the pile element, gave the dimensions of $1.4m$ pile foundation length and $0.26m$ diameter which were employed in the research to determine the lateral and pull-out capacity. Firstly, a full-scale experiment was performed to evaluate the ultimate lateral capacity of the pile foundation. Secondly, experimental results were compared with analytical ones as a step of in-depth understanding of the lateral and the axial/pull-out loading behaviour. Thirdly, a numerical model considering soil-structure interaction was also developed to determine the lateral and the pull-out capacity of the foundation. Finite difference method was adopted to solve the numerical

model in large deformation condition, while FISH programming designed to facilitate the problem with automatic mesh generation and solver. Strength evaluation was done through numerical simulation using FLAC2D which uses the finite difference method (FDM) to evaluate the input codes in step by step manner while integrating the input parameters in a stress strain relation as described in the numerical model code. The dimensions of the model mesh were twice the pile foundation depth, $2L$ in the *y-direction* and $2L$ in the *x-direction* from the pile vertical axis. Strength evaluation was done on *dense sand*, *clay* and *silty* medium to determine the vast array of data for engineering design measures.

Ultimately, this research entailed a detailed numerical and parametric study on the lateral behavior of piles in foundation designs. For this reason, a detailed study on the influence generated on the *p-y* curves was mandatory to create a numerically valid model for use in the process of foundation design without much ado. FDM was used to implement a solution to the coded input for example soil and pile element parameters. The model validation process under lateral study done in this paper involved the variation of some of the critical parameters such as the *variation on the type of soil* in the area under consideration. Next, *modification of the elastic modulus* of the given soil as a check on the cohesiveness, *change on the loading velocity* at the top of the pile, a *variation of the pile material stiffness* and the *difference of the pile eccentricity*. Considering the pull-out study, the parametric study was done by *varying the foundation depth* from $0.7m$ to $2.0m$, *soil angle of internal friction* from 10° to 40° and the *inclusivity of gap* upon failure. The results obtained from the *p-y curves* generated from the parameters, underwent sifting through for any effects on the ultimate loading capacity of the pile to the allowed design loading limits upon full structural installation. This variation was necessary for the approval of the validity of the model in engineering design. The parametric study from this study shows that the structure is of functional

strength and a tolerable factor of safety. The design dimensions show good lateral capacity of 15kN and pull-out capacity up to 94kN, 90kN and 80kN for dense sand, silty soil and clay soil respectively. The suggested relations for the lateral capacity and pull-out capacity of the composite single pile regarding the lateral and axial ability are within design limits, 4kN. The suggested relations for the lateral and pull-out capacity of the single pile regarding the lateral and axial ability are within design limits.

Keywords: *Lateral load, pull-out capacity, p-y curve, skin friction, finite difference method, stress-strain relation, Soil-pile interaction, FLAC2D*

OUTLINE OF THE THESIS

Chapter 1: Introduction, Background Study, Problem Definition, Scope of Study and Objectives of the study

Chapter 2: Preliminary Design of foundation depth with respect to wind loads and the ground forces

Chapter 3: Modelling Technique using FLAC2D and the stress and strain relation matrixes.

Chapter 4: Presents the approaches used in the analysis of the Lateral loading evaluation.

- ❖ Introduction,
- ❖ Analytical Approaches, Materials and Methods
 - Full-scale experiment approach
 - Analytical approach
 - Numerical modelling approach

Chapter 5: Presents the approaches used in the analysis of the Pull-out loading evaluation.

- ❖ Introduction,
- ❖ Analytical Approaches, Materials and Methods
 - Full-scale experiment approach
 - Analytical approach
 - Numerical modelling approach

Chapter 6: Results and discussions & Parametric study on Lateral and Pull-out forces.

Chapter 7: Conclusions

OWINO ALEX OTIENO

JOURNAL PUBLICATIONS

1. Alex Otieno Owino, Zakaria Hossain, and Jim Shiau: Parametric Study on the Response of Composite Single Piles to Lateral Load by Numerical Simulation (FDM): European Journal OF Engineering Research and Science, Vol.3, No.10, pp. 16-20, October 2018
DOI:10.24018/ejers.2018.3.10.899
<http://www.ejers.org/index.php/ejers/article/view/899>
2. Alex Otieno Owino, Zakaria Hossain, and Jim Shiau: Pull- out Resistance of Single Piles and Parametric Study Using the Finite Difference Method (FDM): American Journal of Civil Engineering and Architecture, Vol.6, No.5, pp. 193-198, Accepted October 19, 2018
DOI: 10.12691/ajcea-6-5-4
<http://www.sciepub.com/ajcea/content/6/5>: <http://pubs.sciepub.com/ajcea/6/5/4>

CONFERENCE PROCEEDINGS

1. Alex Otieno Owino, Hossain, M.Z., Ojiro C., Ozumi, S., Harada, H. and Okuyama, S.: Analytical Study on Single Pile Design for Solar Foundations for Sloping Land, Proc. of the 3rd International Conference on Science, Engineering & Environment, USQ Springfield Brisbane, Australia, Nov.21-23, ISBN: 978-4-9905958-9-0 C3051, 査読有, Vol.3, pp.172-177, 2017.
2. Alex Otieno Owino, Zakaria Hossain and Jim Shiau: Design and Investigation of Single Pile Composite Foundation for Solar Panels Subjected to Lateral Loading (横荷重を受ける太陽光パネル複合基礎の設計に関する研究), Poster presentation for The Japan Society of Irrigation, Drainage and Rural Engineering, Kyoto University, Kyoto, Sept.4-7, 2018.
3. Alex Otieno Owino, Zakaria Hossain and Jim Shiau: Parametric Study on the Response of Composite Single Piles to Lateral Load by Numerical Simulation (FDM), Proc. of the 4th International Conference on Science, Engineering & Environment, Nagoya, Japan, Nov.12-14, 2018, ISBN: 978-4-909106018 C3051, 査読有, Vol.4, pp. 255-260, 2018.
4. Alex Otieno Owino, Zakaria Hossain and Jim Shiau: Pull-out resistance of Single Piles and Parametric Study based on Numerical Simulation Approach (FDM) using FLAC2D, Proc. of 8th International Conference on Geotechnique, Construction Materials and Environment, Kuala Lumpur, Malaysia, Nov. 20-22, 2018, ISBN: 978-4-909106001 C3051, 査読有, Vol.8, pp. 6-11, 2018.

TABLE OF CONTENTS

ACKNOWLEDGEMENT	iv
ABSTRACT	v
OUTLINE OF THE THESIS	viii
JOURNAL PUBLICATIONS AND CONFERENCE PROCEEDINGS	ix
CONTENT	x
LIST OF FIGURES	xiii
LIST OF TABLES	xv
CHAPTER 1	1
1.0 INTRODUCTION	1
1.1 BACKGROUND STUDY.....	2
1.2 PROBLEM DEFINITION.....	7
1.3 SCOPE OF THE STUDY.....	9
1.4 OBJECTIVES OF THE RESEARCH.....	11
CHAPTER 2	12
2.0 PRELIMINARY DESIGN OF THE FOUNDATION DEPTH	13
2.1 WIND LOAD CALCULATIONS.....	13
2.2 FOUNDATION DEPTH L_1	14
2.3 ULTIMATE DESIGN DIMENSIONS AND INSTALLATION.....	16
CHAPTER 3	18
3.0 NUMERICAL MODELLING USING FLAC2D.....	19
3.1 STRUCTURE ELEMENT	19
3.2 GRID/SOIL ELEMENT.....	20
3.3 INTERFACE ELEMENT.....	21
3.4 STRESS STRAIN LAWS GOVERNING ELASTIC, MODELS	23
3.5 STRESSES AND STRAIN INCORPORATION INTO FLAC2D	27
CHAPTER 4	30
4.0 LATERAL CAPACITY OF COMPOSITE SINGLE PILES.....	31

4.1 INTRODUCTION.....	31
4.2 ANALYTICAL APPROACHES, MATERIALS AND METHODS.....	34
4.2.1 Full-scale experiment approach.....	34
4.2.2 Analytical approach	36
4.2.3 Numerical modelling approach.....	38
CHAPTER 5	41
5.0 PULL-OUT CAPACITY OF SINGLE PILES	42
5.1 INTRODUCTION	42
5.2 ANALYTICAL APPROACHES, MATERIALS AND METHODS	45
5.2.1 Full-scale experimental approach	45
5.2.2 Numerical modelling approach	46
CHAPTER 6	50
6.0 RESULTS AND DISCUSSION	51
6.1 LATERAL LOADING	51
6.1.1 Full-scale experiment approach on lateral loading	51
6.1.2 Analytical approach on lateral loading	52
6.1.3 Numerical simulation on lateral loading	53
6.2 PARAMETRIC STUDY ON LATERAL LOADING	62
6.2.1 Effects different soils: silty soil and clay soils	62
6.2.2 Effects of soil elastic modulus	64
6.2.3 Effects of loading velocity with depth on ultimate load	65
6.2.4 Effects of pile stiffness: Stiffness of normal coupling spring	67
6.2.5 Effects of eccentricity, e	69
6.3 PULL-OUT/ AXIAL LOADING	71
6.3.1 Full-scale experiment approach on Pull-out loading	71
6.3.2 Numerical simulation on Pull-out loading	72
6.4 PARAMETRIC STUDY ON LATERAL LOADING	78
6.4.1 Variation of the Pile Foundation Depth	78
6.4.2 Variation of the Angle of Internal Friction	79
6.4.3 Influence of Gap Formation during Loading	81
6.5 FACTOR OF SAFETY (FoS)	84

CHAPTER 7 85

 7.0 CONCLUSION..... 86

 7.1 CONCLUSION BASED ON LATERAL CAPACITY STUDY 86

 7.2 CONCLUSION BASED ON LATERAL PARAMETRIC STUDY 86

 7.3 CONCLUSION BASED ON PULL-OUT CAPACITY STUDY 87

8.0 SUMMARY..... 88

REFERENCES 90

LIST OF FIGURES

Figure 1 Concrete pier foundation	4
Figure 2 Helical pile foundation structure and material	5
Figure 3 Driven pile foundation setup and installation technique	6
Figure 4: ballasted foundations set-up	6
Figure 5 Composite foundation structural component	7
Figure 6 (a) Fixed orientation two pillar support system on slopping ground	8
Figure 6 (b) Flexible composite single pile foundation on slopping ground	8
Figure 7 Sites for the foundation full-scale control experiments	9
Figure 8 Pile forces and ground forces	15
Figure 9 Pile Shaft Diameter against Pile Length	17
Figure 11 Mesh, boundary condition and structural element(pile)	19
Fig 12 An interface represented by sides A and B connected	21
Figure 13 Coordinate axes for a transversely isotropic model	24
Figure 15 Basic explicit calculation cycle	28
Fig 16 full scale experiment and plot of results	31
Figure 17 Lateral loading functions	33
Figure 18 Full-scale experimental setup	35
Figure 19 Full-scale experimental setup	35
Figure 20 Cross-sectional area of the pile element inside the soil medium	36
Figure 21 Model details before the application of the lateral load	39
Figure 22 Uplift capacity function and the failure pattern by Kulhawy	44
Figure 23 Full-scale experimental set up	46
Figure 24 LVDT for vertical displacement	46
Figure 25 Axial loading scale.....	46
Figure 26 Pull-out numerical simulation mesh for FLAC2D	47
Figure 27 Full-scale experimental setup	51

Figure 28 Full-scale experimental data plot for Matsusaka city	52
Figure 29 Analytical data plot for Matsusaka city	53
Figure 30 Mesh, boundary condition, and pile element displacement pattern	55
Figure 31 Soil movement and pile displacement pattern	55
Figure 32 Soil movement and pile normal pressure distribution	56
Figure 33 Load-deflection curve at Matsusaka testing site	57
Figure 34 The gap	58
Figure 35 Contour zone for effective stress distribution on grid	59
Figure 36 Maximum shear strain increment around the pile element	60
Figure 37 Maximum shear strain rate on the grid	61
Figure 38 Effects Different Soils: Silty soil and clay soils	62
Figure 39 soil-pile displacement patterns for silty soil	63
Figure 40 soil-pile displacement patterns for clayey soil	63
Fig. 41 Effects of elastic modulus for silty soil	64
Fig. 42 Effects of elastic modulus for clayey soil	65
Figure 43 Effects of loading velocity with depth on ultimate load at 0.7m depth	66
Figure 44 Effects of loading velocity with depth on ultimate load at 1.4m depth	66
Figure 45 Effects of loading velocity with depth on ultimate load at 2.8m depth	66
Figure 46 Effects of Loading velocity with depth on ultimate load	67
Figure 47 Effects of pile stiffness silty soil	68
Figure 48 Effects of pile stiffness clayey soil	69
Fig. 49 Effects of pile eccentricity in silty soil	70
Fig. 50 Effects of pile eccentricity in clayey soil	70
Figure 51 Full-scale experiment plot in Matsusaka Site	71
Figure 52 Comparison of the experimental plot for the full-scale experiment	72
Figure 53 Pile head displacements at different axial loads	73
Figure 54a Clayey soil	74
Figure 54b Sand soil	74

Figure 54c Silty soil	75
Figure 55 Contour zone for effective stress distribution on the grid	75
Figure 56 Effective Principal stress tensor distribution on axial loading	76
Figure 57 Maximum shear strain increment around the pile element	77
Figure 58 Variation of the foundation depth	78
Figure 59 Variation of the Angle of Internal Friction for dense sand	79
Figure 60 Variation of the Angle of Internal Friction for silty soil	80
Figure 61 Variation of the Angle of Internal Friction for clayey soil	80
Figure 62 Influence of the angle of internal friction of the soil	81
Figure 63 Influence of Gap Formation during Loading for dense sand	82
Figure 64 Influence of Gap Formation during Loading for silty soil	82
Figure 65 Influence of Gap Formation during Loading for clayey soils	82
Figure 66 Effects of the gap on the ultimate axial load	83

LIST OF TABLES

Table 1 Wind load calculation on panel surface	14
Table 2 Ground forces subjected to the pile and soil parameters	14
Table 3 Soil Properties	39
Table 4 Pile Element Properties	40
Table 5 Soil properties	48
Table 6 Pile element properties	48

CHAPTER 1

INTRODUCTION

1 INTRODUCTION

1.1 BACKGROUND STUDY

In accordance to the rising fluctuation in the global environmental concerns such as climate change, environmental sustainability has become handy so as to rescue the environment from further degradation. With reference to these problems the innovation on renewable energy solutions have paved the road towards saving the ecosystem. Energy demand is a growing level worldwide with figures up to 559.8 EJ as stated in Energy and the Challenge of Sustainability (2000) during the United Nations World Energy Council summit. This high energy consumption mainly reflects in production industries and governments. With the influx in the commodity demand, most of the attention is focusing towards the production of green energy sources like solar energy. Solar energy is a green energy source that utilises the radiant heat from the sun and is harnessed using different technologies like solar heaters, photovoltaic cells, solar thermal energy absorbers and solar architecture innovations. As at now much of the research are based on the innovation on a wide variety of the solar cells and the architectural design of different size, shape, and structure of the solar harnessing material. Little research is available on the determination of economically viable foundation structures to support the ever evolving industry on tapping the green energy source. To begin with, a clear reflection on the merits and the demerits of solar energy is mandatory so as to identify the areas of interest that will be tackled in my research such as the reducing the installation costs. The advantages of solar energy are:

- ❖ Solar energy is a renewable source.
- ❖ Abundant source of energy in most parts of the world especially the tropics.
- ❖ A sustainable source of energy due to the continuous presence of the sun.
- ❖ Environmentally friendly due to the fact that there are no harmful emissions

- ❖ Solar has diverse applications from electricity generation to solar thermal sources.
- ❖ Solar energy has low maintenance cost once installed.
- ❖ Have a large room for technological development and advancement in future.
- ❖ Ensures a reduction in the cost of electricity due to the abundance depending on the size of the solar firm and the amount of usage.
- ❖ A silent source of energy with no noise pollution to the environment.

The disadvantages of the solar energy on the other hand, brings in the urge to develop new ways on how to make the abundant energy source easily available to the consumers. Some of the demerits that motivated me to undertake this research include:

- ❖ High initial investment capital to build a solar firm.
- ❖ Solar firms require large spaces to install the panels.
- ❖ Some plants employ the use of exotic material for construction.
- ❖ Solar energy is intermittent: dependent on the position of the sun and its availability.

My focus in this research is to reduce the installation cost by designing a simple composite single pile foundation. The aim of this foundation is to cut costs by using easily available construction materials and application on different land topography for installation of the panels especially in regions having financial constraints such as the developing countries. Another motivation is on curbing the energy challenges faced in the developing countries by tapping the abundant source of energy with simple foundation designs.

Some of the foundations being used today in the installation of the solar firm projects include the following:

- ❖ Concrete piers

- ❖ Helical piles
- ❖ Driven piers
- ❖ Ballasted foundations.

Each of these foundations have a strength and a weakness in accordance to the strength evaluation, durability of the foundation, topography of the land under consideration, number of piles/piers to be used and the initial cost needed for its construction as discussed in details below.

Concrete piers: This foundation used concrete at the main material to bond the piers to the ground. Concrete requires three components that is cement, sand and gravel to get the good strength. The foundation has good axial and lateral resistance but requires high initial cost for installation and is best suited for flat surfaces. In common practices today the panels have multiple foundation support systems to support the panels from both the four sides hence four piers as shown in Figure 1.

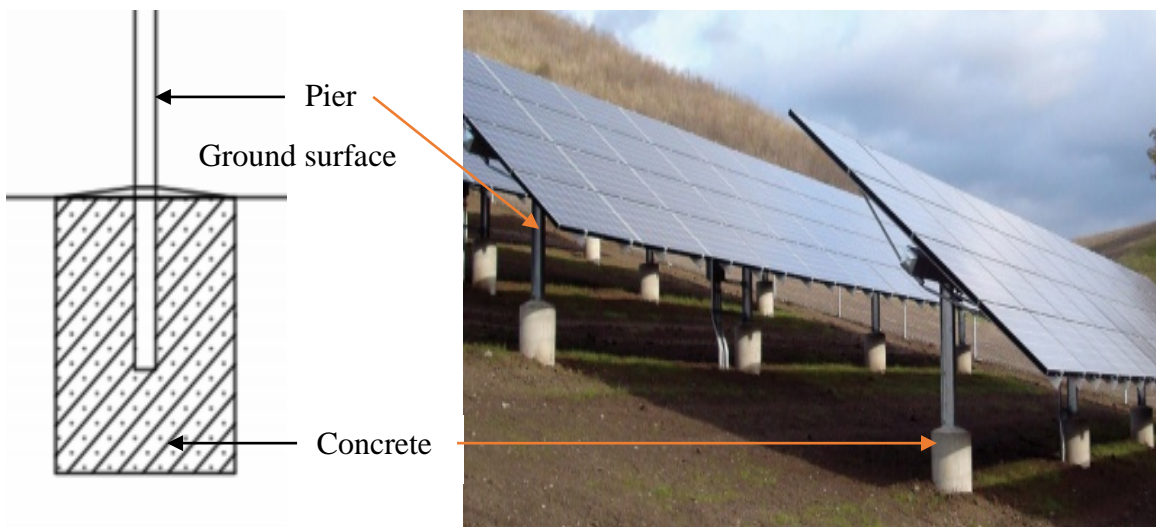


Figure 1 Concrete pier foundation

Helical pile: This type of foundation consists of an additional helical shape part to improve on the bonding mechanisms with the soil component upon installation. The design includes a large split disc welded at the bottom of the pile at an angle. The disc worms into the soil during rotation. This makes the foundation not suitable for regions with high refusal rates. Helical foundations have good axial capacity and low lateral capacity. In addition to this, the helical pile requires great ground embedment depth hence the use of more material on the pile length. The additional bracing increased the installation costs as well as the high number of piles required to support the given design load of the panels. Due to the low lateral capacity its use on sloping ground is fully restricted. Figure 2 is a clear representation of the helical pile.

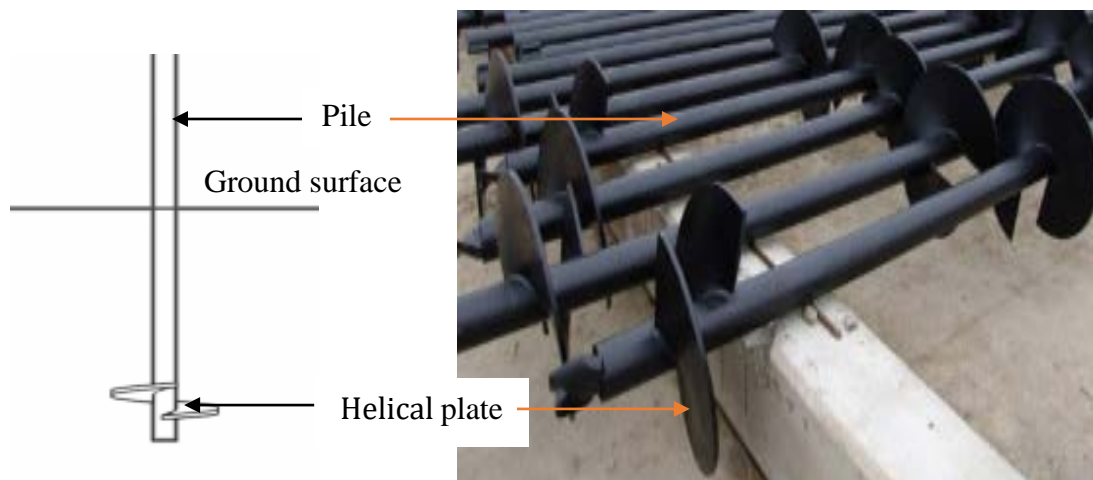


Figure 2 Helical pile foundation structure and material.

Driven piles: this setup includes piles driven into the ground using special equipment thus increasing the installation costs. The first step is to understand the bearing capacity and the corrosivity of the given type of soil. This type of foundation doesn't employ the use of the helical plates hence lower resistance to the axial forces. To achieve good resistance to subjected forces, the piles must be of great depth into the ground and as a result more material needed for its construction. In addition to the great depth, more pile will be required and at closer spacing to

support a given design load. An illustration of the foundation type and the precision installation method is shown in figure 3.

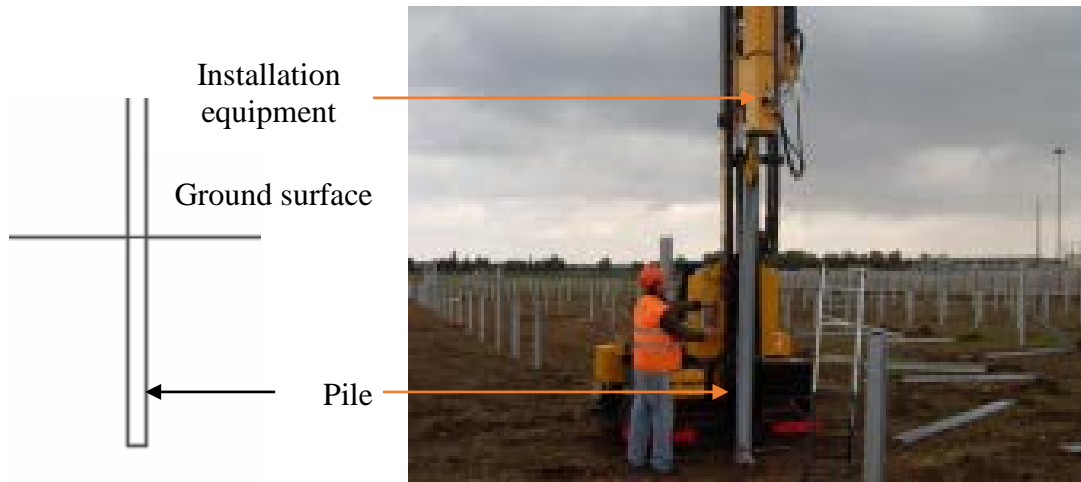


Figure 3 Driven pile foundation setup and installation technique.

Ballasted foundation: This is a very expensive foundation set-up that uses heavy ballasted reinforced concrete section installed above ground. Its suitable for regions with high refusal rates towards penetration. The sections are made of precast material to be shipped to the required destination or casted on site. Have low economic viability in regions having financial constraints like the developing countries. Figure 4 represents ballasted foundations.



Figure 4: ballasted foundations set-up.

1.2 PROBLEM DEFINITION

Figure 5 shows an explicit representation of the composite single pile solar foundation structure with more focus on the foundation depth L_1 , pile diameter D_1 , foundation excavation diameter D_2 and pile clearance at the bottom L_2 . The new foundation design consists of a hollow steel pile anchored to the ground by a thin layer of mortar (sand and cement). The high tensile steel section increases the resistance of the foundation towards the axial or pull-out forces and the lateral forces subjected to it during loading. The main function of the mortar is to improve on the foundation bearing capacity and a bonding interface between the steel section and the surrounding soil component. The mortar provides enough frictional resistances (skin friction) hence high tolerance to pull-out forces due to increased roughness coefficient as compared to conventional foundations.

The synergetic combination between the steel and the mortar and between the mortar and the soil gives the desired composite foundation strength.

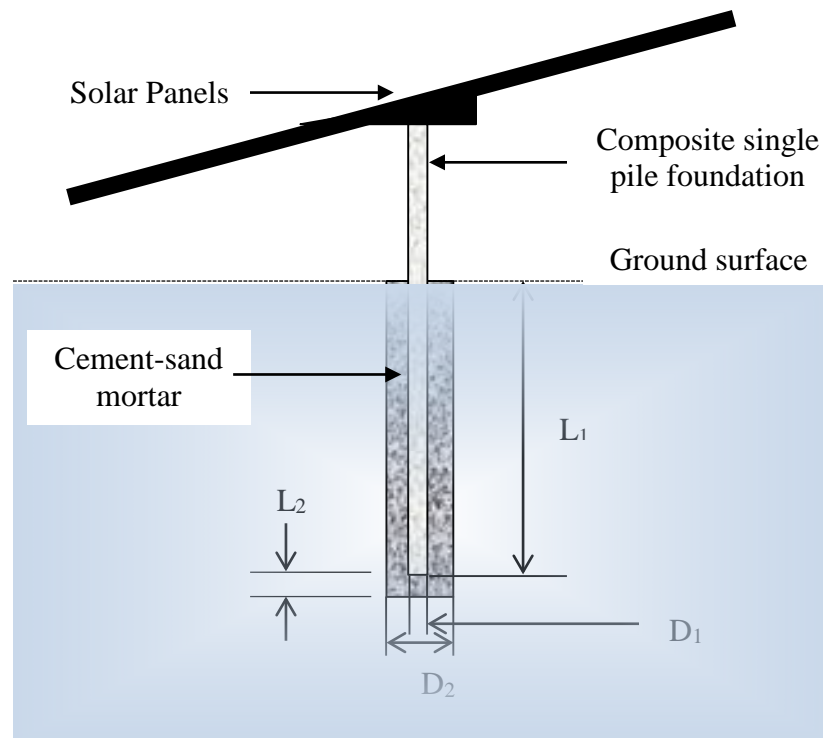


Figure 5 Composite foundation structural component

The composite single pile foundation also aims to provide proper utilization of the sunshine hours by ensuring that the panels face the sun at all times during the day. Most fundamental solar panel foundations, tend to have fixed orientations to the sun due to the multiple number of support structures involved. In addition to the flexibility, the single pile foundation will be able to utilize the sloping lands with ease as shown in Figure 6 (a) and (b). Rather than adopting the four pillar or two pillar set up, the single pile composite foundation allows for the change in orientation of the panel surface hence, maximum energy tapping to the consumer.

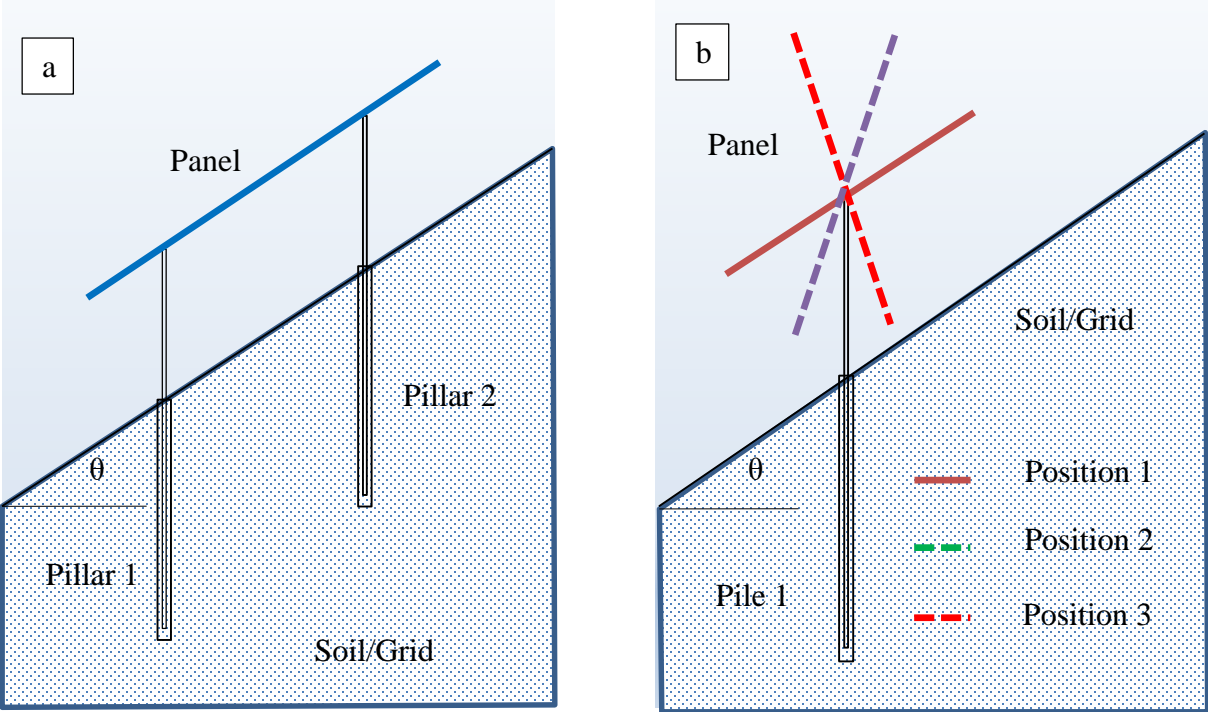


Figure 6 (a) Fixed orientation two pillar support system on sloping ground.

Figure 6 (b) Flexible composite single pile foundation on sloping ground.

1.3 THE SCOPE OF THE STUDY

In this research the first step was to identify a site to conduct the control full scale experiment. The full scale set up was done in two regions namely Matsusaka City in Mie Prefecture, Japan and Kasugai City in Aichi Prefecture, Japan. These two regions experience frequent rainfall throughout the year and also strong winds during natural calamities such as the typhoon. Matsusaka city has saturated silty soils while Kasugai City has saturated clayey soils which give a good comparison in terms of the soil component variation. A google map presentation of the two regions is shown in Figure 7.

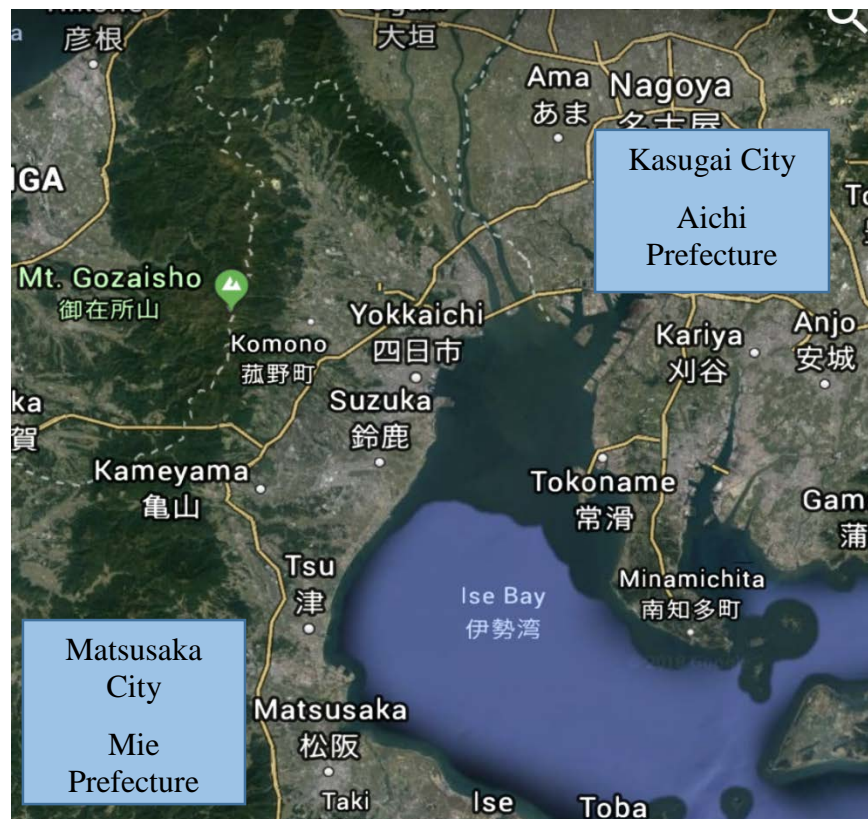


Figure 7 Sites for the foundation full-scale control experiments

Experimental data is collected by the use of linear variable displacement transducers (LVDTs) and load cells to monitor the axial/pull-out loads and the lateral loads. The data is plotted to obtain the p-y curves for the respective types of loading.

A plot of the p-y curves (load against the displacements) can be further analyzed to obtain the bearing capacity of the composite single pile as well as the evaluation of the factor of safety (FoS). The FoS is a quality check of the redundancy of the foundation structure upon failure.

Analytical methods which involve the use of theoretical equations are used to compare the results by substituting in the loads obtained from the full-scale experiment. The main Theoretical equation used in this study is the Reese and Matlock load deflection equation for lateral loading.

The next step involves the development numerical simulation code for both lateral loading and axial/pull-out loading. This code is aimed at offering engineers with easy methods of analyzing engineering problems associated with composite foundations through computer generated simulations using civil engineering software. This is a good approach in reducing the costs of full-scale experiments and also shortening the time requires for project designs. This research involves the use of FLAC2D software to monitor pile response. FLAC2D used the finite difference method for the step by step integration of the stresses and strains relations to give the desired output on the grid through zonal deformations at the specific applied velocity in the grid nodes.

Ultimately, parametric study is done so as to refine the coded parameters into FLAC2D and program validation for use in the design of Composite single pile foundation for solar support structures.

Nevertheless, the approaches above follows the Japanese Industrial Standards, (JIS C8917) which proposes the need for foundations designs to withstand extreme environmental condition such as typhoons, cyclones, soil cohesion variability and any other natural or artificial calamity that may lead to structural failure. My new technological approach for foundation design bears in mind the cost- performance relations and financial implications during project execution.

1.4 OBJECTIVES OF THE RESEARCH

- ❖ To validate the single pile composite foundation design using simple engineering techniques taking in to consideration the economic factors such as minimum cost evaluation and minimum material usage.

- ❖ To determine the optimum permissible load that the single pile composite foundation can withstand with respect to Lateral and Pull-out Forces

- ❖ To determine the soil/ground reaction to the Lateral and Axial/Pull-out forces during loading for different types of soil depending on the site conditions.

- ❖ To provide numerical solutions to Engineers hence reducing design costs by replacing full-scale experiments. Validation of the program code for the analysis of composite single piles.

- ❖ To maximize solar ray utilization by the solar panels by flexibility on panel orientation on slopping lands with minimum material usage.

- ❖ To attain the environmental sustainability goals by the production of clean green energy across all economic divides.

CHAPTER 2

PRELIMINARY DESIGN OF THE FOUNDATION DEPTH

2.0 PRELIMINARY DESIGN OF THE FOUNDATION DEPTH

To understand the soil and foundation interaction, it is necessary to develop a control experimental set up which acts as a focal point for the comparison of the model data output. This design gives a proper comparison of the pile deflection hence validating the eligibility of the model. Economic limitations encountered in the majority of the developing countries, cost evaluation of projects lead to the development of new designs while keeping in mind the maintenance of strength and durability of the project at hand. The solution to this is a composite single pile foundation. A composite solar foundation design is studied using experimental, analytical and numerical simulation approaches. The primary objective is to determine the optimum permissible loading that the foundation can withstand for lateral loading. The essential lateral load, in this case, is the wind load subjected to the panel surface considering the angle of attack and wind speed. It is possible to attain the lateral force created by the wind. The wind force and ground reaction forces are used in this paper to express an equation that can be solved to obtain a suitable foundation depth.

2.1 WIND LOAD CALCULATIONS

Wind is one of the significant forces that require load transmission to the ground, (Akins and Cermak 1975). The maximum wind load is assumed to act at an angle of 45° when the pressure is applied to the panel surface (Aihara, 2008). Wind is a crucial loading vector as it helps in establishing a strong foundation that will resist any horizontal loading subject to fluctuating wind speeds. Aihara et al. (2008) stated that the coefficients of wind load pressures can be obtained to design the foundation depth. In this study wind speed is taken as 40m/s and slope 10° . The wind loads can be evaluated using the formulas shown in Table 1. This calculation gives a wind load of 3.28kN.

Table 1 Wind load calculation on panel surface.

Item	Formula
Effective projection area	(Length *Width)
Wind load (kg/m ²)	{1/16 *(wind speed m/s) ² * Resistance coefficient}
Wind load on effective area	(Effective projection area * Wind load)
Horizontal wind load	(Wind load on effective area* Sin 45°)
Right angle wind load	(Wind load on effective area* Cos 45°)
Horizontal wind load Force	{(Horizontal wind load* Sin 10°) + (Right angle wind load* Cos 10°)}

2.2 FOUNDATION DEPTH L₁

Ground reaction force (GRF) considers the toleration of the force exerted by the ground to the foundation pillar in contact with it. This GRF acts as a baseline parameter in the calculation of foundation strength taking into account the overhead load to be transmitted, the bending moment of the pile extension above the ground and the soil parameters as shown in Table 2.

Table 2 Ground forces subjected to the pile and soil parameters.

	Item	Value
Working Load; Applied	The horizontal force, H	4 kN
Load	Moment Bending, M	4 kN.m
Pile dim.	The width of column, D	0.13 m
	Unit vol. weight, γ	18kN/m ³
Ground Condition	Internal friction angle, ϕ	30
	Wall friction angle, δ	10
	Adhesive force, C	0kN/m

Engel (2012) shows that the root penetration length can be determined when the maximum ground reaction force (P_{max}) is less than or equal to the passive soil pressure strength (P_p). Considering a rigid foundation in Figure 8, taking into account the depth, bottom surface resistance, and an increase of horizontal ground reaction force coefficient (K_h) as shown in figure 8, both the rotation angle (θ) and the center depth (h) are obtained using equations 1 and 2.

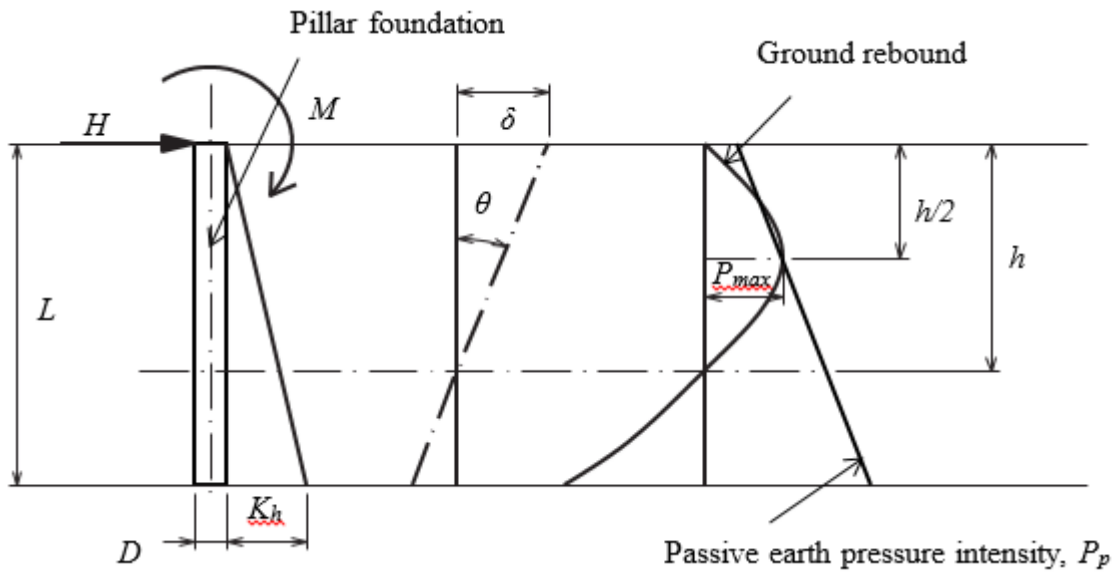


Figure 8 Pile forces and ground forces

$$\text{Rotational angle } (\theta) = \frac{12(3M+2HL)}{K_h} \quad (1)$$

$$\text{Rotational center depth } (h) = \frac{L(4M+3HL)}{2(3M+2HL)} \quad (2)$$

Maximum Ground reaction force occurs at $h/2$, hence;

$$P_{max} = \frac{1}{2}(h\theta)K_h \frac{h}{2L} \quad (3)$$

$$P_p = \frac{1}{2}hK_p\gamma + 2c\sqrt{K_p} \quad (4)$$

$$K_p = \frac{\cos^2 \varphi}{\cos \delta \left\{ 1 - \frac{\sin(\varphi+\delta) \sin(\varphi+\beta)}{\cos \delta \cos \beta} \right\}} \quad (5)$$

When P_{max} is equal to P_p ;

$$\frac{1}{2}(h\theta)K_h \frac{h}{2L} - \frac{1}{2}hK_p\gamma + 2c\sqrt{K_p} = 0 \quad (6)$$

Substituting equation (1) and (2) into equation (6);

$$3K_p\gamma DHL^4 + 4D(K_p\gamma M + 4c\sqrt{K_p}H)L^3 - 3(9H^2 - 8c\sqrt{K_p}DM)L^2 - 72MHL - 48M^2 = 0 \quad (7)$$

Resistance width of the pile is considered to be, $D = 3D$, according to Broms (1964). Therefore, equation (7) becomes,

$$3K_p\gamma DHL^4 + 4D(K_p\gamma M + 4c\sqrt{K_p}H)L^3 - (9H^2 - 24c\sqrt{K_p}DM)L^2 - 24MHL - 16M^2 = 0 \quad (8)$$

Replacing the coefficients of L with C_1, C_2, C_3, C_4 , and C_5 , we have;

$$C_1L^4 + C_2L^3 - C_3L^2 - C_4L - C_5 = 0 \quad (9)$$

Using equation (8), a desirable foundation depth L can be calculated by evaluating the fourth order equation as shown in the simplified equation (9). This solution is based on the known parameters such as the lateral load H , ground reaction coefficient K_p , the moment of the force M , overburden soil weight γ , soil cohesion c , and the diameter of the pile section D .

2.3 ULTIMATE DESIGN DIMENSIONS AND INSTALLATION

Using equation (8), Figure 9 shows the relationship between the foundation depth and the pile shaft diameter. The width of the pile shaft has an inverse proportionality with reference to the length of the foundation. Therefore, from an economic point of view, the choice of minimum dimension parameters ($D = 0.13m$; $L = 1.4m$) is necessary without any detrimental effect (reduction) on the factor of safety and strength of the foundation structure.

The steel pipe has a diameter of 130mm and a total length of 2 meters. The sand-cement mortar was mixed at a ratio of 2:1 with a water-cement ratio of 2:1. A burrow with a clearance of 0.065m was drilled using a precision drilling machine set at right angles to the field. This clearance gave an overall foundation diameter of 0.260m. The steel section is anchored into the ground at a depth of 1.4m.

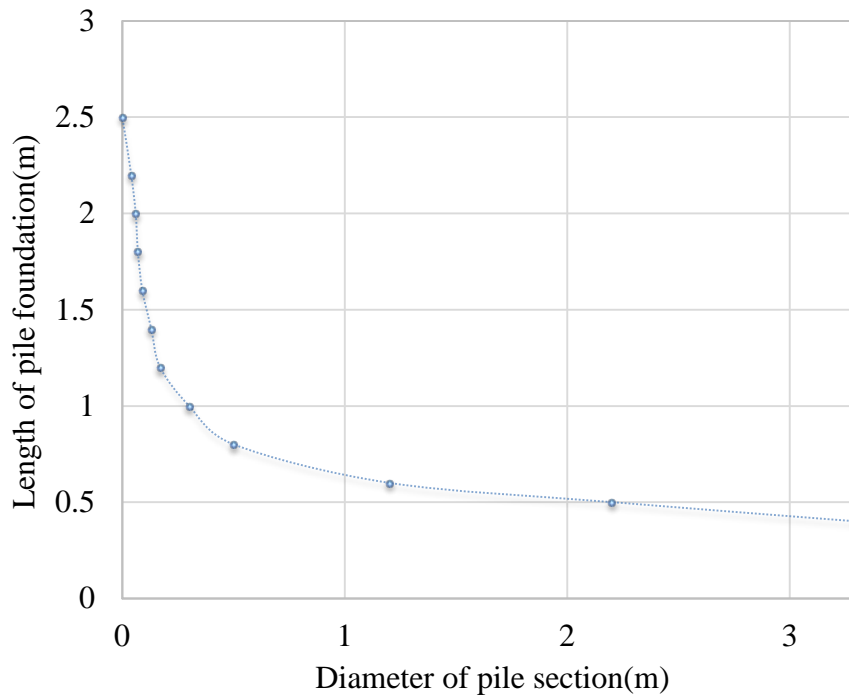


Figure 9 Pile Shaft Diameter against Pile Length

A comprehensive foundation construction procedure and the project evaluation and testing is as shown in Figure 10.

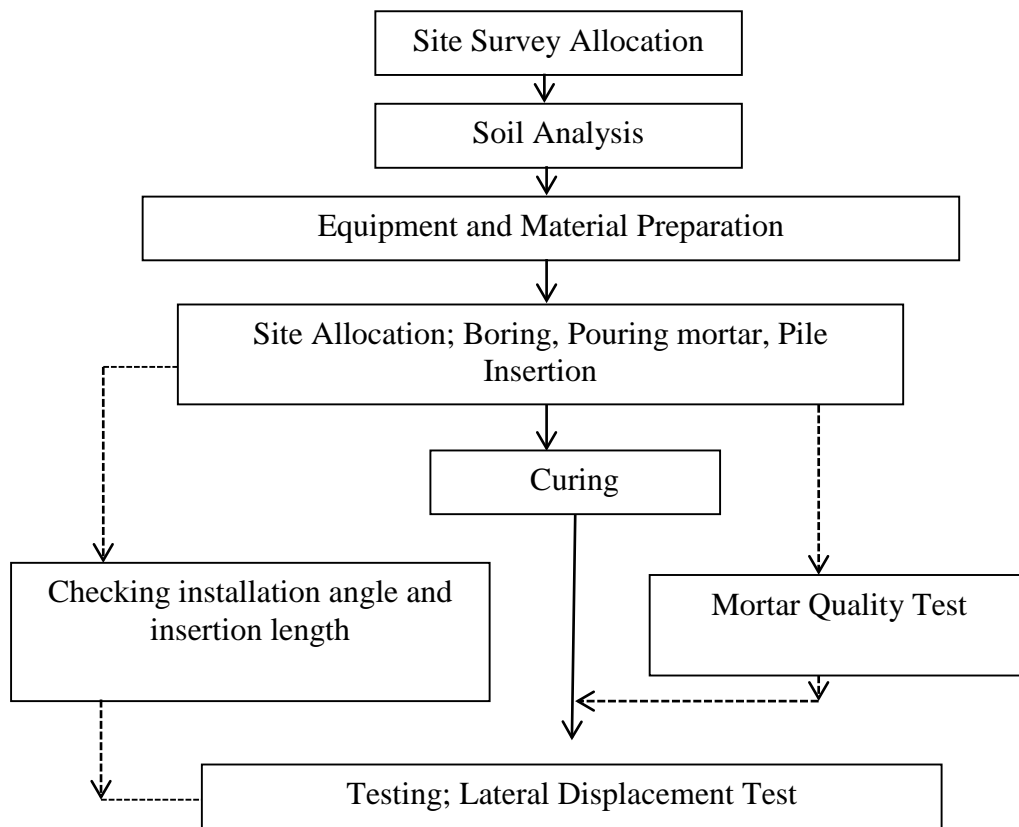


Figure 10 Workflow diagram

CHAPTER 3

NUMERICAL MODELLING USING FLAC2D

3.0 NUMERICAL MODELLING USING FLAC2D

In this chapter, the following three components are used in the building of a desirable model to replicate the composite single pile foundation. Figure 11 is the model that will be used in this research.

- Structural element
- Grid/Soil element
- Interface element/component

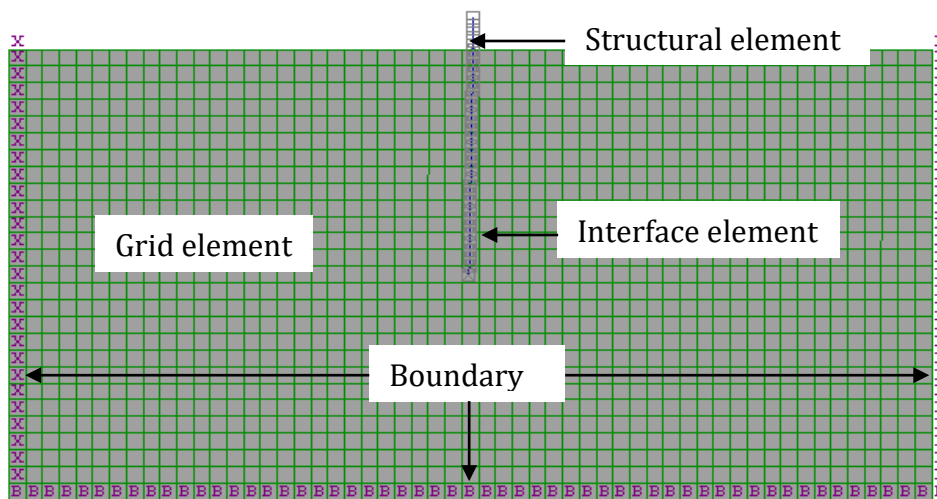


Figure 11 Mesh, boundary condition and structural element(pile)

3.1 STRUCTURE ELEMENT

In this research the type of the structural element involves is known as a pile element with 32 segments. A pile element is a two-dimensional element that transfers normal, shear forces and bending moments to the model grid as depicted in the beam and cable elements. The shear forces and normal forces subjected to the pile element acts in the parallel direction and perpendicular direction respectively. The pile elements are designed to represent the behavior of foundation piles. Therefore, the factors to consider include the cross-sectional area of the pile, A second moment of Area also known as the moment of inertia, I density of the pile

material, ρ elastic modulus of the pile, E the spacing between the piles which is always considered to be in a continuous direction in the out-of-plane direction.

In addition to these, the exposed perimeter of the pile itself also plays a major role in the analysis as it is the part in contact with the soil medium. Since in this case the exposed perimeter is in contact with the soil, then the interaction is expressed in terms of a normal response when the normal force is applied. Considering the fact that the pile in this case was cast in place, the stiffness of normal coupling spring, cs_{nstiff} and stiffness of shear coupling spring, cs_{sstiff} which are functions of the force applied, pile length and displacement are also important as they give a clear simulation of the behavior of the interface during lateral loading. In the evaluation of the structural element strength with respect to structural failure, then the lower limits of the frictional resistance of the shear coupling spring, cs_{sfric} and the cohesive strength of the shear coupling spring, cs_{scoh} can be related to those of the soil.

3.2 GRID/SOIL ELEMENT

These properties are essential in the estimation of the pile-soil shear and normal response during lateral loading. The soil element is represented by the grid. In FLAC2D the grid is a flexible function that carries in shape and size according to the problem being analysed. The grid consists of rows and columns that can be deformed to different shapes to suit the model at hand. The finer the grid mesh is, the more accurate the results obtained. In addition to this the aspect ratio (the ratio of the height of a zone to the width) also has a greater influence in the accuracy of the results obtained when the model is run. The grid in this research bears the soil component properties with the structural element installed in it. This analyses the stress and strain relations between the grid and the pile element. The grid component bares the soil properties of Matsusaka city that had silty soils and Kasugai City that had Clayey soils.

3.3 INTERFACE ELEMENT

The interface is the region between the structural component and the soil component/ grid using the contact logic. The interfaces may include, joint or bedding plane in a geologic medium, the area between a foundation and the soil, a contact plane between a chute and the materials in it or the contact between two or more colliding objects. In this case FLAC is characterized by Coulomb sliding/tensile separation. At the element-grid interface there exists the properties of dilation, normal stiffness, shear stiffness, friction, cohesion and the tensile strength. Never the less an interface can also exist between two structural elements laid side by side. The figure 12 below by Cundall and Hart (2003) shows a representation of normal and shear stiffness between two elements in contact with one another.

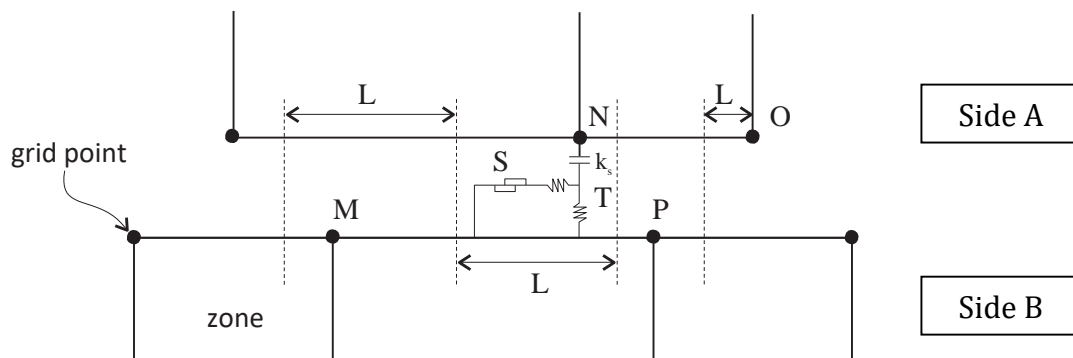


Fig 12 An interface represented by sides A and B connected by a shear, k_s and a normal, k_n stiffness springs.

Where, S = slider, T = tensile strength, k_n = normal stiffness, k_s = shear stiffness, L_n = length associated with grid-point N , L_m = length associated with grid-point M ,denotes limits for joint segments (placed halfway between adjacent grid-points). Referring to Figure 12, grid-point N is checked for contact on the segment between grid-points M and P . If contact is detected, the normal vector, \mathbf{n} , to the contact grid-point, N , is computed. A “length,” L , is also defined for the contact at N along the interface. This length is equal to half the distance to the nearest grid-point to the left of N plus half the distance to the nearest grid-point to the right, irrespective of whether the neighboring grid-point is on the same side of the interface or on the

opposite side of N . In this way, the entire interface is divided into contiguous segments, each controlled by a grid-point. During each time-step, the velocity, \dot{u}_i of each grid-point is determined. Since the units of velocity are displacement per time-step, and the calculation time-step has been scaled to unity to speed convergence, the incremental displacement for any given time-step is: $\Delta u_i \equiv \dot{u}_i$

The incremental relative displacement vector at the contact point is resolved into the normal and shear directions, and total normal and shear forces are determined by:

$$F_n^{(t+\Delta t)} = F_n^{(t)} - k_n \Delta u_n^{(t+(1/2)\Delta t)} L$$

$$F_s^{(t+\Delta t)} = F_s^{(t)} - k_s \Delta u_s^{(t+(1/2)\Delta t)} L$$

Where the stiffnesses, k_n and k_s , have the units of stress/displacement.

The shear force, F_s and the normal forces, F_n are calculated by the incorporation of the shear coupling spring and the normal coupling springs which are a representative of the pile/grid interface. The shear coupling spring consists of the spring slider system analyzed above at the nodal points of the pile element. On the other hand, the normal coupling spring is represented by a linear spring with a force that relies on the pile node movement direction. Equations 10 and 11 shows the function required for the calculation of both forces.

$$F_s = c_{s_{stiff}} (u_p - u_m) L \quad (10)$$

$$F_n = c_{n_{stiff}} (u_p^n - u_m^n) L \quad (11)$$

Where for Equation 10: F_s = shear force that develops in the shear coupling spring (i.e., along the interface between the pile element and the grid); $c_{s_{stiff}}$ = coupling spring shear stiffness ($c_{s_{stiff}}$); u_p = axial displacement of the pile; u_m = axial displacement of the medium (soil); and L = contributing element length.

For equation 11: F_n = normal force that develops in the normal coupling spring (i.e., along the interface between the pile element and the grid); $c_{n_{stiff}}$ = coupling spring normal stiffness ($c_{n_{stiff}}$); u_p^n = displacement of the pile normal to the axial direction of the pile; u_m^n =

displacement of the medium (soil) normal to the axial direction of the pile; and L = contributing element length.

3.4 STRESS STRAIN LAWS GOVERNING ELASTIC, TRANSVERSELY ISOTROPIC MODELS IN FLAC2D

The analysis of piles, combines the study on the response produced by beams elements and cable elements during loading. Each of these elements are a good example in the elastic modelling field hence governed by the elastic model laws. The primary representative of these laws is the Hooke's law that includes the stresses and strains involves during any type of loading subjected to the given element. The Hooke's law representation of the stress strain relation for an elastic isotropic model is represented by the *plain strain* and *plain stress* matrix as shown in matrix equation 12 and 13 respectively.

$$\begin{aligned}\Delta \sigma_{xx} &= \alpha_1 \Delta e_{xx} + \alpha_2 \Delta e_{yy} \\ \Delta \sigma_{yy} &= \alpha_2 \Delta e_{xx} + \alpha_1 \Delta e_{yy} \\ \Delta \sigma_{xy} &= 2G\Delta e_{xy} : (\Delta \sigma_{yx} = \Delta \sigma_{xy}) \\ \Delta \sigma_{zz} &= \alpha_2 (\Delta e_{xx} + \Delta e_{yy})\end{aligned}\tag{12}$$

Where $\alpha_1 = K + (4/3) G$, $\alpha_2 = K - (2/3) G$, K = Bulk modulus and G =Shear modulus.

$$\begin{aligned}\Delta \sigma_{xx} &= \beta_1 \Delta e_{xx} + \beta_2 \Delta e_{yy} \\ \Delta \sigma_{yy} &= \beta_2 \Delta e_{xx} + \beta_1 \Delta e_{yy} \\ \Delta \sigma_{xy} &= 2G\Delta e_{xy} : (\Delta \sigma_{yx} = \Delta \sigma_{xy}) \\ \Delta \sigma_{zz} &= 0\end{aligned}\tag{13}$$

Where, $\beta_1 = \alpha_1 - (\alpha_1^2 / \alpha_1)$ and $\beta_2 = \alpha_1 - (\alpha_1^2 / \alpha_1)$

Considering a transversely isotropic model, the plane of isotropy lies in the xz -plane as shown in figure 13. FLAC2D deforms a transversely isotropic elastic element when acted upon

by plane stress or plain strain boundary conditions such that the z -axis lies parallel with the planes of Isotropy (xy plane)

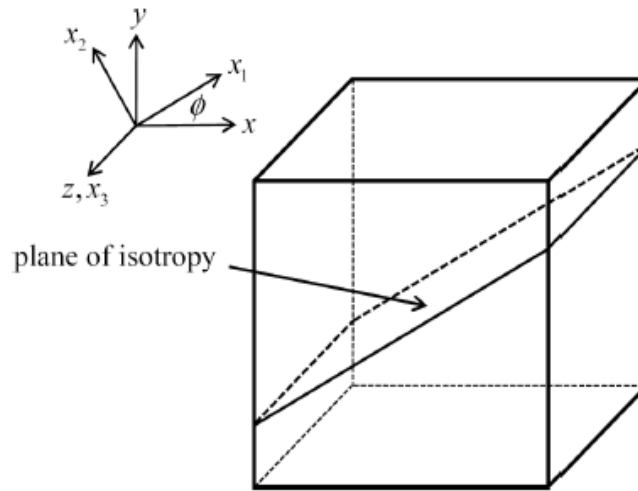


Figure 13 Coordinate axes for a transversely isotropic model.

Using FLAC2D, the elastic moduli are then defined as follows. E_1 or E_x is the modulus of elasticity in the plane of isotropy, E_2 or E_y is the modulus of elasticity in the plane perpendicular to the plane of isotropy, G_{12} or G_{xy} is the cross shear modulus between the plane of isotropy and the perpendicular plane, G_{13} or G_{xz} is the shear modulus in the plane of isotropy, ν_{21} or ν_{yx} is the Poisson's ratio for the normal strain in the x -direction related to the normal strain in the y -direction due to the uniaxial stress in the y -direction and lastly ν_{31} or ν_{zx} is the Poisson's ratio for the normal strain in the x -direction related to the normal strain in the z -direction due to uniaxial stress in the z -direction. From these elastic moduli then the following relations can be obtained:

$$E_z = E_x: \nu_{zx} = \nu_{xz}: \nu_{yz} = \nu_{yx}: G_{yz} = G_{xy}: G_{xz} = E_x / (2(1 + \nu_{zx})):$$

$$\nu_{xy} = \nu_{yx}(E_x / E_y) \tag{14}$$

According to Amadei 1982 on rock anisotropy on medium that are transversely isotropic, he found out that the following limitations are useful in variation of the elastic moduli. $E_x > 0$, $E_y > 0$, $G_{xy} > 0$, $\nu_{xy}^2 \leq 1$, $\nu_{xz}^2 \leq 1$ and $(1 - \nu_{xz}) - (2E_x \nu_{yx}^2 / E_y) \geq 0$. These limitations are vital in the

computation of the stress strain equations as illustrated by Lekhnitskii (1981). The matrix of the stress strain equation is as illustrated in Equation 15.

$$\begin{aligned}
\Delta e_{xx} &= S_{11} \Delta \sigma_{xx} + S_{12} \Delta \sigma_{yy} + S_{13} \Delta \sigma_{zz} + S_{16} \Delta \sigma_{xy} \\
\Delta e_{yy} &= S_{12} \Delta \sigma_{xx} + S_{22} \Delta \sigma_{zz} + S_{23} \Delta \sigma_{zz} + S_{26} \Delta \sigma_{xy} \\
\Delta e_{zz} &= S_{13} \Delta \sigma_{xy} + S_{23} \Delta \sigma_{yy} + S_{33} \Delta \sigma_{zz} + S_{36} \Delta \sigma_{xy} \\
\Delta e_{yz} &= 1/2[(S_{44} \Delta \sigma_{yz}) + (S_{45} \Delta \sigma_{xz})] \\
\Delta e_{xz} &= 1/2[(S_{45} \Delta \sigma_{yz}) + (S_{55} \Delta \sigma_{xz})] \\
\Delta e_{xy} &= 1/2[(S_{16} \Delta \sigma_{xx}) + (S_{26} \Delta \sigma_{yy}) + (S_{36} \Delta \sigma_{zz}) + (S_{66} \Delta \sigma_{xy})]
\end{aligned} \tag{15}$$

Where,

$$\begin{aligned}
S_{11} &= \frac{\cos^4 \phi}{E_1} + \left(\frac{1}{G_{12}} - \frac{2\nu_{12}}{E_1}\right) \sin^2 \phi \cos^2 \phi + \frac{\sin^4 \phi}{E_2} \\
S_{22} &= \frac{\sin^4 \phi}{E_1} + \left(\frac{1}{G_{12}} - \frac{2\nu_{12}}{E_1}\right) \sin^2 \phi \cos^2 \phi + \frac{\cos^4 \phi}{E_2} \\
S_{12} &= \left(\frac{1}{E_1} + \frac{1}{E_2} + \frac{2\nu_{12}}{E_1} - \frac{1}{G_{12}}\right) \sin^2 \phi \cos^2 \phi - \frac{\nu_{12}}{E_1} \\
S_{13} &= -\left(\frac{\nu_{23}}{E_2}\right) \sin^2 \phi - \left(\frac{\nu_{13}}{E_1}\right) \cos^2 \phi \\
S_{23} &= -\left(\frac{\nu_{23}}{E_2}\right) \cos^2 \phi - \left(\frac{\nu_{13}}{E_1}\right) \sin^2 \phi \\
S_{33} &= \frac{1}{E_3} \\
S_{44} &= \frac{\cos^2 \phi}{G_{23}} + \frac{\sin^2 \phi}{G_{13}} \\
S_{45} &= \left(\frac{1}{G_{23}} - \frac{1}{G_{13}}\right) \sin \phi \cos \phi \\
S_{55} &= \frac{\sin^2 \phi}{G_{23}} + \frac{\cos^2 \phi}{G_{13}} \\
S_{16} &= \left[2\left(\frac{\sin^2 \phi}{E_2} - \frac{\cos^2 \phi}{E_1}\right) + \left(\frac{1}{G_{12}} - \frac{2\nu_{12}}{E_1}\right) (\cos^2 \phi - \sin^2 \phi)\right] \sin \phi \cos \phi \\
S_{26} &= \left[2\left(\frac{\cos^2 \phi}{E_2} - \frac{\sin^2 \phi}{E_1}\right) - \left(\frac{1}{G_{12}} - \frac{2\nu_{12}}{E_1}\right) (\cos^2 \phi - \sin^2 \phi)\right] \sin \phi \cos \phi \\
S_{36} &= 2\left(\frac{\nu_{13}}{E_1} - \frac{\nu_{23}}{E_2}\right) \sin \phi \cos \phi
\end{aligned}$$

$$S_{66} = 4 \left(\frac{1}{E_1} + \frac{1}{E_2} + \frac{2\nu_{12}}{E_1} - \frac{1}{G_{12}} \right) \sin^2 \phi \cos^2 \phi + \frac{1}{G_{12}}$$

Φ is the angle of anisotropy that is measured in an anticlockwise direction from the x axis. To obtain plain stress with respect to the xy plane, the following stresses in the matrix are set to zero as shown in equation 16. These values substituted into equation 15 gives the plain stress matrix shown in equation 17.

$$\Delta\sigma_{zz} = \Delta\sigma_{xz} = \Delta\sigma_{yz} = 0 \quad (16)$$

$$\Delta e_{xx} = S_{11} \Delta\sigma_{xx} + S_{12} \Delta\sigma_{yy} + S_{16} \Delta\sigma_{xy}$$

$$\Delta e_{yy} = S_{12} \Delta\sigma_{xx} + S_{22} \Delta\sigma_{yy} + S_{26} \Delta\sigma_{xy}$$

$$\Delta e_{xy} = 1/2(S_{16} \Delta\sigma_{xx} + S_{26} \Delta\sigma_{yy} + S_{66} \Delta\sigma_{xy})$$

This can be rewritten as shown in matrix equation 6

$$\begin{bmatrix} \Delta e_{xx} \\ \Delta e_{yy} \\ \Delta e_{xy} \end{bmatrix} \begin{bmatrix} S_{11} & S_{12} & S_{16} \\ S_{12} & S_{22} & S_{26} \\ S_{16} & S_{26} & S_{66} \end{bmatrix} \begin{bmatrix} \Delta\sigma_{xx} \\ \Delta\sigma_{yy} \\ \Delta\sigma_{xy} \end{bmatrix} \quad (17)$$

The plain strain matrix can be obtained by equating the strain values in equation 18 to zero then substituting into the matrix in equation 15 to obtain the matrix illustrated by equation 19.

$$\Delta e_{zz} = \Delta e_{xz} = \Delta e_{yz} = 0 \quad (18)$$

$$\Delta e_{xx} = S_{11}\Delta\sigma_{xx} + S_{12}\Delta\sigma_{yy} + S_{13}\Delta\sigma_{zz} + S_{16}\Delta\sigma_{xy}$$

$$\Delta e_{yy} = S_{12}\Delta\sigma_{xx} + S_{22}\Delta\sigma_{yy} + S_{23}\Delta\sigma_{zz} + S_{26}\Delta\sigma_{xy}$$

$$0 = S_{13}\Delta\sigma_{xx} + S_{23}\Delta\sigma_{yy} + S_{33}\Delta\sigma_{zz} + S_{36}\Delta\sigma_{xy}$$

$$0 = S_{44}\Delta\sigma_{yz} + S_{45}\Delta\sigma_{xz}$$

$$0 = S_{55}\Delta\sigma_{xz} + S_{45}\Delta\sigma_{yz}$$

$$\Delta e_{xy} = 1/2 (S_{16}\Delta\sigma_{xx} + S_{26}\Delta\sigma_{yy} + S_{36}\Delta\sigma_{zz} + S_{66}\Delta\sigma_{xy}) \quad (19)$$

The matrix Equation 19 can also be rewritten as shown in equation 20

$$\begin{bmatrix} \Delta e_{xx} \\ \Delta e_{yy} \\ 0 \\ 2\Delta e_{xy} \end{bmatrix} \begin{bmatrix} S_{11} & S_{12} & S_{13} & S_{16} \\ S_{12} & S_{22} & S_{23} & S_{26} \\ S_{13} & S_{23} & S_{33} & S_{36} \\ S_{16} & S_{26} & S_{36} & S_{66} \end{bmatrix} \begin{bmatrix} \Delta \sigma_{xx} \\ \Delta \sigma_{yy} \\ \Delta \sigma_{zz} \\ \Delta \sigma_{xy} \end{bmatrix} \quad (20)$$

3.5 STRESSES AND STRAIN INCORPORATION INTO THE FLAC2D MODELS

Figure 14 is a representative of an extended view of the top of the model with 1,2 and 3 indicating the zones and inscribed within the zones ($i-1$, i , and $i+1$), shows the stresses involved during stress and strain development process. On the other hand, a , b and c indicated the grid points upon which the velocities are applied to produce deformations that lead to the grid displacement.

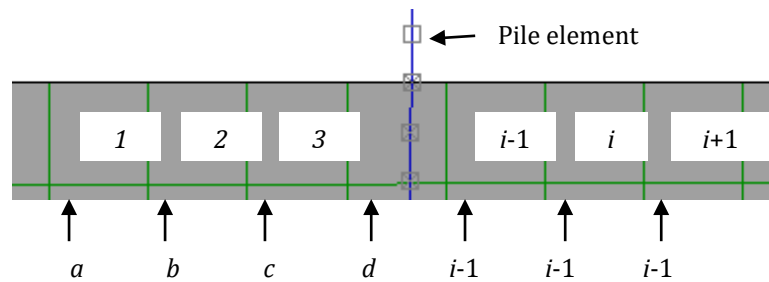


Figure 14 Schematic representation of the grid points and the zones

Finite-difference method (FDM) is numerical methods for solving differential equations by approximating them with difference equations, in which finite differences approximate the derivatives. FDMs (Cundall, P) are thus discretisation methods and are the dominant approach to numerical solutions of partial differential equations. FLAC2D applies the FDM to implement a solution to the coded input, for example, the analysis of the pile foundation. FLAC2D therefore, allow for the vector quantities for example forces, velocities and displacements storage in the finite difference grid generated while all scalar quantities, for example, stresses, pressure, and material properties stored in the zone locations. To ensure stability in the numerical scheme, FLAC2D includes the dynamic equations of motion (equilibrium equation) in the formulation. The balance thus provides there is no sudden failure or collapse to the structural component during the lateral loading procedures (Britto and Gunn, 1987). The primary explicit calculation cycle is as shown in figure 15.

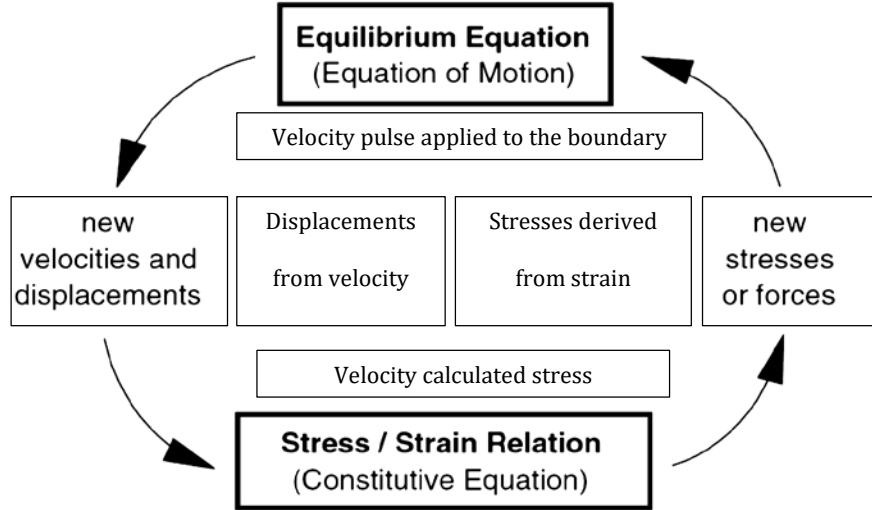


Figure 15 Basic explicit calculation cycle

The behaviour of a pile element during loading is similar to the elastic model in FLAC2D. Regarding figure 15, three main equations that dictate the response of the pile element include Stress-Strain Constitutive Law (Hooke's Law), Equation of Motion for Dynamic Equilibrium (wave equation) and FDM formulation using central finite difference equation as shown in equation 21, 22 and 23 respectively.

$$\sigma_{xx} = E (\partial u_x / \partial x) \quad (21)$$

$$\rho (\partial \dot{u}_i / \partial t) = \partial (\sigma_{ij} / \partial x_j) + \rho g_i \quad (22)$$

$$\sigma_{xx}^i(t) = E [(u_x^{i+1}(t) - u_x^i(t)) / \Delta x] \quad (23)$$

Where ρ is the mass density, u_x is the velocity component, E is the elastic modulus, t is the time, x_i is the component of the coordinate vector, g_i is the component of gravitational acceleration and σ is the component of the stress tensor. Equation 22 illustrates the dynamic force equilibrium which indeed shows the relationship between gravitational forces and the changes in stress in the model grid. As reflected earlier in this paper, FLAC2D consists of mainly useful formulations where the variations in velocity are quickly solved. Consequently, the rate at which strain is experienced in the model grid can be related to the velocity. The finite difference equation for the equation of motion using central finite difference equation 23, can further be simplified and classified into two sections, with the left side of the equation showing the changes in velocity while the right side represents the changes in the stresses involved during the model code execution as shown in equation 24.

$$\frac{\rho}{\Delta t} \left\{ \dot{u}_x^i \left(t + \frac{\Delta t}{2} \right) - \dot{u}_x^i \left(t - \frac{\Delta t}{2} \right) \right\} = \frac{1}{\Delta x} \left\{ \sigma_{xx}^i(t) - \sigma_{xx}^{i-1}(t) \right\} \quad (24)$$

Equation 24 is then rearranged to equation 25 which upon integration produces the deformations in the grid (equation 26) and the histogram thereby generated is a plot of the p-y curves of the pile at the prescribed loading velocity.

$$\dot{u}_x^i \left(t + \frac{\Delta t}{2} \right) = \dot{u}_x^i \left(t - \frac{\Delta t}{2} \right) + \frac{\Delta t}{\rho \Delta x} \left\{ \sigma_{xx}^i(t) - \sigma_{xx}^{i-1}(t) \right\} \quad (25)$$

$$u_x^i(t + \Delta t) = u_x^i(t) + \dot{u}_x^i \left(t + \frac{\Delta t}{2} \right) \Delta t \quad (26)$$

Ultimately, these p-y curves produces are used in the analysis of the pile element response to various types of loading for example lateral loading, axial loading and compression loading as discussed in this study. The FISH program embedded in FLAC2D runs equation 26 so as to obtain the desired deformations that will be experience in the grid/soil. The deformations are due to the stresses and the strains developed in the model grid hence the measurement of the corresponding deflections through the p-y curves.

More explanation on the model parameters and the mode in which the forces are subjected to the numerical model are discussed in Chapter 4 and Chapter 5 based on lateral capacity evaluation and pull-out capacity evaluation respectively.

CHAPTER 4

LATERAL CAPACITY OF COMPOSITE SINGLE PILES

4.0 LATERAL CAPACITY OF COMPOSITE SINGLE PILES

4.1 INTRODUCTION

The response of laterally loaded piles is a function that is dictated by many related parameters that act upon the pile foundation during loading. At any considerable time of loading, the effects of each parameter input can cause a substantial influence on the reaction of the pile foundation and the adjacent soil components. Engineers always propose pile foundation for the transfer of loads of overlying structures as it offers adequate bearing capacity for lateral loads and also gravity loads. Somekawa et al. (2012) studied the effects of the wind loading on the solar panels as this is one of the major forces to be transmitted by the foundation into the ground. In the past studies on pile foundations, several approaches have been carried out to analyze this response from loads. Firstly, the method that have been employed in the analysis of laterally loaded piled is the full-scale experimental model. In this case, the whole experimental set-up is done on the fields and tests done on real time upon completion of the pile foundation structure. Examples of full scale experiments are as shown the Figure 16.

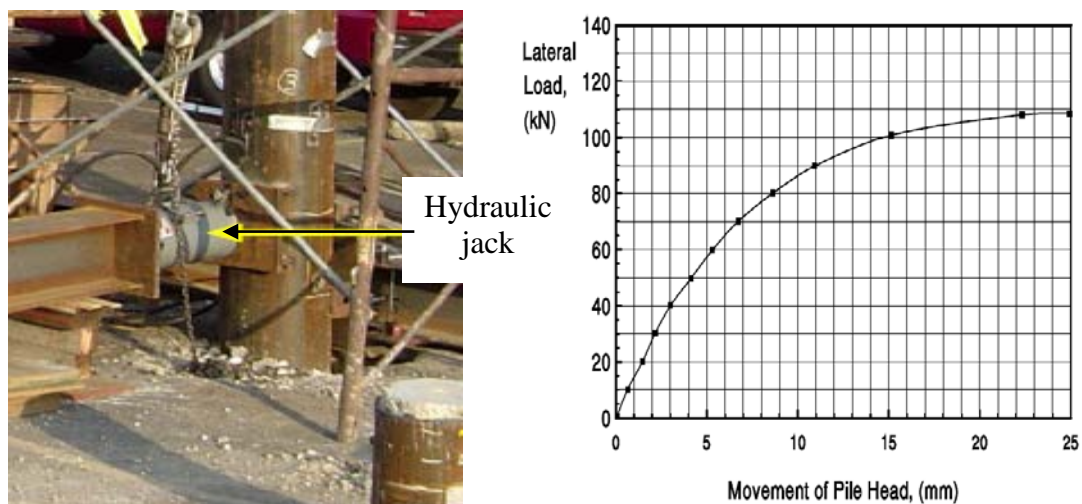


Fig 16 full scale experiment and plot of results

Secondly, the analytical approach involved the development of analytical models that provided a scaled model to replicate what would have existed in the real ground. Klepikov

(1965), conducted a study using such analytical models to examine the influence generated by the modulus of subgrade reaction at the ground surface as the primary parameter influencing the lateral capacity of the pile structure and its response to the soil grid. The subgrade reaction has also enabled engineers to develop models that can withstand seismic activities without the fear of structural failure as stipulated by Caseiro (1986), who predicted the foundation response to seismic and dynamic loads. In addition to this, the development of analytical equations taking into consideration all the input parameters the foundation is subjected to when acted upon by the horizontal or lateral loads were also considered. Considering an analytical approach by Reese and Matlock (1971), the lateral displacement of the pile, y when subjected to the lateral forces was a function of the lateral force H , bending moment M , foundation depth z , length of the pile L , relative stiffness factor T , pile material modulus of elasticity E , the moment of inertia I , and the unit modulus of subgrade reaction of the soil K_h . These parameters are shown in Figure 17 and equation (1).

$$y = \beta \{H(T^3)/EI\} A_y + \beta \{M(T^2)/EI\} B_y; T = 5\sqrt[3]{(EI/K_h)} \quad (27)$$

Where $H=3.28 \text{ kN}$, $T=0.186$, $EI=5607.94 \text{ Nm}^2$, $K_h=25000 \text{ kNm}^3$, $A_y=2.435$, $B_y=1.623$

A_y and B_y are the coefficients for the Matlock-Reese model solution. Given a lateral loading H , equation (1) can be used to calculate the corresponding deflection y .

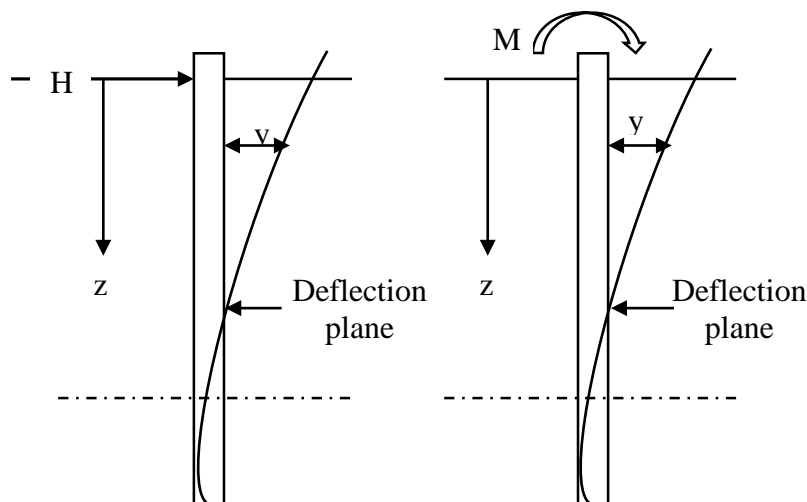


Figure 17 Lateral loading functions

So as to validate the calculations from the classical equations, safety measures such as in AIJ (2004), on horizontal pile bearing capacity analysis was helpful for the determination displacement that occurs at the ground level. The allowable empirical horizontal movement was 10mm in typical situations and 15mm in the areas prone to seismic process such as earthquakes. Okahara et al. (1991a) also stated that the permissible horizontal displacement is the more considerable value of 1% of the pile diameter or 15mm in both areas of normal conditions and seismic activity-prone regions. The value comes from the study of pile bearing capacity by Okahara et al. (1991b) focusing on the examination of piles subjected to horizontal loads and the observation of the elastic limits displacements on the load-displacement curves.

The third approach involved the use of numerical simulations to get a clear picture of what happens within the soil medium and the pile element. These approaches included force method, beam on elastic foundation method, soil plasticity, and elasticity continuum method. But most recently the practice of finite element method FEM (Poulos, 1971), finite difference method FDM (Brown, Shie & Kumar, 1989) is being put in to use. FEM and FDM are flexible and can be manipulated to give a variety of responses and an in-depth analysis of the pile and the soil interface. The analysis of laterally loaded piles in most cases is expressed mostly by using the load-displacement curve methods also referred to as the p-y curve method. Using the p-y curves, the response of the soil during loading is shown by a series of springs that produce the resistance offered by the load when acting upon them. The curvilinear load-displacement p-y characteristics of the springs are given as input to the analysis, and numerical methods are used to obtain the pile load-displacement response (Cox & Reese, 1978). From the p-y curve obtained, the pile foundations, in this case, the single pile foundation should be able to withstand the imposed load with a reasonable factor of safety, the pile head displacement should not exceed the tolerable movements for the structure it supports, for example, the solar

panels in this study and lastly the intermediate soil should not receive excessive stresses that may make it achieve the ultimate load carrying capacity upon full construction and operation (Duncan, Jr. Evans & Ooi, 1994). A closer consideration was given on the response of the soil to the short piles as this provides a clear understanding of the pile element because at this depth the displacement was entirely reliant on the resistance of the soil as illustrated by (Broms, 1964).

4.2 ANALYTICAL APPROACHES, MATERIALS AND METHODS

In this research the three approaches were done to design and analyse the single pile composite foundation as illustrated below:

- Full-scale experimental approach. Conducted in Matsusaka and Kasugai Cities.
- Analytical methods using theoretical equations and developed classical equation.
- Numerical modelling/ simulation approach using civil engineering software. In this research thesis uses FDM procedures embedded in FLAC2D software.
- Parametric study using FLAC2D

4.2.1 Full-scale experiment approach

The development of an experimental control foundation setup can be useful for preliminary designs. This study shows a simple composite foundation design taking in to account cost and performance relation, made from a hollow steel pipe to curb the tension forces involved when acted upon by dead loads and external loads and anchored to the ground by a cement-sand mortar to ensure effective frictional resistance as it bonds well with steel section and the soil medium. The steel pile channels the entire load to the ground while the sand – cement mortar improves the soil bearing capacity as well as bonding the foundation to the next soil structure, thus providing adequate frictional resistances and improved cohesion owing to its relatively greater surface area and roughness as compared to conventional foundation. The test piles were installed in Matsusaka city and Kasugai city which had Silty soils and clayey soils respectively.

All the tests were carried out in accordance to the Japanese Geotechnical Society (JGS), 2014. Monitoring was done using the Linear Displacement Transducers (LDT) and readings recorded automatically with respect to loading variations as shown in Figure 18 and 19.



Figure 18 Full-scale experimental setup



Figure 19 Full-scale experimental setup

4.2.2 Analytical approach

Development of a classical equation for the deflection of a laterally loaded single pile

As a key part of research and development, the development of new approach to engineering problems is necessary to obtain a more simplified view of the problem. In accordance to this, below is the derivation of an equation that can be used to evaluate the deflection of the composite single pile using the ground reaction approach. Figure 20, is a clear representation of the cross-sectional area of the pile element inside the soil medium. Where H is the lateral load, y_1 is the deflection at the top of the pile, y_2 is the deflection at the bottom of the pile, L is the length of the pile in the soil, θ_1 is the pile rotation angle, θ_2 is the ground slope and O is the rotational centre depth.

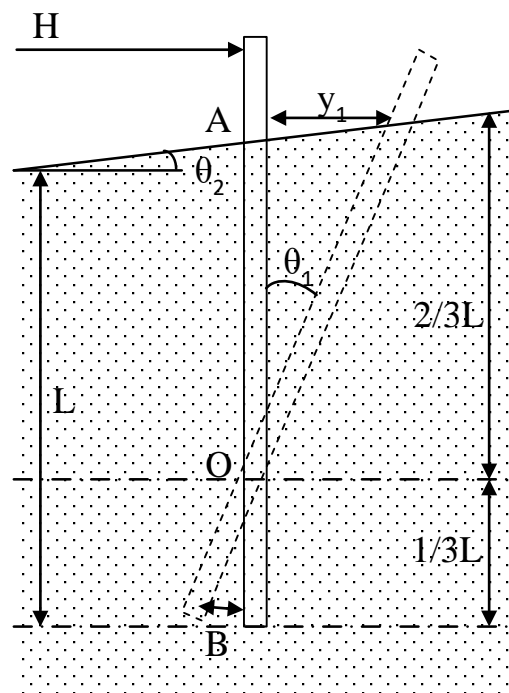


Figure 20 Cross-sectional area of the pile element inside the soil medium

From figure 20 the derivation steps to obtain a classical equation for the deflection, y , of the composite single pile head when subject to lateral loading are as follows:

- Determination of the modulus of subgrade reaction of the soil
- Evaluation of soil pressures at different depths of the pile

- Evaluation of the pile element displacement angle using Reese approach.
- Correcting the pressure values considering the ground slope at the surface
- Using the corrected soil reaction pressure to derive the new pile head deflection equation, y .

The following equations are therefore applicable.

$$y_1 \text{ is the deflection at the top of the pile. Where } y_1 = 2/3 \tan \theta \quad (28)$$

$$y_2 \text{ is the deflection at the bottom of the pile. Where } y_2 = 1/3 \tan \theta \quad (29)$$

θ_1 is the pile rotation angle at $2/3L$, θ_2 is the ground slope, point O is the rotational center depth while H is the lateral load. Pressure applied by soil due to the lateral load at the top of the pile σ_1 , is obtained as shown in equation 30.

$$\sigma_1 = (K_h y_1) = 2/3 K_h L_1 \tan \theta : L_1 = z_o - z \quad (30)$$

Pressure applied by soil due to the lateral load at the bottom of the pile σ_2 is obtained as shown in equation 31.

$$\sigma_2 = (K_h y_2) = -(1/3 K_h L_2 \tan \theta) : L_2 = z - z_o \quad (31)$$

Effective soil pressure acting on the composite single pile foundation pile therefore becomes:

$$\sigma_1 + -\sigma_2 = (K_h y_1) = 2/3 K_h L_1 \tan \theta + -(K_h y_2) = -(1/3 K_h L_2 \tan \theta) \quad (32)$$

By the introduction of the ground slope (10), then soil pressure adjustments is necessary to portray the real effects of the ground topography and effects of the overlying soil layers. Soil Pressure adjustment due to the introduction of the slope (10) are evaluated at the top of the pile and the bottom of the pile as shown in equations 33 and equation 34.

Corrected soil Pressure at the top of the pile σ_1 :

$$\sigma_1 / (1 + \tan \theta) = (2/3 K_h L_1 \tan \theta_1) / (1 + \tan \theta_2) \quad (33)$$

Corrected soil Pressure at the top of the pile σ_2 :

$$\sigma_2 / (1 + \tan\theta) = (1/3K_h L_1 \tan\theta_1) / (1 + \tan\theta_2) \quad (34)$$

θ_1 is the pile element rotation angle, proposed by Reese by the equation 35,

$$\theta_2 = A_\theta \frac{Q_g T^2}{E_p I_p} + B_\theta \frac{M_g T}{E_p I_p} \quad ; \quad T = \sqrt[3]{\frac{E_p I_p}{n_h}} \quad (35)$$

Where; Q is the lateral load, T is the pile stiffness, E is the pile modulus of elasticity, I, is moment of inertia, Moments about the pile and A/B are the Reese slope factors. σ_2 is the angle of the slope at the ground surface. Ultimately the deflection, y becomes:

Deflection, y = (Soil pressure acting on the pile / Modulus of subgrade reaction)

$$\text{Deflection, } y = \frac{\frac{0.67K_h L \tan\theta_1}{1 + \tan\theta_2}}{K_h} - \frac{\frac{0.33K_h L \tan\theta_1}{1 + \tan\theta_2}}{K_h} \quad (36)$$

$$\text{Where } K_h = \frac{2E_s}{\pi D^2 (1 - \mu^2)}$$

Where: K_h is the modulus of subgrade reaction, E_s soil elastic modulus, D is the diameter of the pile element, μ is the poisson ratio of the soil, L values for top of the pile = $(z_0 - z)$ and L values for bottom of the pile = $(z - z_0)$.

4.2.3 Numerical modelling approach

Nowadays, numerical modelling is becoming a popular tool to obtain a clear picture of the interaction between soil and the foundation. This research as shown in Figure 21 therefore uses FLAC2D (Billiaux et al. 2001) which is a popular two-dimensional explicit finite difference program for geotechnical modelling. The program is capable of providing the performance in different types of medium like soil, rock and all materials that can experience plastic flow when the material yield limits. In a numerical model, the material is represented in zones/elements and upon the application of forces, the elements behave in accordance to the subjected linear

or non-linear stress/strain laws. Hence, showing the pressure distribution along the pile foundation, the intensity of the bending moment during lateral loading and the displacement patterns of the soil and pile foundation. The accuracy of the model is based on Lagrangian calculation scheme and also the mixed discretion zoning technique accorded to the structure as discussed in Chapter 3.

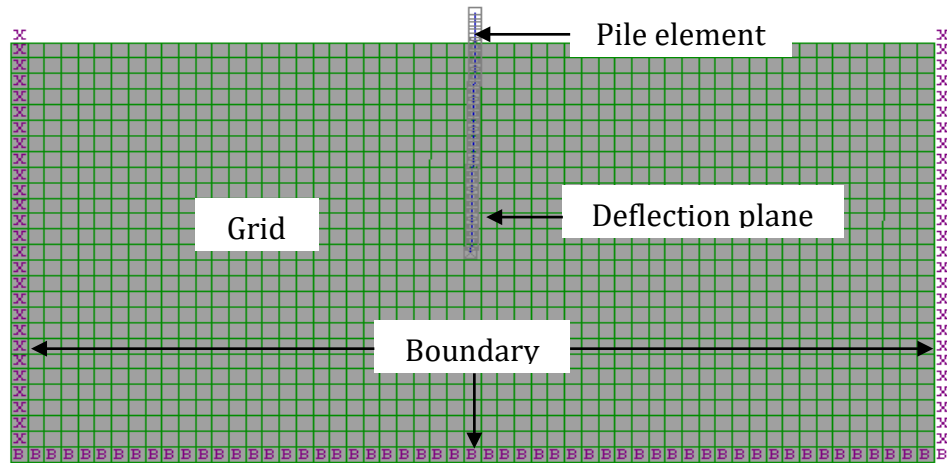


Figure 21 Model details before the application of the lateral load.

The input parameters into the FLAC2D model code include the soil properties and the pile element properties are as shown in Table 3 and Table 4 respectively.

Table 3 Soil Properties

Item	Type of soil		Units
	Silty soil	Clayey soil	
Soil Density	1750	1750	kg/m ³
Soil Cohesion	25e3	50e3	N/m ²
Soil Friction	30	0	Degree
Soil Dilatancy	15	0	Degree
Soil Tension	50e3	50e3	N/m ²
Young's Modulus	21e6	50e6	N/m ²
Poisons Ratio	0.3	0.49	Ratio

Table 4 Pile Element Properties

Item	Value	Units
Pile length below the ground surface	1.4	m
Pile diameter	0.26	m
Pile Young's modulus	8e10	N/m ²
Stiffness of shear coupling spring (cs sstiff)	1.3e11	N/m ²
Cohesive strength of the shear coupling spring (cs scoh)	30e3	N/m
Frictional resistance of the shear coupling spring (cs sfric)	20	Degree
Stiffness of normal coupling spring (cs nstiff)	1.3e8	N/m ²
Cohesive strength of the normal coupling spring (cs ncoh)	30e3	N/m
Frictional resistance of the normal coupling spring (cs nfric)	20	Degree

The numerical study thus investigates the effects of several parameters such as pile head displacement variations for two types of soil (silty soil and clayey soil), soil elastic modulus, loading velocity, stiffness of the standard coupling spring represented by the pile element and the pile eccentricity on the p-y curves. The p-y curves will help in the determination of the pile bearing capacity with respect to lateral loading.

CHAPTER 5

PULL-OUT CAPACITY OF SINGLE PILES

5.0 PULL-OUT CAPACITY OF SINGLE PILES

5.1 INTRODUCTION

Pile foundations are commonly used in support of engineering structures to prevent them from overturning moments produced by winds and earthquakes in most cases. To understand how piles, transmit the loads to the ground, several experiments are necessary before construction. In literature, the pull-out capacity of pile foundations has been carried out in a few studies most of which employ full-scale field experiments. In the previous research (Begemann, 1965) it is suggested that static cone penetration test can be used in the estimation of the pile ultimate lifting capacity with the most determining factor being the uplift skin friction. The value obtained however needed some adjustments which led to the introduction of the reduction factor which was highly dependent on the soil type and the type of pile used in the construction and reduction values on the uplift load if the force was oscillating.

A large-scale experimental set up in (Downs, and Chieurzzi, 1966) focused on the analysis of the pull-out loads. Their experiment was mainly based on fixed pile dimension installed in soft moist silty to fine clayey sand. The results obtained were

used in the formulation of the equation: $P_u = \pi d L/2 (KL \tan \theta + 2c)$ where K represented the coefficient of lateral earth pressure. However, their approach reflected the effect of type of casing and method of backfilling on the uplift capacity.

In accordance to the fact that the uplift capacity of the pile is dependent on the relative skin friction on the pile-soil interface, Sowa (1970), analysis on the field tests on cast piles depicted that the coefficient of the earth pressure was considerably less during loading than the ratio of earth pressure at rest and Rankine's active earth pressure coefficient. Due to this variation, it was perverse to set value during the preliminary design.

To counter the fluctuation of the earth pressure coefficient, Meyerhof (1973), introduced the uplift coefficient in place of the factor of earth pressure. For a pile installed at an angle of shearing resistance θ , the uplift coefficient increased with the increase in the slenderness ratio L/d up to a maximum value, then remained constant. However, the limiting factor was shown to increase with an increase in angle of shearing resistance.

McClelland (1974), demonstrated the effects of installation on the uplift capacity of piles by field tests on same steel pipe piles of diameter 508 mm installed to penetration of 14.63m in uniform beach sand by four different techniques. The driven pile exhibited net uplift capacity, which was 1.4 times that of a pile installed by jetting with external return flow. He concluded that the ultimate shaft resistance was dependent on the methods of driving/installation.

More research by Sharma (1988), suggested the evaluation of the ultimate loading capacity of the piles was by the assessment of the skin friction along the pile and soil interface and the bearing pressure along the perimeter of the pile. Using this proposed approach, the ultimate bearing capacity became a function of the diameter of the pile, d , depth of the centre of the first under-reamed bulb, d_1 , thickness of the center of the last under-reamed bulb, d_n , diameter of the under-reamed bulb, B_1 , number of under-reamed bulb, n , coefficient of earth pressure and the bearing capacity depending on the angle in friction. This relationship is as shown in equation 37

$$Q = \pi / 2dk_y \tan \theta (d_1^2 + L^2 + d_n^2) + \pi / 4 (B_1^2 - d^2) (1 / 2n\gamma B_1 N_\gamma + \gamma N_\gamma + N_q d_1). \quad (37)$$

The effects of pull-out load on piles were further analyzed with the coexisting relations to the stress-strain relations (Poorooshasb and Paramesw, 1982). This analysis was done in frozen sandy soils, and the stress-strain relationship proved to be linear. This approach was found to apply to the short pile only installed in moderately to densely over-consolidated clay soils

hence a limiting factor in the predesign considering the fluctuating soil layers. The study further showed that during the loading process, the deformation of the earth along the pile perimeter acted similarly as the shearing of concentric cylinders hence the linearity in the stress and strain relations.

In the process of determining the pile failure mechanism, Kulhawy (1979), came up with a general analytical model for the drained uplift capacity of drilled pile foundations. The main aim was to establish the main determining variables that will lead to the calculation of the ultimate loading capacity that produced the pile failure pattern. From his study, the uplift capacity, Q_u was a function of the foundation weight, W , pile tip resistance, Q_{tu} , pile side resistance, Q_{su} , length of the pile, D , and the shearing resistance along a general shear surface as shown in Figure 22.

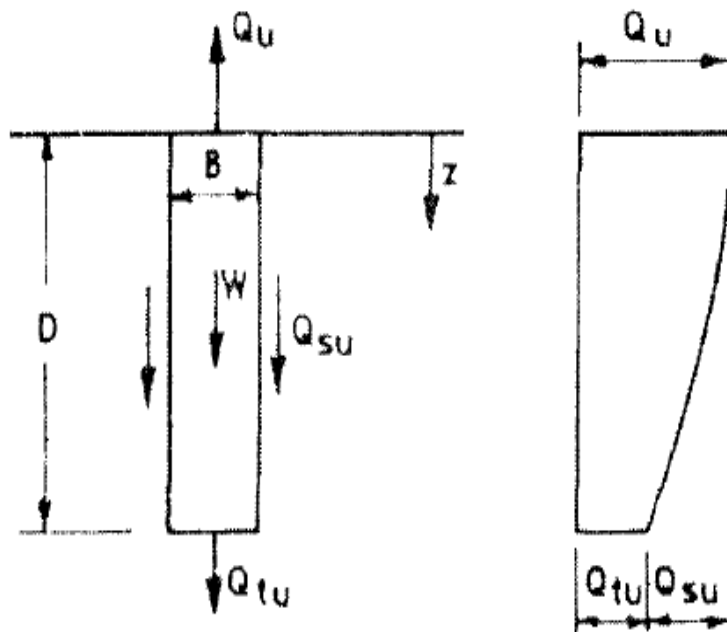


Figure 22 Uplift capacity function and the failure pattern by Kulhawy

Following these essential researches on the pile foundations, several experimental models have been developed to have an understanding of the pile-soil interaction during loading. These include the effects of repeated loading on the drained uplift capacity of the piles in granular

soils (Kulhawy, 1985), so as to examine the influence of the soil density and the pile diameter on the mechanism of the drilled shaft resistance, a study on the effects of straight piles and the piles with enlarged bases and roughness variation on the uplift capacity (Turner and Kulhawy, 1990), and a study on the reaction of single piles embedded in layered sand under inclined pulling loads. The most recent researches have involved the development of scaled physical models (Patra and Pise, 2001), to study the responses of pile groups under uplift loads and an analytical method to predict the uplift capacity of the pile under study and, model tests on tubular steel tubes to analyze the effects of compressive load on the uplift capacity (Das and Pise, 2003).

5.2 ANALYTICAL APPROACHES, MATERIALS AND METHODS

This study on the pull-out capacity engages two methods of determining the ultimate axial/pull-out capacity which include:

- Full-scale experimental approach
- Numerical modelling approach
- Parametric study using FLAC2D

5.2.1 Full-scale experimental approach

The full-scale experimental set up involved the installation of composite single piles in two cities namely Matsusaka and Kasugai city which had silty soils and clayey soils respectively. Once the foundation was fully cured it was subjected to pullout test which involved the application of a pulling load in the *y direction* (perpendicular to the ground surface with pulley restrainers to minimize the lateral movements in the *x direction*). All the tests were carried out in accordance to the Japanese Geotechnical Society (JGS), 2014. Monitoring was done using the Linear Variable Displacement Transducers (LVDT) and readings recorded automatically with respect to loading variations. Experimental setup is as shown the Figure 23, 24 and 25 below.

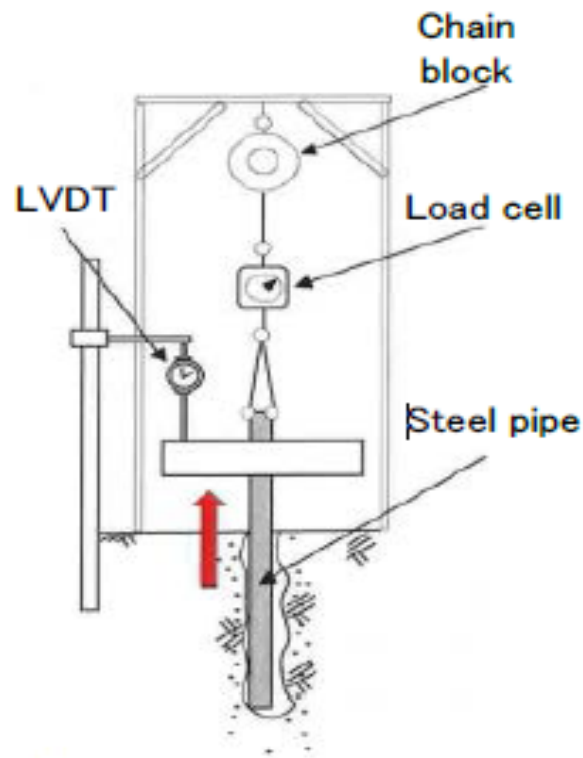


Figure 23 Full-scale experimental set up



Figure 24 LVDT for vertical displacement



Figure 25 Axial loading scale

5.2.2 Numerical modelling approach

The approach engages the use of numerical design of the composite single pile element and the soil/ground simulation to establish the foundation reaction concerning the uplift or pull-out

loading. The numerical model uses the finite difference method embedded into the FLAC2D software to assess and compute the variation of the different input parameters, to obtain the desired output on pile performance. The reckoning is achieved mainly by the simulation of the stresses and the strains developed in the model grid during deformation by the applied corresponding velocities of the uplift load. A numerical approach is a vital tool in the close examination of soil behaviour under complex ground conditions. Most of the engineering problems associated with axial loading are always based on the axisymmetric point load solutions but FLAC2D is adapted to the plane-strain mode which is used to simulate equally spaced single piles. To obtain these critical results a finite element analysis mesh to replicate the real problem (Lysmer, 1970) is necessary as shown in Figure 26. The final model has been chosen so that the overall velocity field is distributed within the domain and no boundary effect is presented. In general, the model size has to be greater than 2 times the pile length (i.e. 2.8 m radius from pile element axis by 2.8 m depth).

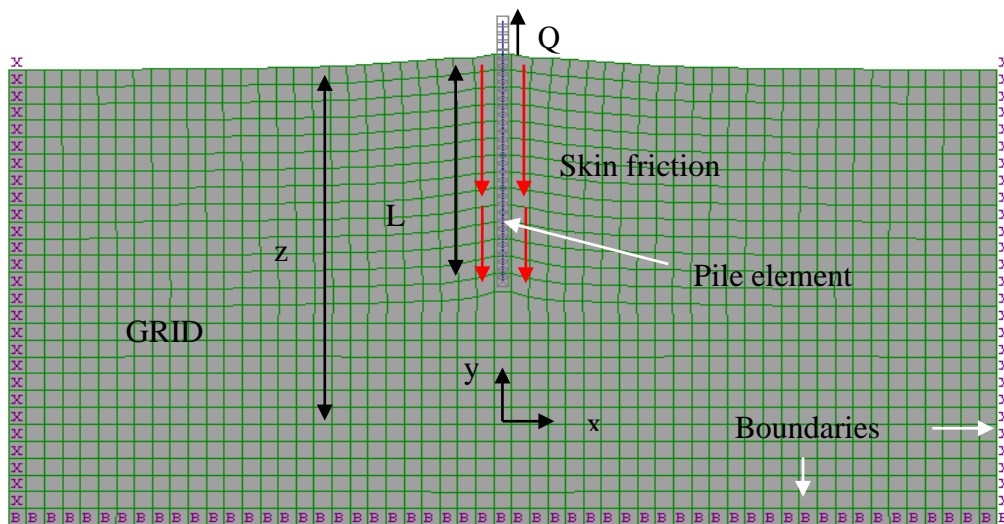


Figure 26 Pull-out numerical simulation mesh for FLAC2D

This mesh places all the parameters to be input into the FLAC2D domain considering the pile and the soil interaction and the desired output. The input parameters which include the soil properties and the pile element properties are as shown in Table 5 and Table 6 respectively.

Table 5 Soil properties

Item	Type of soil			Units
	Silty soil	Clayey soil	Sandy soil	
Soil Density	1750	1750	2100	kg/m ³
Soil Cohesion	25e3	11e3	40e3	N/m ²
Soil Friction	30	0	22	Degree
Soil Dilatancy	15	0	15	Degree
Soil Tension	50e3	50e3	60e3	N/m ²
Young's Modulus	21e6	50e6	65e6	N/m ²
Poisons Ratio	0.3	0.3	0.35	Ratio

Table 6 Pile element properties

Item	Value	Units
Pile length below the ground surface	1.4	m
Pile diameter	0.26	m
Pile Young's modulus	8e10	N/m ²
Stiffness of shear coupling spring (cs sstiff)	1.3e11	N/m ²
Cohesive strength of the shear coupling spring (cs scoh)	5e5	N/m
Frictional resistance of the shear coupling spring (cs sfric)	20	Degree
Stiffness of normal coupling spring (cs nstiff)	1.3e8	N/m ²
Cohesive strength of the normal coupling spring (cs ncoh)	5e3	N/m
Frictional resistance of the normal coupling spring (cs nfric)	10	Degree

FLAC2D software then employs the Finite difference codes to provide a step by step integration of the input parameters for time and the set loading velocity. The products of the combination are summed up in the plane-strain mode which places the pile as a wall extending out of the plane of the cross-section (grid). FLAC2D, therefore, calculates the vertical stresses which area representative of the skin friction along the pile and the grid (soil) interface. These stress calculations are computed by the FISH function embedded in FLAC2D within all the

zonal centroids in the model grid which is a representative of the soil component. Considering the forces represented in Figure 26, the calculated vertical stresses, σ_{yy} in the axial direction, can be described theoretically as shown in Equation 38 for $y_y \geq z-L$ and Equation 39 for $y_y \leq z-L$. Where y_y is the vertical displacement, z is the depth of the overburden soil layer, L is the length of the pile and x is the horizontal displacement.

$$\sigma_{yy} = Q/\pi L \left(\ln \frac{x^2}{(z-y)^2+x^2} + \frac{(z-y)^2}{(z-y)^2+x^2} \right) \quad (38)$$

$$\sigma_{yy} = Q/\pi L \left(\ln \frac{(z-L-y)^2+x^2}{(z-y)^2+x^2} + \frac{x^2}{(z-L-y)^2+x^2} + \frac{x^2}{(z-y)^2+x^2} \right) \quad (39)$$

Once all the input parameters are coded into the program, numerical stepping is therefore initiated, and the results obtained analyzed and plotted to capture the relationship between the axial/pull-out load and the vertical displacement. Also, the deformation of the grid/soil, the stress and strain concentrations and directions on the grid, bending moments on the pile and shear plane of failure as discussed in Chapter 6.

CHAPTER 6

RESULTS AND DISCUSSION

6.0 RESULTS AND DISCUSSION

6.1 LATERAL LOADING

A comprehensive study on foundation-soil interaction is presented using the following three approaches: (1) a full-scale experiment approach for the experimental data; (2) an analytical approach for the calculated data and (3) a numerical modelling approach.

6.1.1 Full-scale experiment approach on lateral loading

Two full-scale testing experiments were conducted in Matsusaka city and Kasugai city in Japan which have silty soils and clayey soils respectively. This region is suitable for the current research since it experiences strong wind, especially during typhoons and the lands are saturated due to the frequent rainfall. The experimental setup includes a meter gauge for monitoring the increment in the subjected horizontal load at the pile top and a linear variable displacement transducer to check the pile head deflection due to the lateral pressure on the composite pile foundation structure as shown in Figure 27.



Figure 27 Full-scale experimental setup

A plot of the pile head deflection against the horizontal/lateral load is as shown in Figure 28 where a curvilinear relationship having two phases of load-deflection ties are evident. The first

phase is a slow and linear deflection phase from 0mm to 13mm as the load increases rapidly from 3kN to 13kN. The second phase shows a direct linear relationship of rapid deflection from 13mm to 26 mm with a 1kN rise in loading up to the failure point of 14kN horizontal/lateral loading for Matsusaka test site. The output of the Kasugai test site also shows a curvilinear relationship with the composite single pile attaining maximum loads of 8kN at deflections of 13mm.

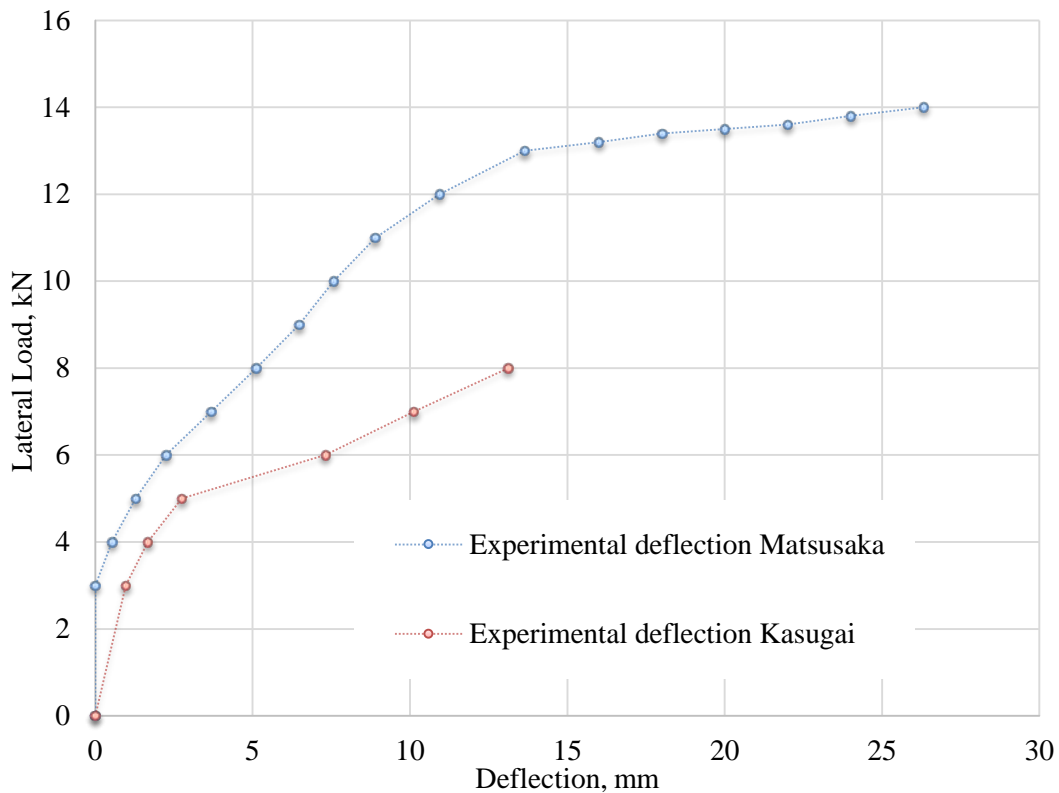


Figure 28 Full-scale experimental data plot for Matsusaka city

6.1.2 Analytical approach on lateral loading

The formulation in Reese and Matlock (1971) is issued to analyze the lateral displacement considering unit modulus of subgrade reaction and foundation material stiffness, as shown in equation (1). During lateral loading, the intensity of the horizontal load is also dependent on the foundation depth, with more deflection experienced at the pile tip at the ground surface than at the base of the foundation. To obtain the foundation equilibrium status, the soil offers

a reaction force on the pile foundation, and this ground reaction force acts in the opposite direction to the direction of the applied horizontal force.

The load-deflection relationship from this logical point of view depicts a curvilinear curve as shown in Figure 29.

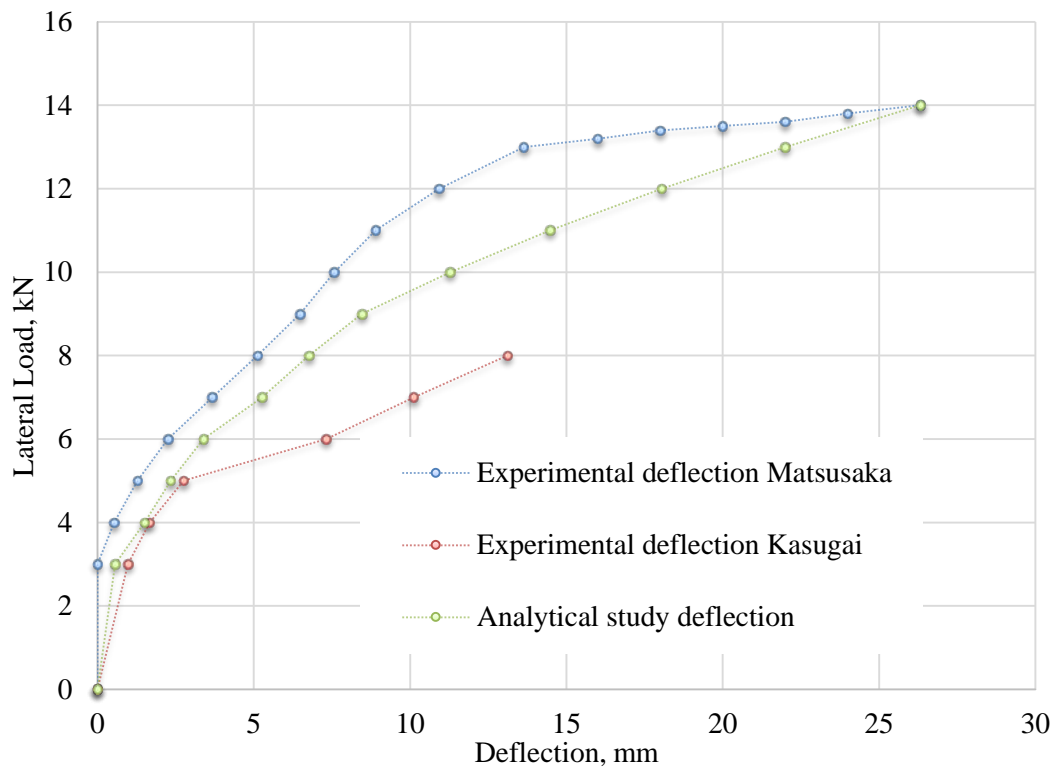


Figure 29 Analytical data plot for Matsusaka city

As seen from the graph, the deflection increased as the loading are increased until the bearing capacity is attained. This gave a value of 14kN with a maximum deflection of 26mm on the pile head. The load-deflection relationship exhibited a similar trend to the experimental one with minimal deviations.

6.1.3 Numerical simulation on lateral loading

The type of the structural element involved in the simulation is known as a pile element with 32 segments. A pile element is a two-dimensional element that transfers normal, shear forces and bending moments to the model grid as depicted in the beam and cable elements. The shear forces and normal forces subjected to the pile element acts in the parallel direction and

perpendicular direction respectively. The pile elements are designed to represent the response of foundation piles. Therefore, the factors to consider include the cross-sectional area of the pile, $A(0.053m^2)$, the second moment of area also known as the moment of inertia, $I(1.4E-5m^4)$, density of the pile material, $\rho (8,050 kg/m^3)$, elastic modulus of the pile, $E (4E8Nm^2)$, frictional resistance of the shear coupling spring, $cs_sfric (20^\circ)$, the cohesive strength of the shear coupling spring, $cs_scoh (30E3 N/m^2)$. The spacing between the piles which is always considered to be in a continuous direction in the out-of-plane direction. In addition to these, the stiffness of normal coupling spring, $cs_nstiff (1.3E8 N/m^2)$ and stiffness of shear coupling spring, $cs_sstiff (1.3E11 N/m^2)$ which are functions of the force applied, pile length and displacement is also crucial as they give an apparent simulation of the behaviour of the interface during lateral loading.

Similarly, soil parameters (silty soil) must also be input as this will be the framework of the grid. The soil parameters include, soil density $\rho (1750 kg/m^3)$, soil cohesion $c (50E3 N/m^2)$, soil friction $\phi (30^\circ)$, soil dilatancy (15°) , soil tension $(50E3 N/m^2)$, soil young's modulus $E (21E6Nm^2)$ and poisons ratio $\mu (0.3)$

The interaction between the pile and the soil grid is through shear and normal coupling springs. It is through the coupling springs that the force transfer occurs between the pile elements and the soil grid. The model consists of a fixed grid point with pinned boundary condition applied along the bottom of the model and roller boundary conditions employed on both sides with a prescribed displacement value set at 20mm. Figure 30 shows the mesh, boundary conditions, and the pile element displacement pattern during lateral loading.

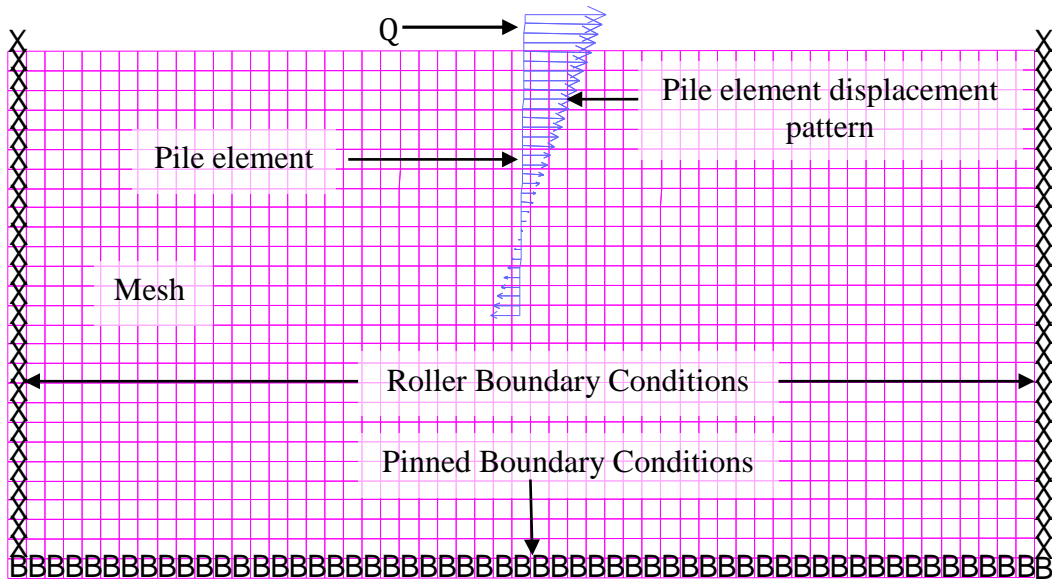


Figure 30 Mesh, boundary condition, and pile element displacement pattern

The pile element interaction with the surrounding soil can be seen by plotting the soil movement and pile displacement patterns using the FLAC2D model as shown in Figure 31.

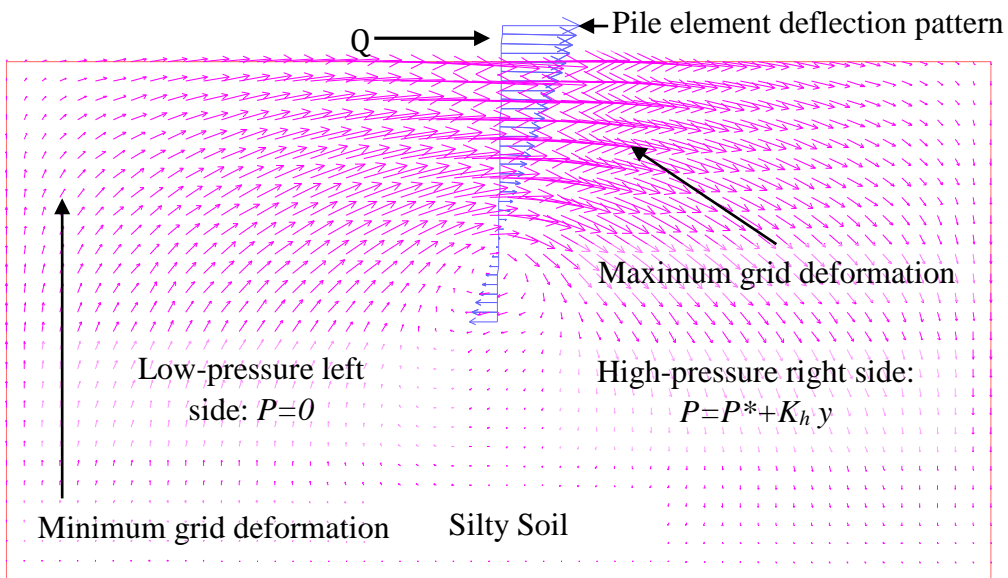


Figure 31 Soil movement and pile displacement pattern

The output plot shows large displacements at the surface of the ground and decreases with depth. Movements are dependent on the cohesive strength of the interface and the stress-dependent frictional resistance along the soil-pile interface.

During normal loading of the pile, the normal behaviour of the pile and the grid/soil interface corresponds to a spring with a limiting force that largely depends on the direction of movement of the composite pile head. Considering the course of the horizontal force, in this case from left to right, the mean stress increases towards the left up to the rotational centre depth of approximately $\frac{2}{3}L$. The direction changes as a result of the change in the direction of soil movement as the pile rotate. In this case, it is a function of the composite material stiffness factor. The mean stress increment is shown qualitatively in Figure 32.

From the load-deflection data collected from the FLAC2D model, the plot shows a curvilinear relationship as the lateral load is increased from 0kN to 15kN at a prescribed $xvel = 2e-7$ in 100000 steps. The pile experiences minimal displacement of 0mm to 10 mm as the loading velocity progressed from 0kN to 15 kN. This gives a deflection of up to 30mm with structural failure realised at a load of 15 kN as shown in Figure 33.

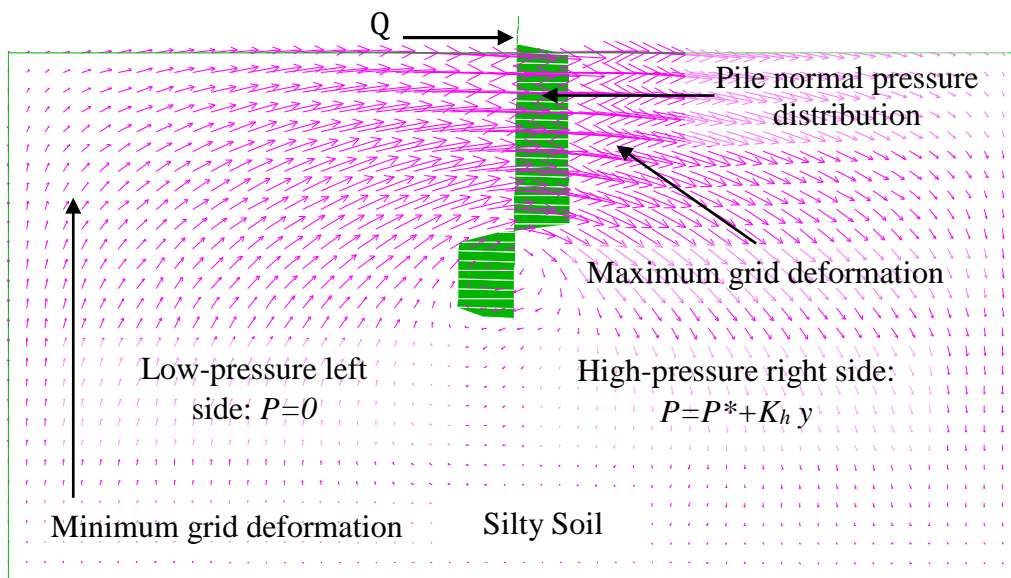


Figure 32 Soil movement and pile normal pressure distribution

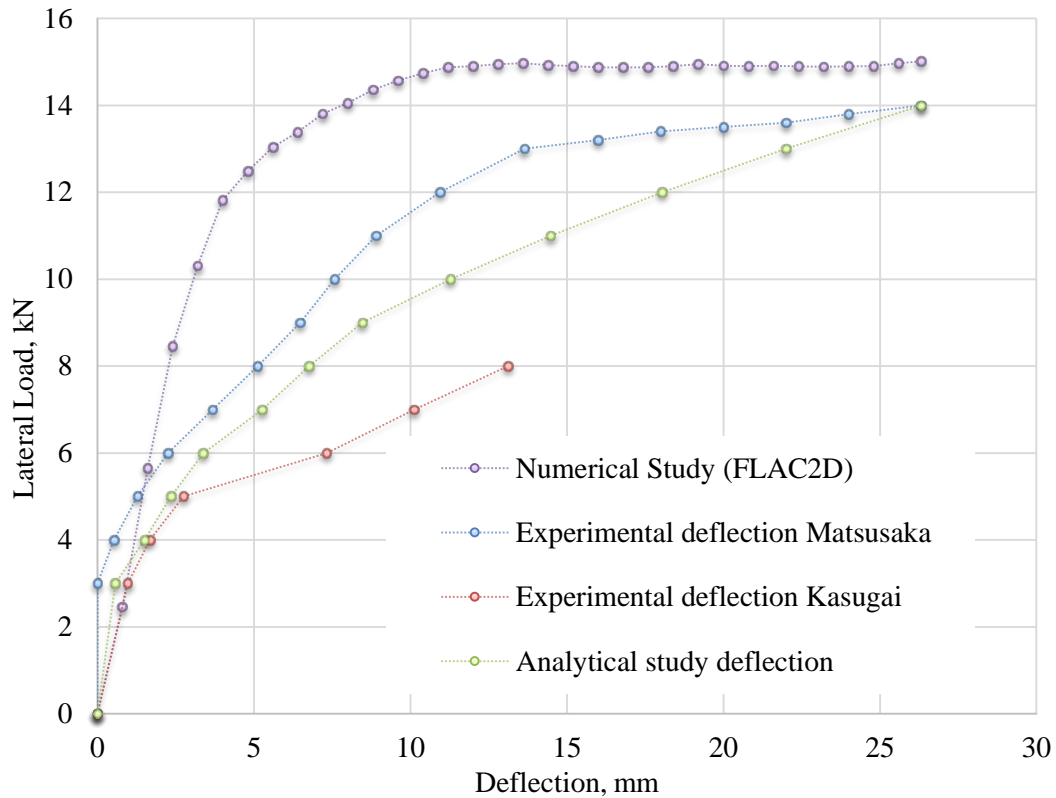


Figure 33 Load-deflection curve at Matsusaka testing site

Normal coupling enables us to model load reversal in soil spring cases and also the formation of a gap between the pile and the grid. In this case, for the rigid pile subjected to lateral loading, there tended to be the formation of a gap and upward movement of soil on the gap side. This upward movement is due to the rotational centre depth at $2/3 L$ of the pile during loading. This upward movement is a discovery for single piles from numerical modelling. Without numerical investigation, it is not possible to detect such ground responses. Gap formation is as shown in Figure 34.

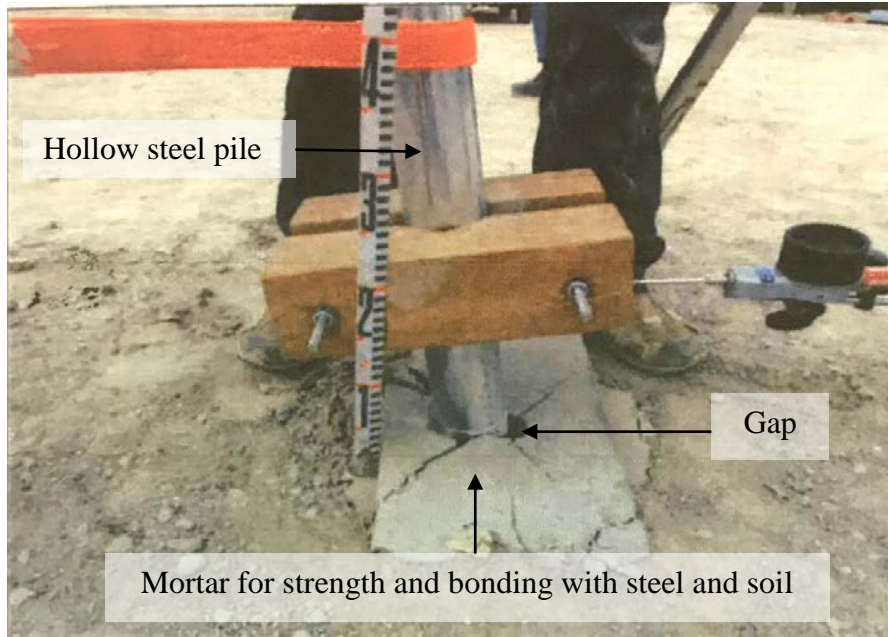


Figure 34 The gap

Figure 35 is a representation of the contour zones for the effective stress distributions on the grid/soil medium. As depicted by the colour coding, the red contours shows the areas with the maximum stresses during the application of the lateral load. The right part of the pile element experiences maximum stresses (20kN) due to the compressive nature the pile tends to offer when being pushed against the grid from left to right. At the lower part of the pile just below the rotational center depth the stresses shift to the left side of the pile due to the switched rigid pile movement from right to left. The blue region experiences low stresses (10kN) as the soil tends to separate from the pile during the formation of Gap.

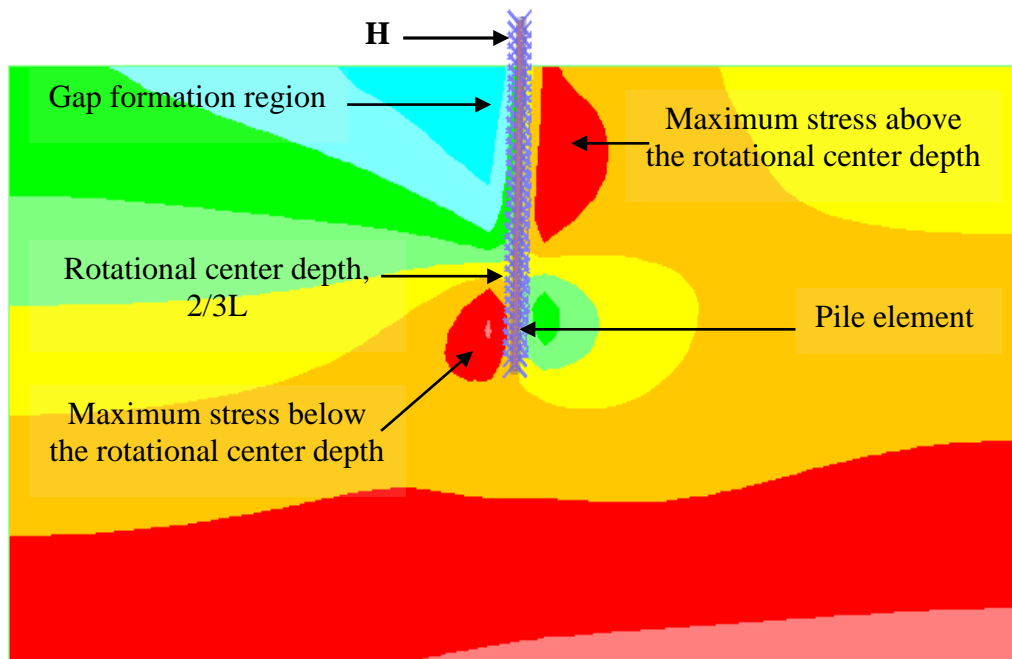


Figure 35 Contour zone for effective stress distribution on grid

During lateral loading, shear strain is experienced at the interface between the grid and the pile. Figure 36 shows the maximum shear strain increment around the pile element. This is the measure of the ratio of the rate of deformation of the grid to the original shape before the application of the lateral load. Upon load application to the pile element, the numerical simulation output shows that maximum shear strain is experienced at rotational center depth where much of the separation and pile rotation occurs. This strain reduces gradually away from the pile center to the outer zones in the grid. The maximum shear strain recorded at the rotational center depth is 0.6mm.

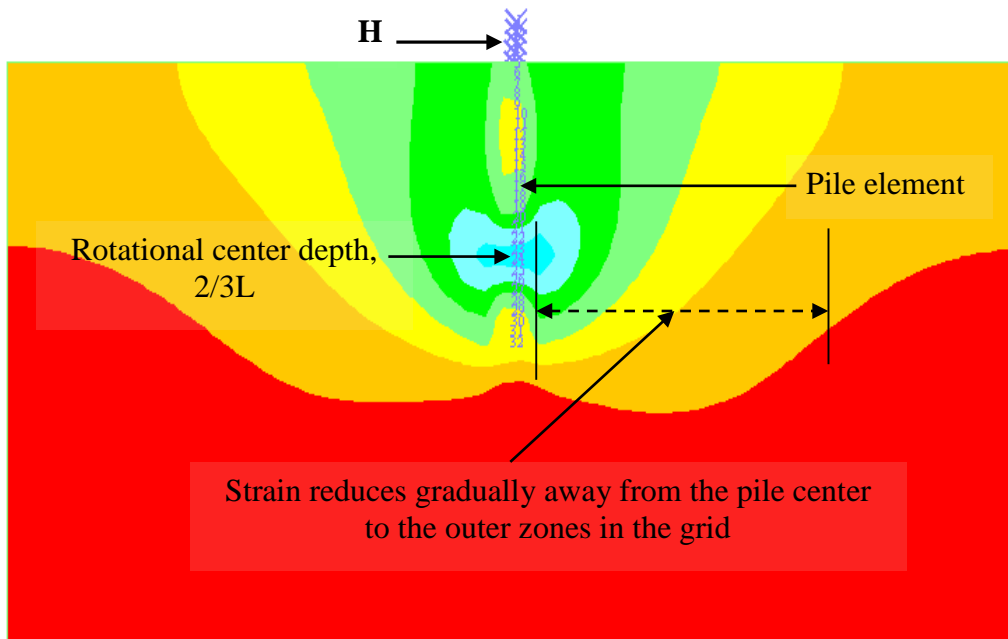


Figure 36 Maximum shear strain increment around the pile element

Figure 36 shows the areas that experience the maximum shear strain increment along the pile, but this does not conclude that this is the only area experiencing the strain. To further understand the region that experiences the shear strains we can have a clear representation by evaluating the shear strain increment rate on the grid.

Figure 37 depicts deformations all through the pile length with upper zones also having maximum deformations and maximum deformations also experienced at the pile bottom. The strains at the bottom are due to the separation that occurs as the pile bottom shifts from right to left when rotating. The maximum shear strain rate recorded is $2.00E-6$ mm at intervals of $2.5E-10$ s

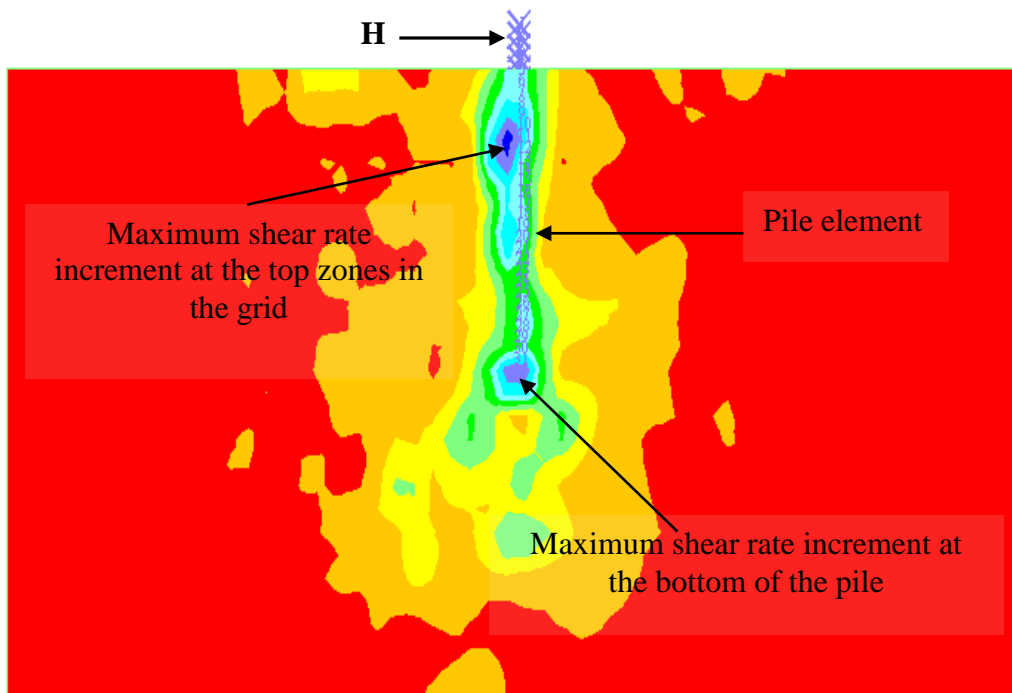


Figure 37 Maximum shear strain rate on the grid.

6.2 PARAMETRIC STUDY ON LATERAL LOADING

6.2.1 Effects different soils: silty soil and clay soils

The type of soil is one of the main parameters to be put into consideration for any construction procedure to be practiced. The cohesive nature of different soils dictates the bearing capacity of the foundation. In addition to bearing capacity, the soil type also dictates the modulus of subgrade reaction, K_s which is a ratio of contact pressure intensity, P and the soil settlement, y . Due to the fact that clayey soil has a higher modulus of subgrade reaction, $80,000 \text{ kN/m}^3$, it attains a higher ultimate load of 15 kN at lower pile head displacement of 4 mm as compare to the silty soils ($K_s=48,000 \text{ kN/m}^3$) that achieves the final pressure at more massive movements of 10 mm as shown in Fig. 38.

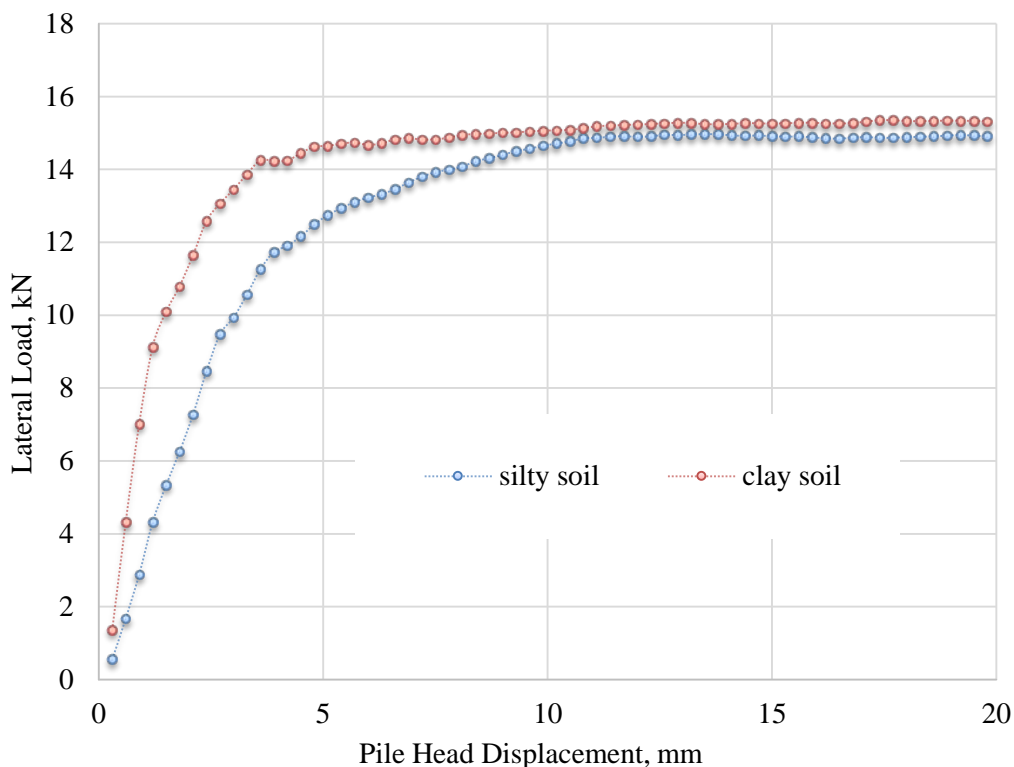


Figure 38 Effects Different Soils: Silty soil and clay soils

A closer examination of the pile element and the soil displacement patterns depicts the more vertical movement of the ground in the clay soil than in the silty soil. This high-intensity soil movement depends on the standard pressure induced by the pressing nature of the pile element

as well as the modulus of subgrade reaction, K_s and the displacement, y produced at the pile head. The soil movements of FLAC2D output are as shown in Fig. 39 and Fig. 40 for silty soil and clayey soil respectively.

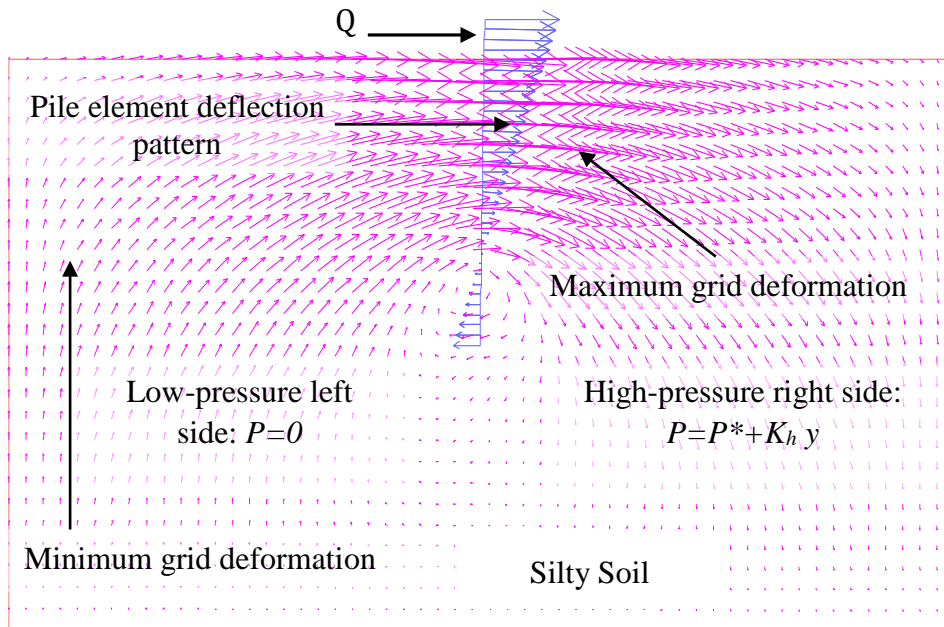


Figure 39 soil-pile displacement patterns for silty soil

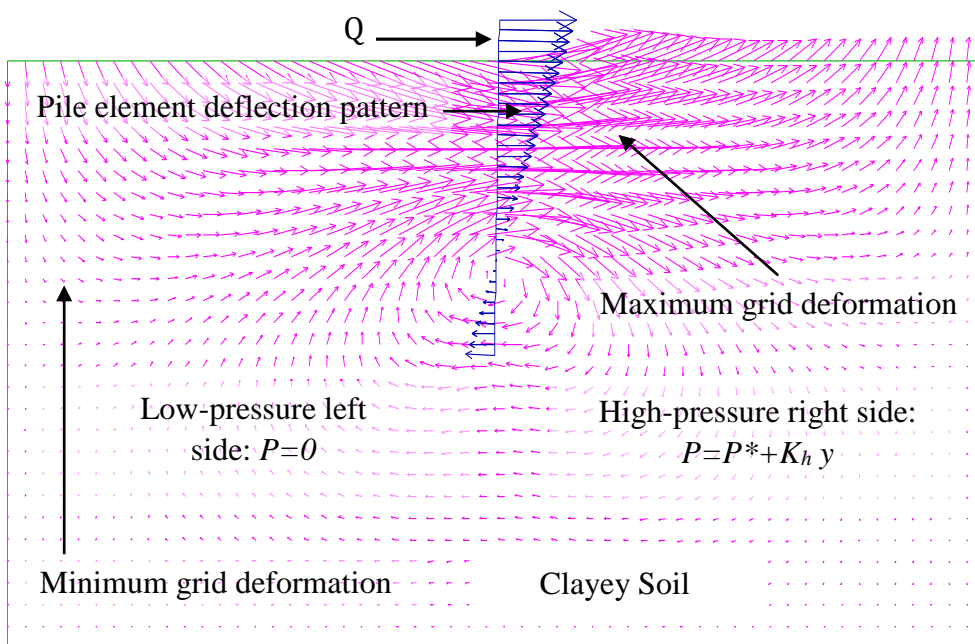


Figure 40 soil-pile displacement patterns for clayey soil

6.2.2 Effects of soil elastic modulus

In this case, it's the elastic modulus of the soil that is studied. The value for the elastic modulus is ranged from $11e6$ to $31e6$ kPa for silty soils and $40e6$ to $60e6$ kPa for the clayey soils. The other conditions are held constant as per the design parameters (*Pile length= 1.4m, pile diameter=0.13m, the rate of loading force constant*). The p-y curves generated from FLAC2D at the design depth shows that the elastic modulus, E , has minimal effects in the silty soils whereas in the clay soils deviations in the ultimate load are noticed at displacements of 5 mm as shown in Figure 41 and 42 respectively. This E variation is a clear indication that the cohesiveness of the soils should be highly considered in the clayey soils if the design bearing capacity is to be achieved.

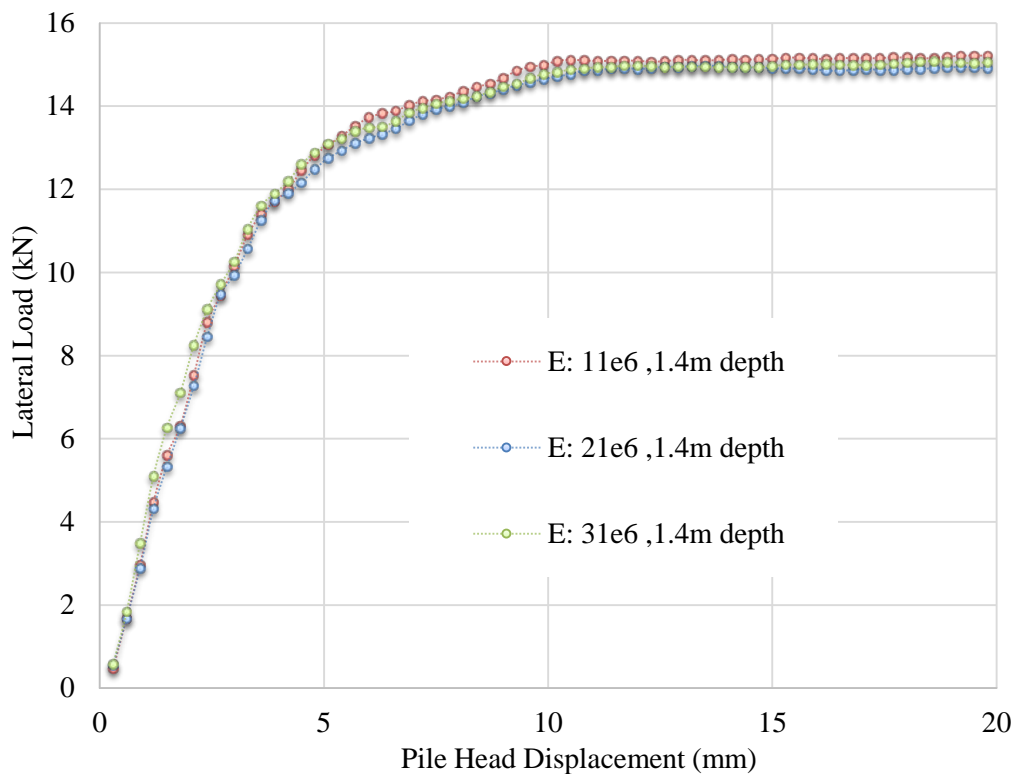


Fig. 41 Effects of elastic modulus for silty soil

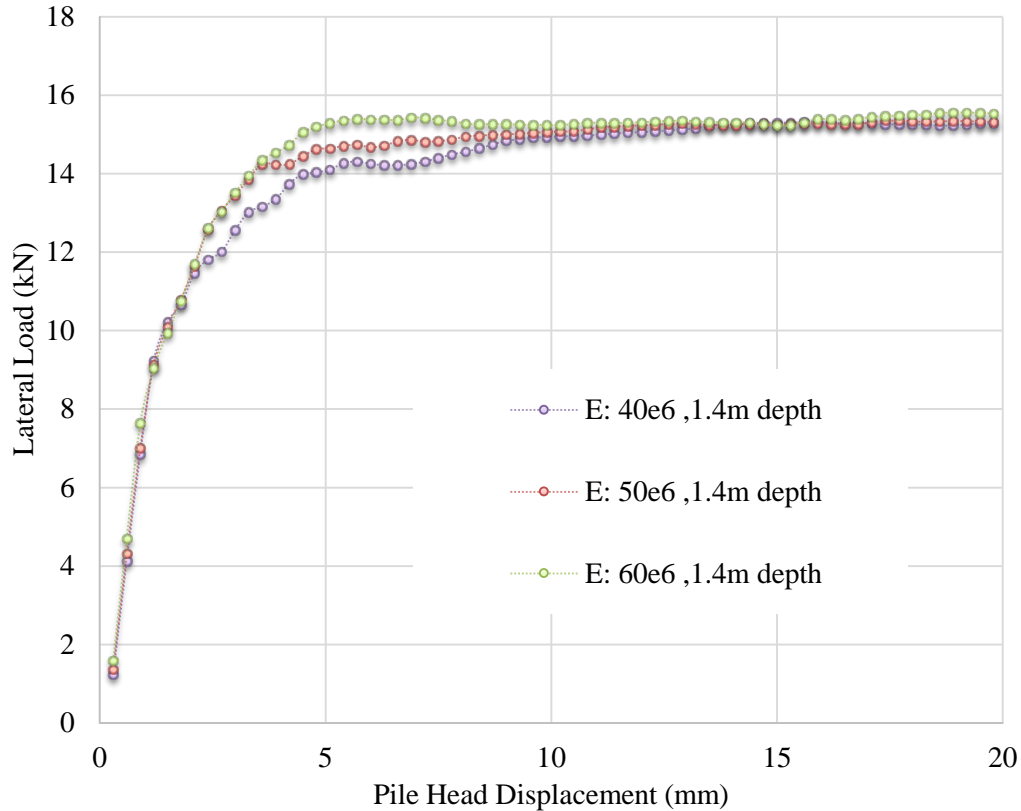


Fig. 42 Effects of elastic modulus for clayey soil

6.2.3 Effects of loading velocity with depth on ultimate load

Velocity is a time-dependent parameter when incorporated into FLAC2D. It ensures that the deformations on the grid follow the stress/strain law. To achieve the ultimate bearing capacity, the correct loading velocity should be determined as it plays a significant role in the damping of the equations of motion to provide static or quasi-static also known as non-inertial solutions. The non-inertial solutions help in achieving the equilibrium state in a numerically stable way with minimal computation effort in FLAC2D. In this study, the velocity was varied from $1.0e7$ to $2.5e7$ for the single pile foundation depths of $0.7m$, $1.4m$, and $2.8m$. Base on the results, it is evident that increasing the velocity at $0.7m$ and $1.4m$ depth increases the ultimate loading capacity in the silty soil, but in the clayey soil, the ultimate loading capacity reduces once the ultimate load is attained at $2.0e7$. At the pile depth of $2.8m$, increasing the velocity have detrimental effects on the ultimate loading capacity as in both cases (silty and clay soils) there is significant decrease in the ultimate loads as shown in Figures 43, 44, 45and 46.

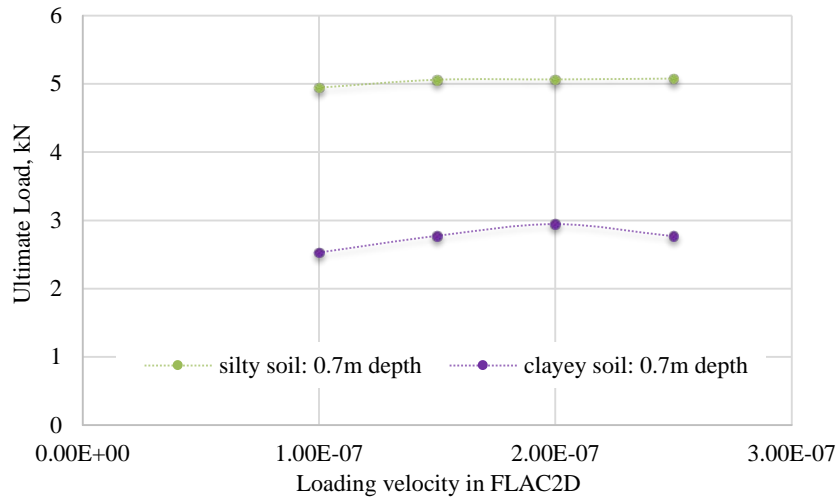


Figure 43 Effects of loading velocity with depth on ultimate load at 0.7m depth

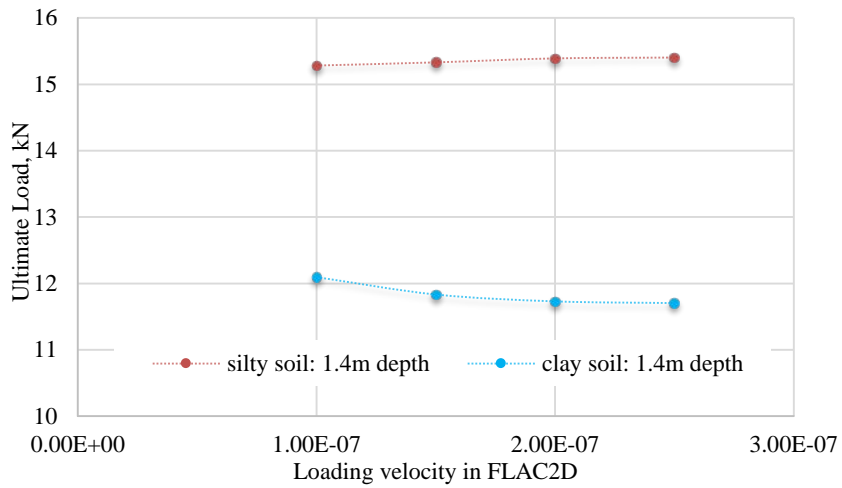


Figure 44 Effects of loading velocity with depth on ultimate load at 1.4m depth

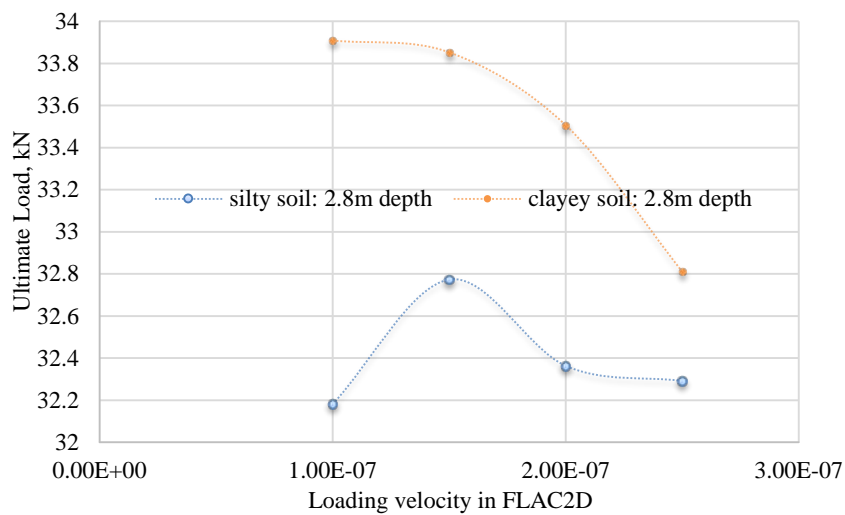


Figure 45 Effects of loading velocity with depth on ultimate load at 2.8m depth

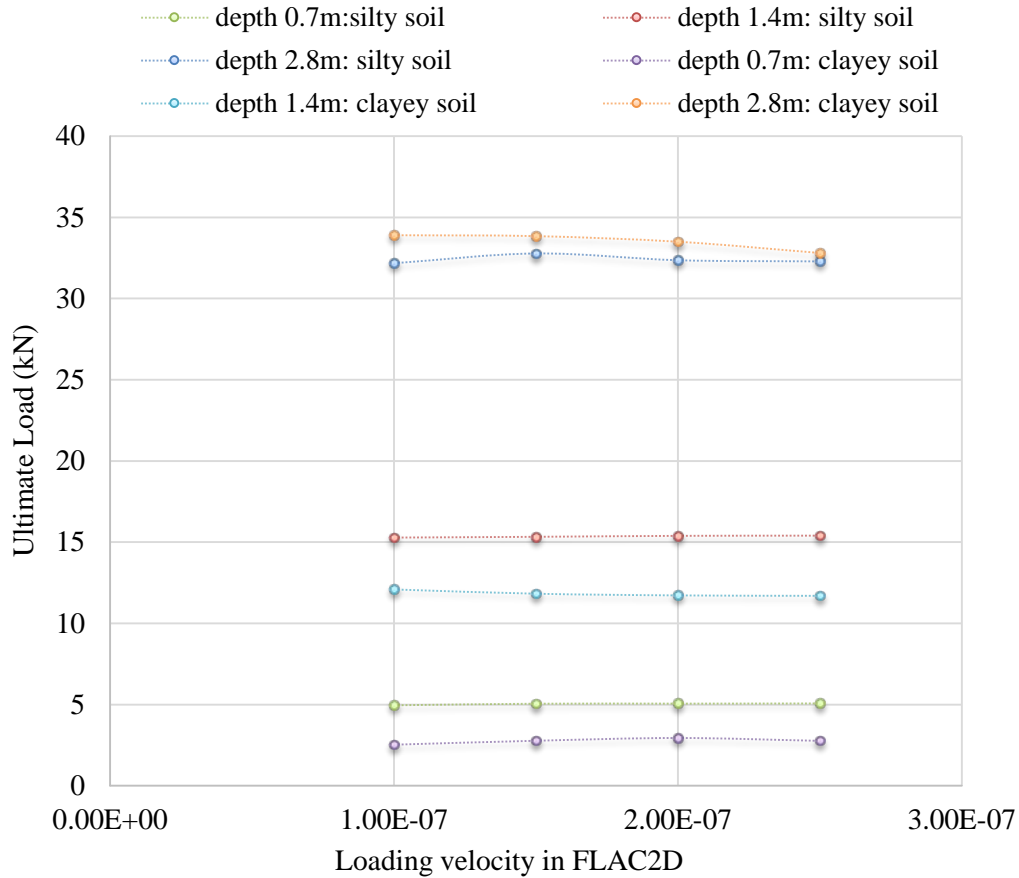


Figure 46 Effects of Loading velocity with depth on ultimate load

6.2.4 Effects of pile stiffness: Stiffness of normal coupling spring

In FLAC2D, the coupling springs are a representative of the interaction between the soil and the pile element under consideration. The normal coupling spring is the medium in which the lateral forces applied at the given velocity transmission, occur to the grid at the prescribed location along the pile element nodes. To obtain a desirable ultimate loading capacity of the pile, then the choice of the pile material should also be put on a check. A numerical description of the action of the normal coupling spring stiffness and the displacements produced during loading is as shown in (8).

$$\frac{F_n}{L} = c s_{\text{stiff}} (u_p^n - u_m^n) \quad (8)$$

Where F_n represents the normal force that develops in the normal coupling spring, c_{Sstiff} is the normal coupling spring stiffness, u_p^n is the displacement of the pile in the axial direction, u_m^n is the displacement of the grid(soil) normal to the axial direction of the pile, and L is the pile element length.

In this study, the stiffness of the normal coupling springs was varied from $1.3e7 \text{ kN/m}^2$ to $1.3e11 \text{ kN/m}^2$ with all other parameters held constant (*Pile length= 1.4m, pile diameter=0.13m, the rate of loading force constant*) for the two types of soils (*silty and clayey soils*). Based on the output, it's seen that an increase in the stiffness of the coupling spring increases the ultimate loading capacity of the pile. Clayey soils depict high ultimate loads up to 16 kN at $1.3e11 \text{ kN/m}^2$ at minimum displacements 7mm as compared to silty soils at 15kN . Figure 47 and Figure 48 shows a plot of the stiffness parameter influence in ultimate loading capacity for silty and clayey soils respectively.

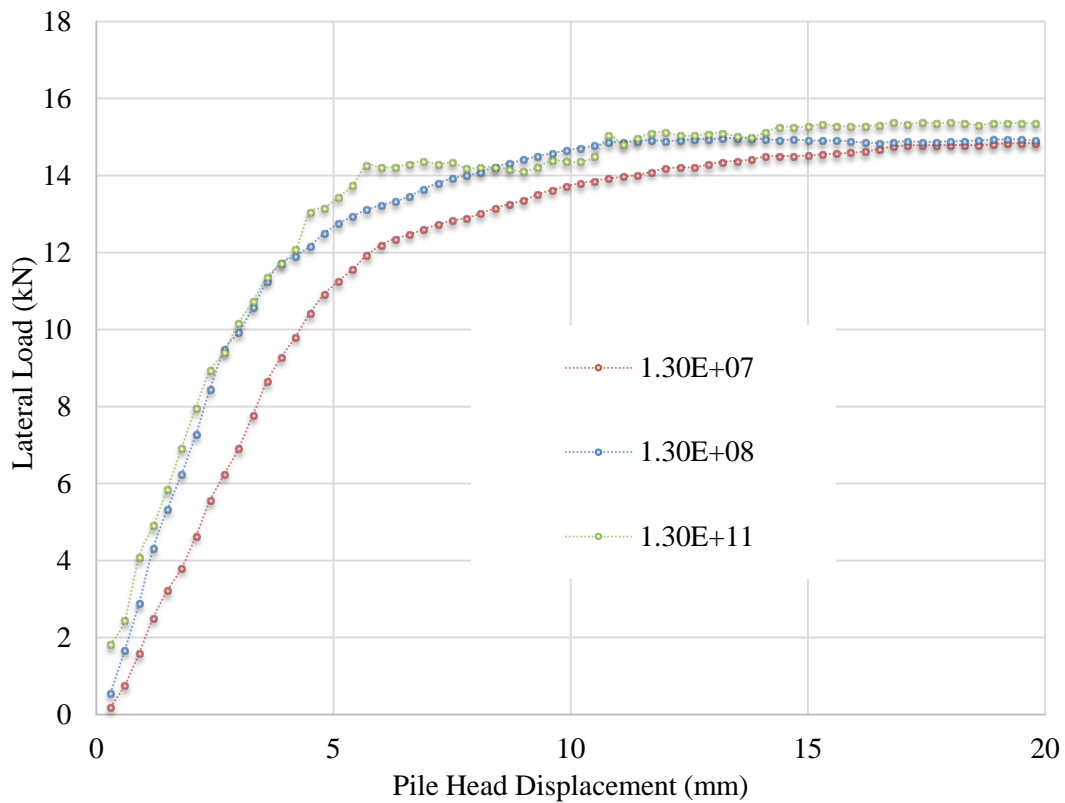


Figure 47 Effects of pile stiffness silty soil

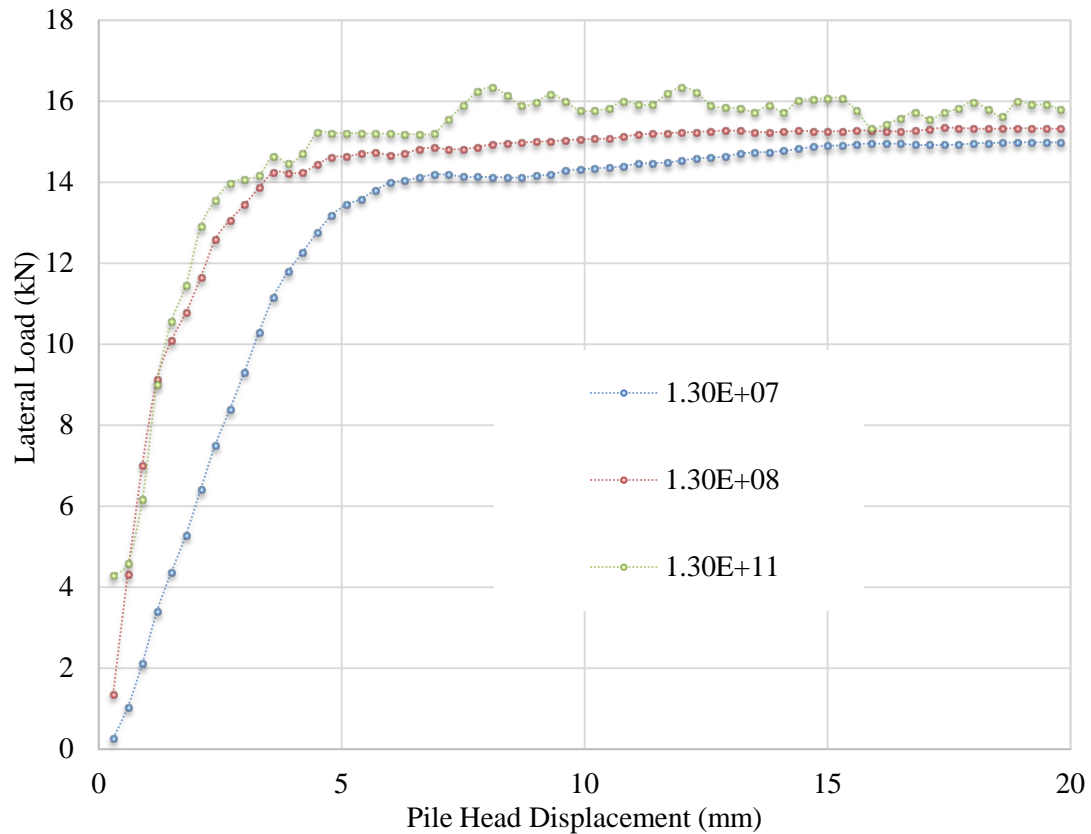


Figure 48 Effects of pile stiffness clayey soil

6.2.5 Effects of eccentricity, e

The height of the pile above the ground is an excellent determinant on the moments above the ground level. The moment equilibrium equation is the product of the lateral force and the eccentricity. When the bending moments tend to increase then the ultimate load that the pile element can withstand reduces considerably. This reduction is due to the rotational effect produced by the lateral pressure above the ground level. When this rotational effect cannot be transmitted to the grid, then the pile tends to fail closer to the ground level at minimal lateral loads. In this study, the eccentricity effect is evaluated at $0.2m$, $0.4m$, $0.6m$ and $0.8m$ for both types of soil and the corresponding ultimate load plotted as shown in Figure 49 and Figure 50 for silty soil and clayey soil respectively. Based on the results, the eccentricity of $0.2m$ produced the highest ultimate loading capacity of $15kN$ in silty soil and $15.8kN$ in clayey soils. An eccentricity of $0.8m$ recorded the minimum value of $8.4kN$ hence this shows that the point

of the load applied to a pile is also a strong determinant of the ultimate strength concerning bearing capacity.

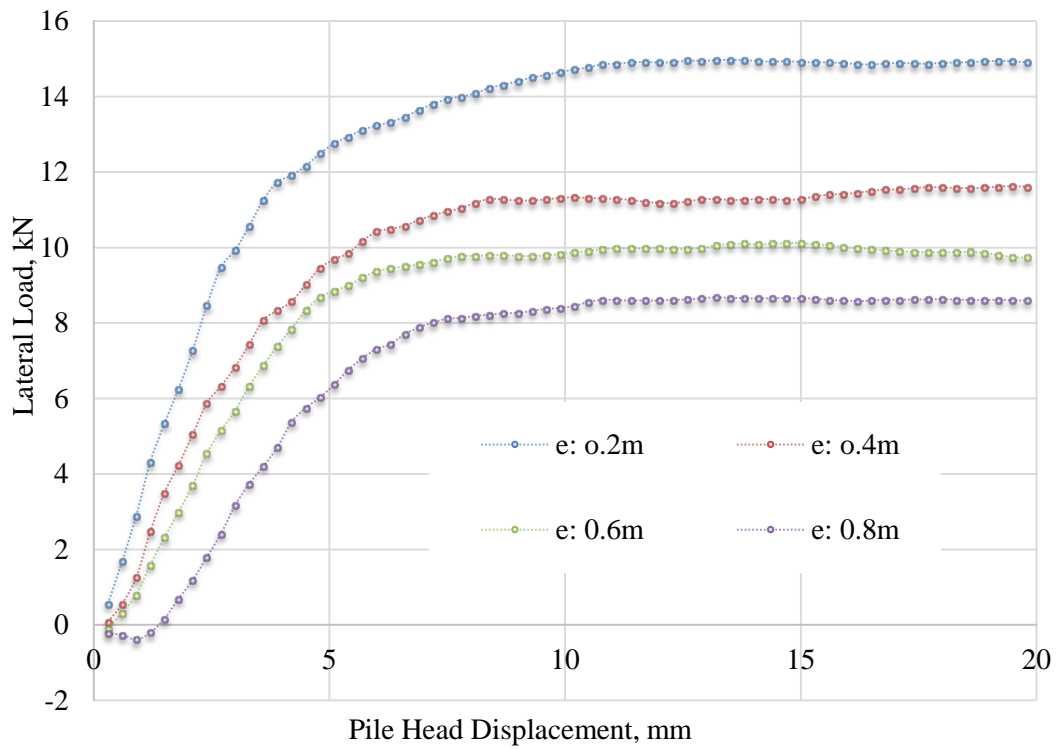


Fig. 49 Effects of pile eccentricity in silty soil

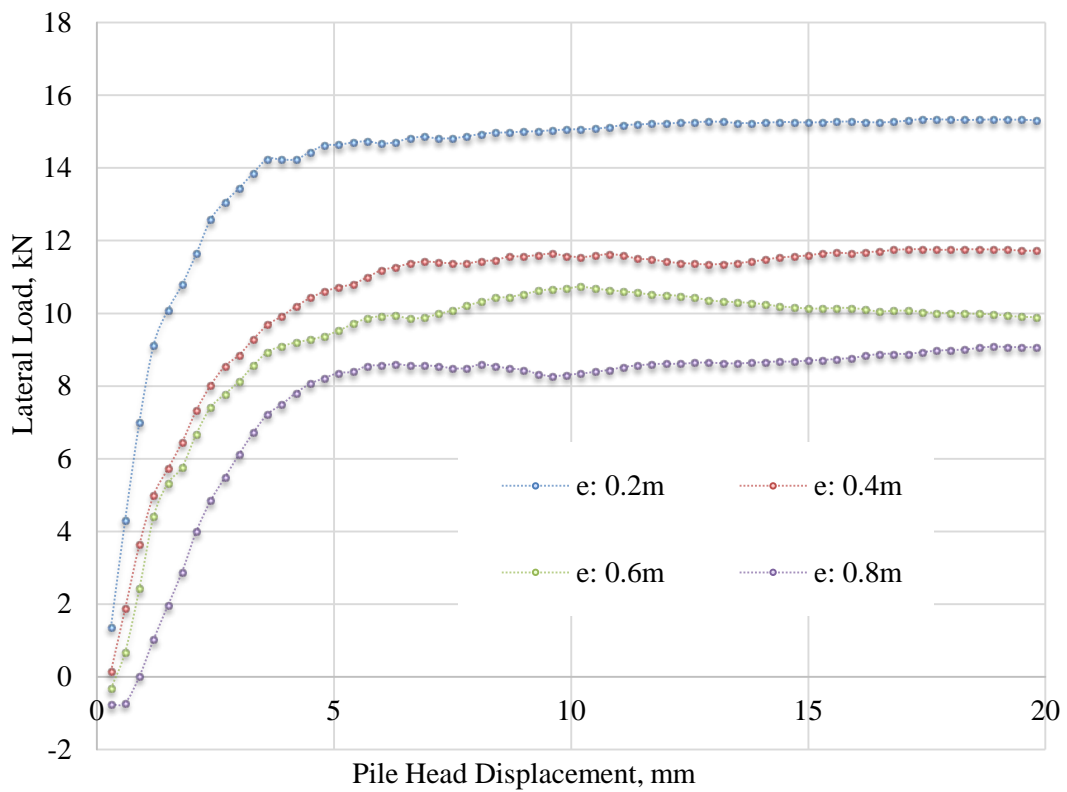


Fig. 50 Effects of pile eccentricity in clayey soil

6.3 PULL-OUT/ AXIAL LOADING

In this section, the (1) Full-scale experimental set up and (2) The finite difference numerical methods are used to analyze the interaction of the pile element and the soil element.

6.3.1 Full-scale experiment approach on Pull-out loading

Figure 51 represents the experimental data plot of axial loading. As discussed in the previous section on the full scale experimental approach, the installation of the composite single piles was done in both Matsusaka and Kasugai cities. The next step was setting up the LVDT and the pulleys to apply the axial loads via a load cell. The results show that the clay soils had more axial capacity to the silty soils. Both output depicted a curvilinear trend with clayey soils in Kasugai test site attaining a maximum axial load of 170kN at pile head displacements of 0.46 mm while the silty soil in Matsusaka test site attaining 150kN at greater pile head displacements of 0.85mm and 0.38mm for Experimental pile 1 and experimental pile 2 respectively.

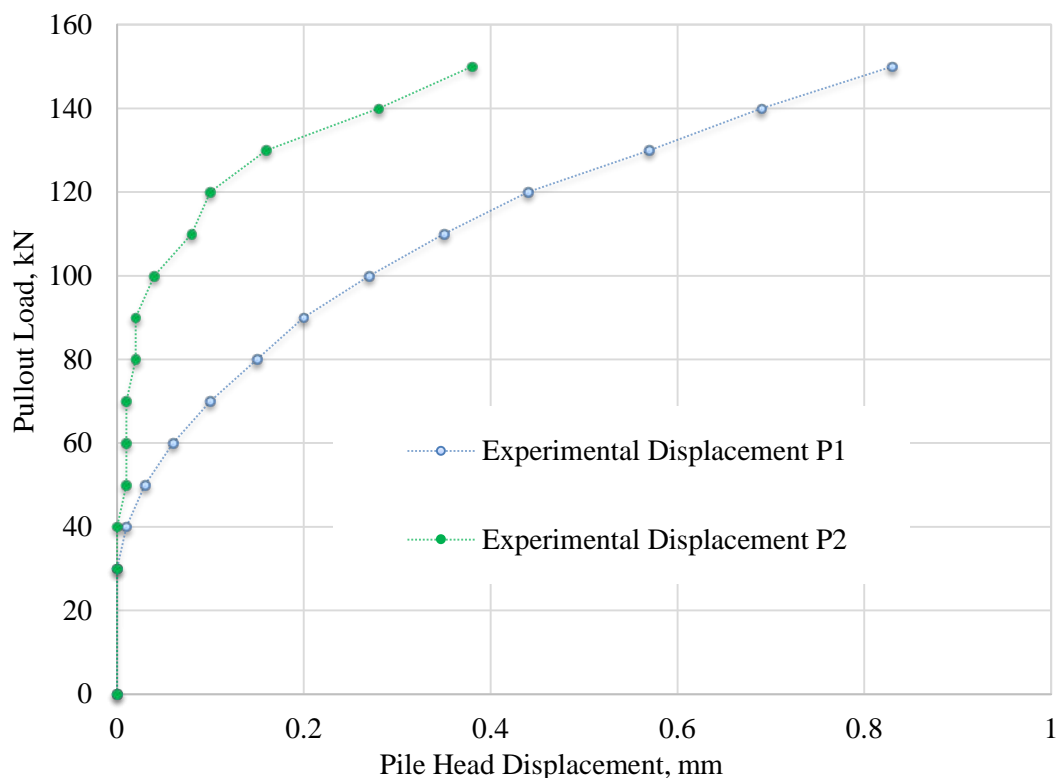


Figure 51 Full-scale experiment plot in Matsusaka Site

A comparison of the experimental plot for the full scale experiment with the Kasugai experimental data is as shown in figure 52. The clay soil in Kasugai City tends to have a higher bearing capacity as compared to the silty soils.

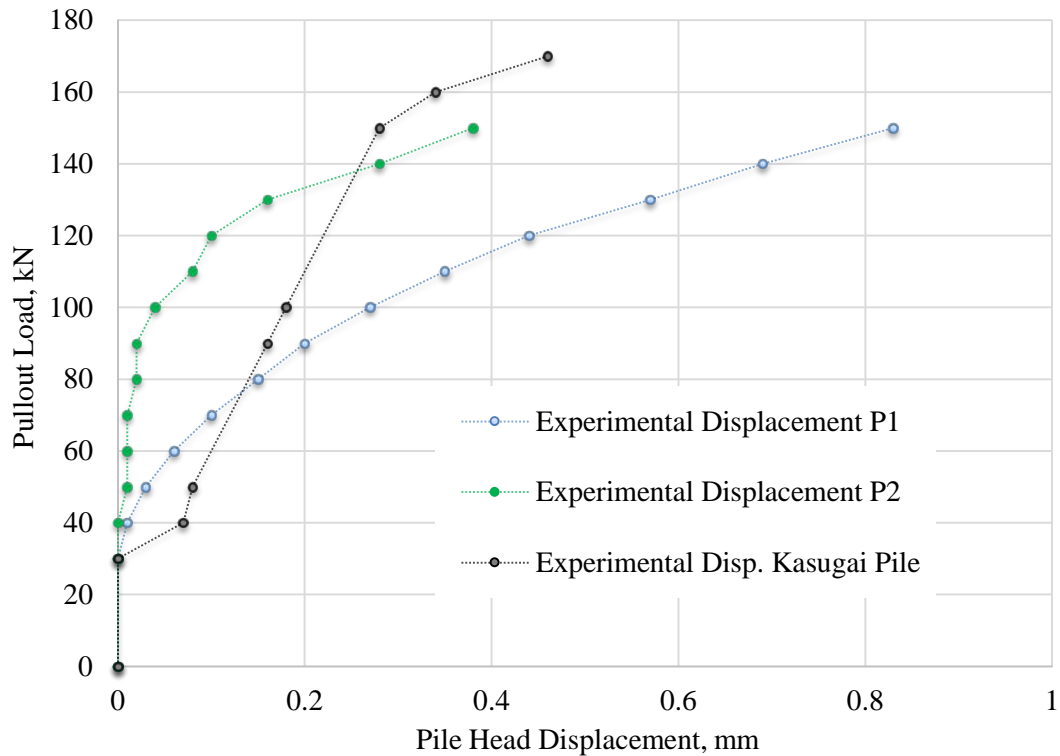


Figure 52 Comparison of the experimental plot for the full-scale experiment in Matsusaka City and Kasugai City

This analysis is done by the presentation of the corresponding pile head displacement curves during axial loading together with a comprehensive parametric study to show a particular design phenomenon. The analysis, therefore, helps engineers in project optimization while maintaining good foundation strength.

6.3.2 Numerical simulation on Pull-out loading

Figure 53 represents the loading characteristics of the pile element under different grid mediums. The pile element is simulated in three types of soils namely, clay soils, silty soils and dense sandy soils. The pile head displacement curves show that sandy soils bear the most robust load handling capacity with maximum axial loads up to 94kN at minimal axial pile head

displacements of 10mm. Silty soils and clay soils attain values of 90kN and 80kN respectively at 10mm axial pile head displacements.

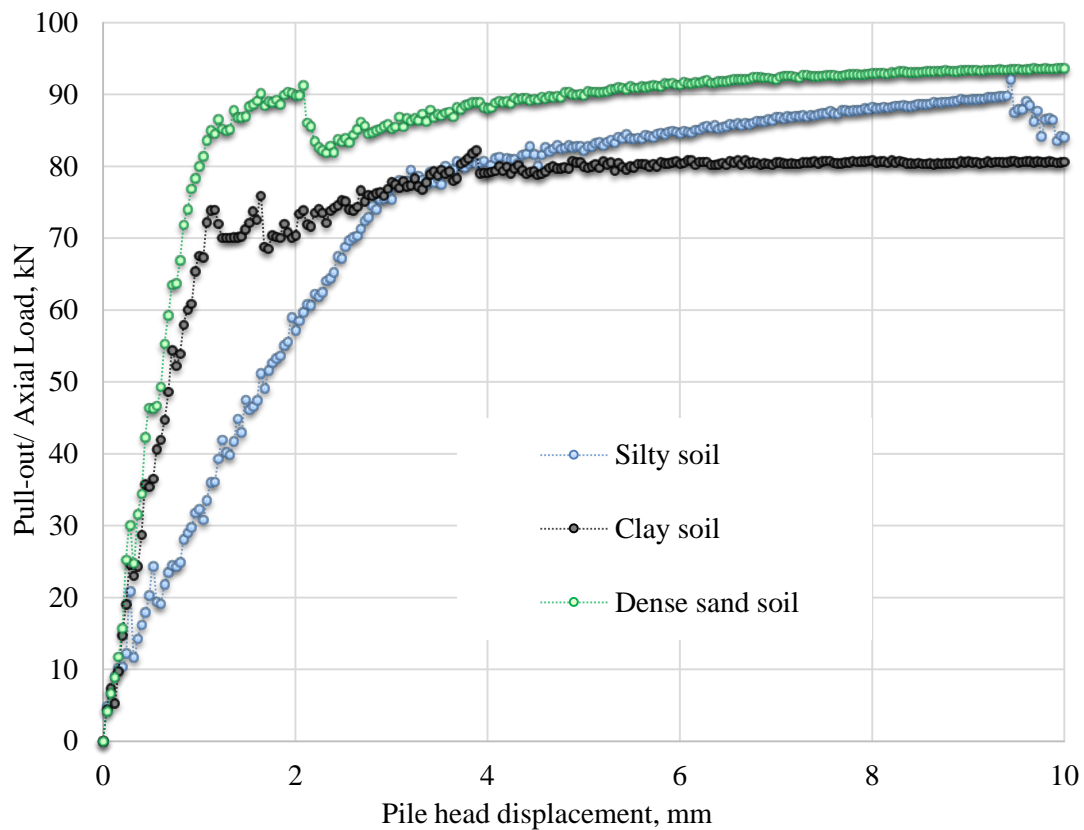


Figure 53 Pile head displacements at different axial loads

FLAC2D provides a visual display of the soil movements during axial loading as shown in Figure 54a, 54b and 54c for clay soils, sandy soils and silty soils respectively. The deformations on the grid show a high upward movement of the overburden soil around the pile and grid interface and this movement reduces as the distance from the center of the pile element increases. This upward movement of the media is due to the vertical stress produced around the pile element due to the skin friction. As the pile tends to move upwards due to the axial load, the skin friction acts in the opposite direction thus creating stresses and strains that lead to the deformation of the zones in the grid. In figure 54a and figure 54b a Gap form at the top of the composite single pile due to the break in contact between the pile element and the grid. This separation between the grid and the pile is not evident in the silty soils as the two components move up as a unit.

As the pile is acted upon by the axial load, maximum strains are also experienced at the bottom of the pile element due to the separation between the pile and the grid together with the vacuum created in the zoned. Effective stress distribution on the grid is also experienced in these regions of maximum grid zones deformations.

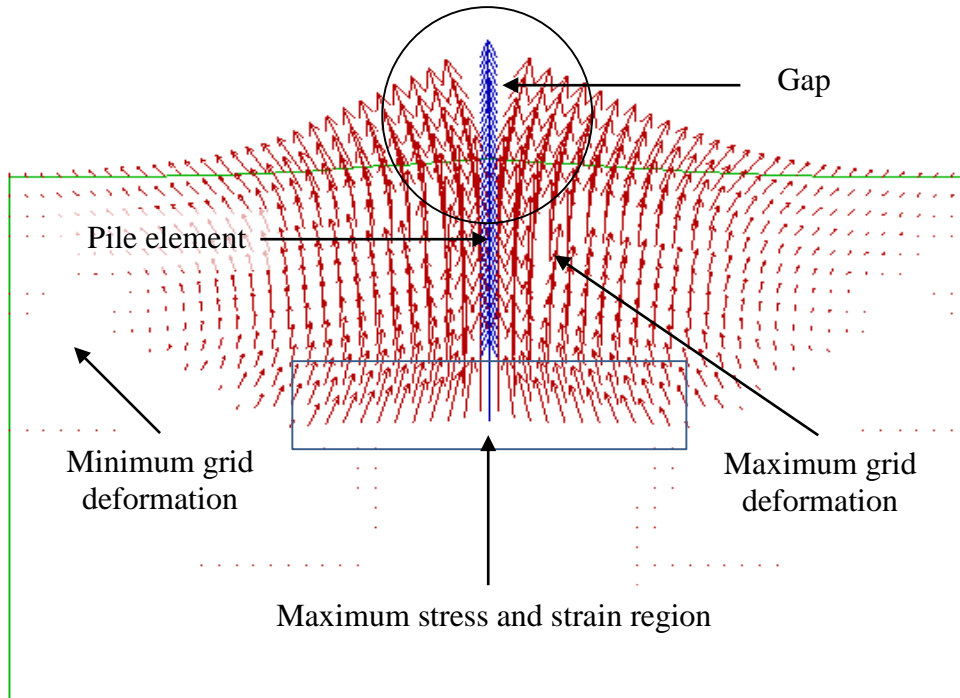


Figure 54a Clayey soil

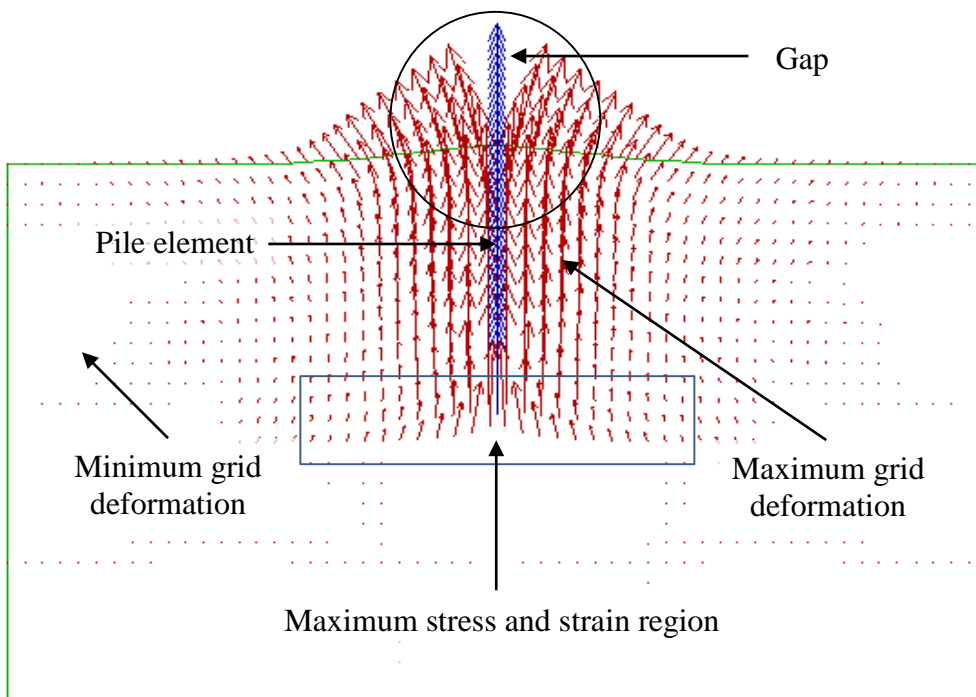


Figure 54b Sand soil

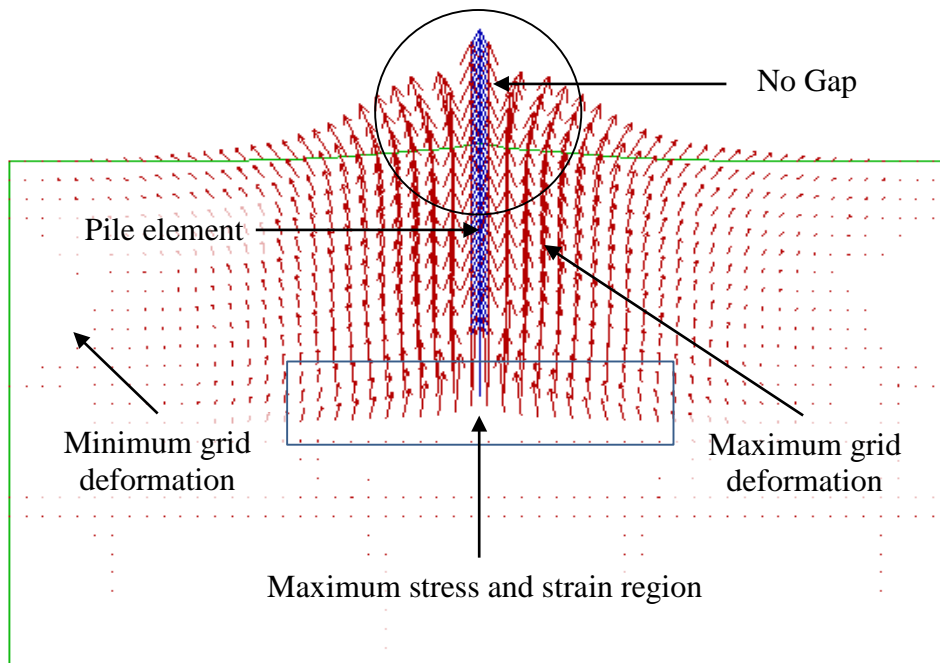


Figure 54c Silty soil

In the process of axial loading, the load is transferred through the specified media by uniform skin friction hence the increment in axisymmetric deformation. This symmetry is shown in Figure 55 which represents the contour map of the effective stress on both sides of the pile elements. The stresses recorded in the grid range from $-3E04$ to $4E04$ N with the intensities demarcated by the colour coding, where light blue and red show the areas that experience maximum stresses and minimum stresses respectively.

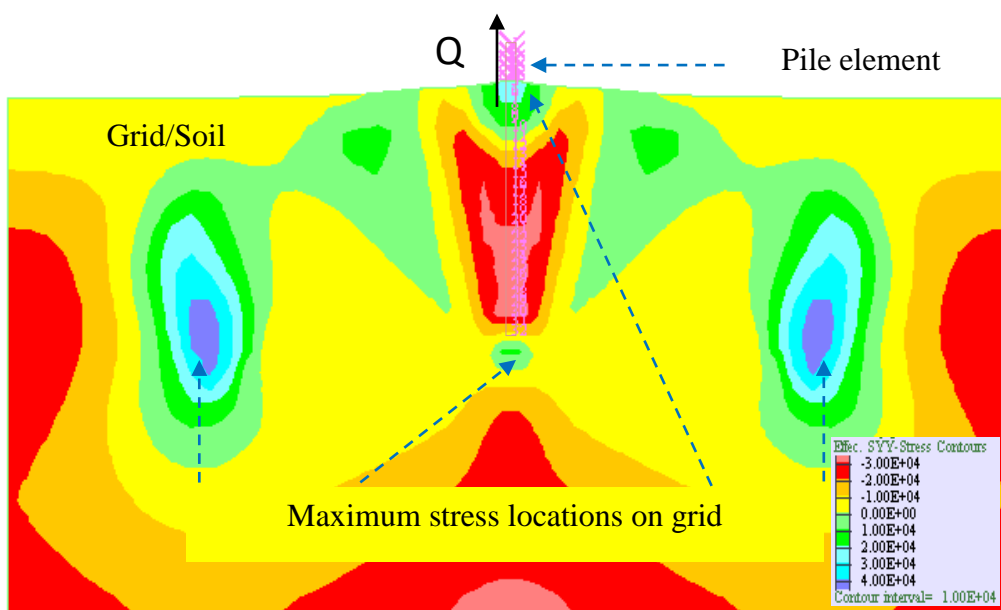


Figure 55 Contour zone for effective stress distribution on the grid

Figure 56 represents an in-depth view of the distribution of the principal stress tensors in the network during axial loading. It is evident that extreme stresses are felt around the pile/grid interface close to the ground surface and axisymmetrically deep into the grid at points that act as the hinges to the vacuum created due to the movement of the overburden weight. These high stresses are due to the high rates of grid deformations at these junctions as the pile element is pulled out. In theory, this behavior is represented by linear springs under the axial force that is dependent on the direction of the pile element movement, in this case along the y-axis.

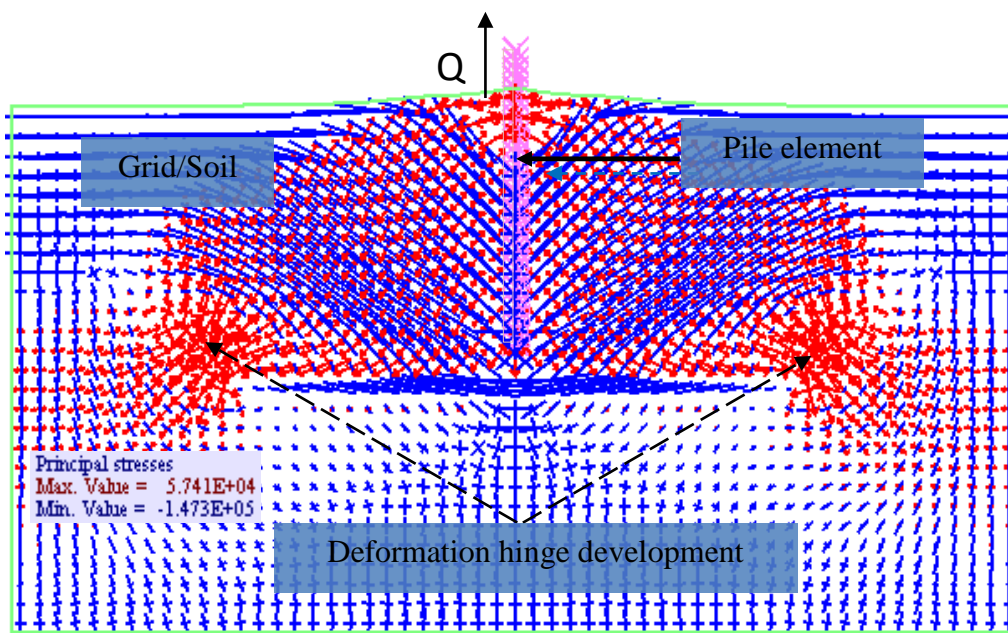


Figure 56 Effective Principal stress tensor distribution on axial loading

To further understand the pile /grid interface, a contour view of the maximum shear strain shows the areas of high deformations as shown in Figure 57. The shear strain developed along the pile is also dependent on the cohesive strength of the pile/grid interface as well as the frictional resistance on the perimeter of the pile element. As the axial load is applied, the strain at the bottom of the pile increase up to $1.5e-1$ which is recorded as the highest due to the high rates of deformations on the grid.

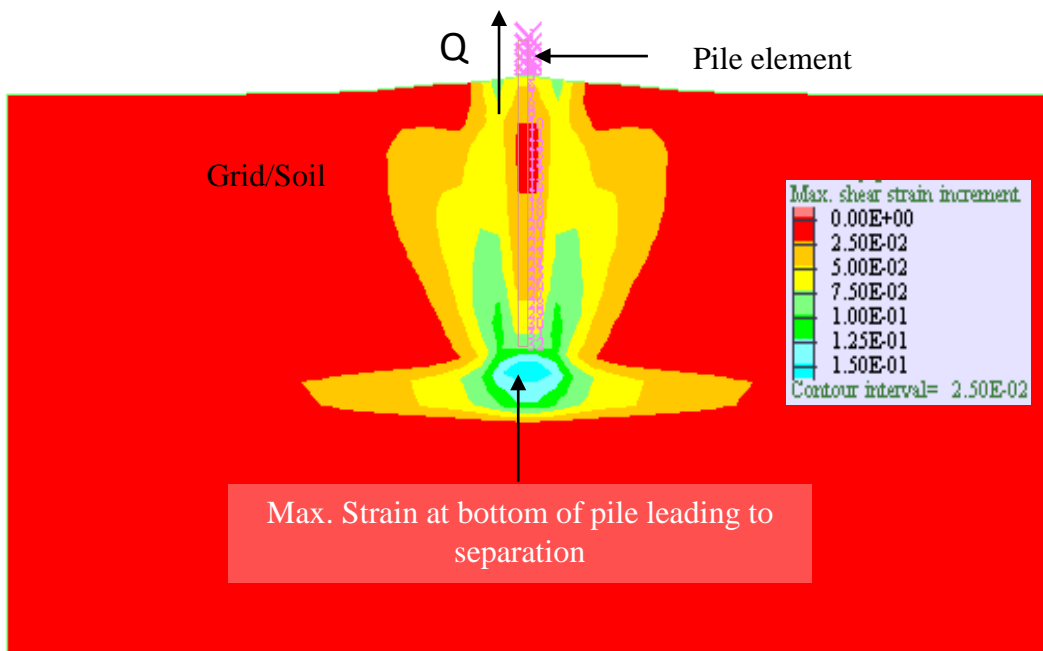


Figure 57 Maximum shear strain increment around the pile element

6.4 PARAMETRIC STUDY ON LATERAL LOADING

6.4.1 Variation of the Pile Foundation Depth

The depth of the foundation is one of the major components that dictate the strength of the structure upon completion. This strength is due to the ability to transmit all the overburden load into the soil without any fear of structural failure. In this study, the depth of the foundation is varied in steps of 0.7m, 1.0m, 1.4m, 2.0m. From the FLAC2D output, it's evident that there is a linear relationship between the depth of the foundation and the ultimate axial load the pile can withstand before failure point. Considering the three types of soil involved in this model i.e. dense sand, silty soil and clay soil, dense sand has the highest permissible ultimate axial load of 130.22kN at 2.0m depth and the minimum allowable axial load of 38.54kN obtained from the clay soil at 0.7m depth as shown in Figure 58.

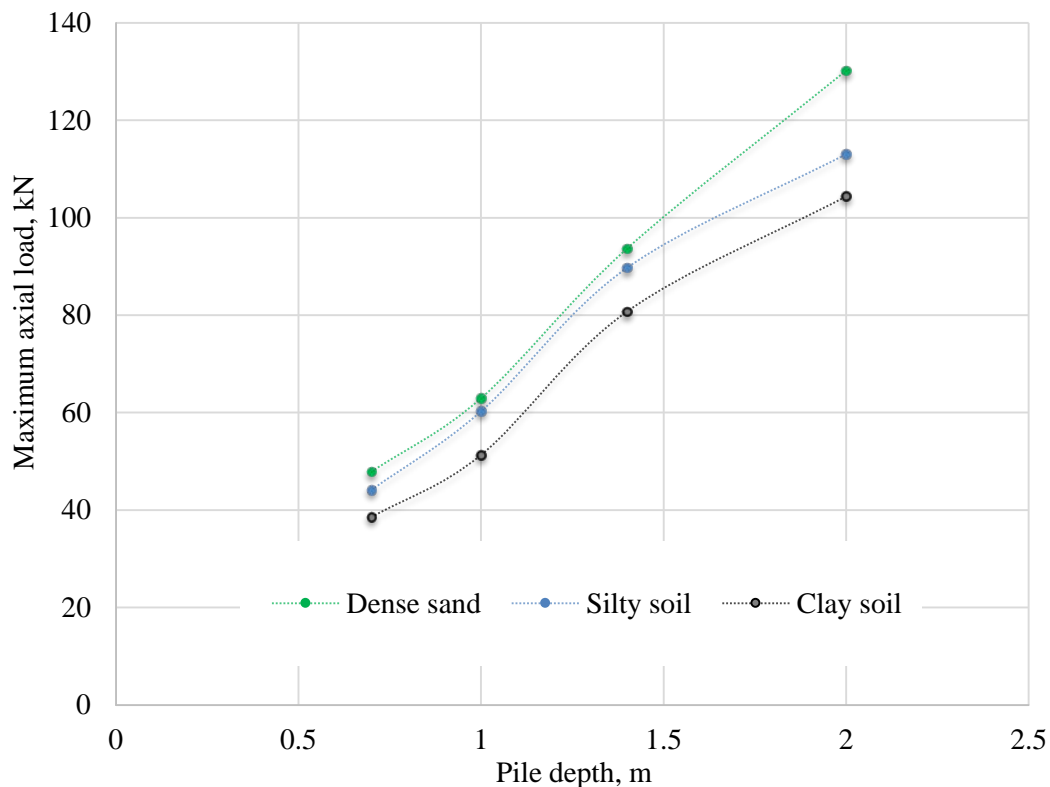


Figure 58 Variation of the foundation depth

6.4.2 Variation of the Angle of Internal Friction

The angle of internal friction is an essential parameter in the estimation of the ability of the soil to withstand the shear stresses experienced within the ground during loading. By replicating this into the input parameters of FLAC2D software, the effects of a range of the angle of internal friction gives a corresponding impact on the bearing capacity of the pile foundation. This angle is the angle measured between the normal force and the resultant force that is attained upon failure in response to the shearing stress. In this model, the angle of internal friction is analyzed at 10°, 20°, 30° and 40° for silty soil, dense sand and clay soils with increasing sand component.

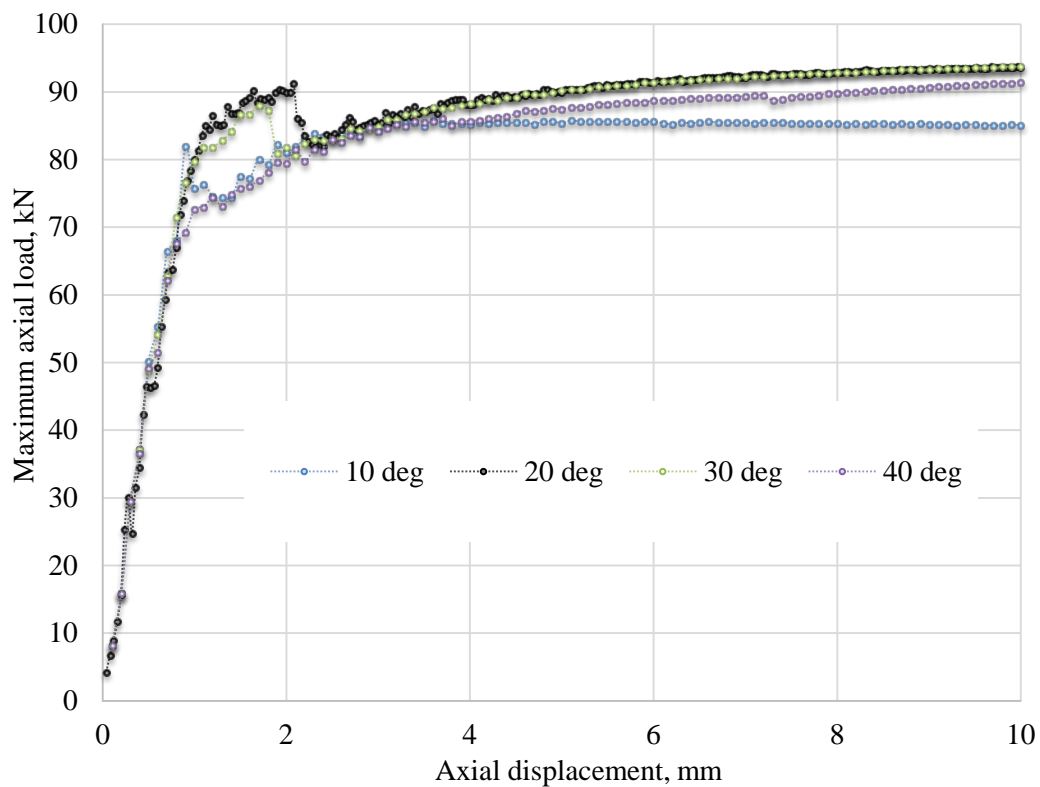


Figure 59 Variation of the Angle of Internal Friction for dense sand

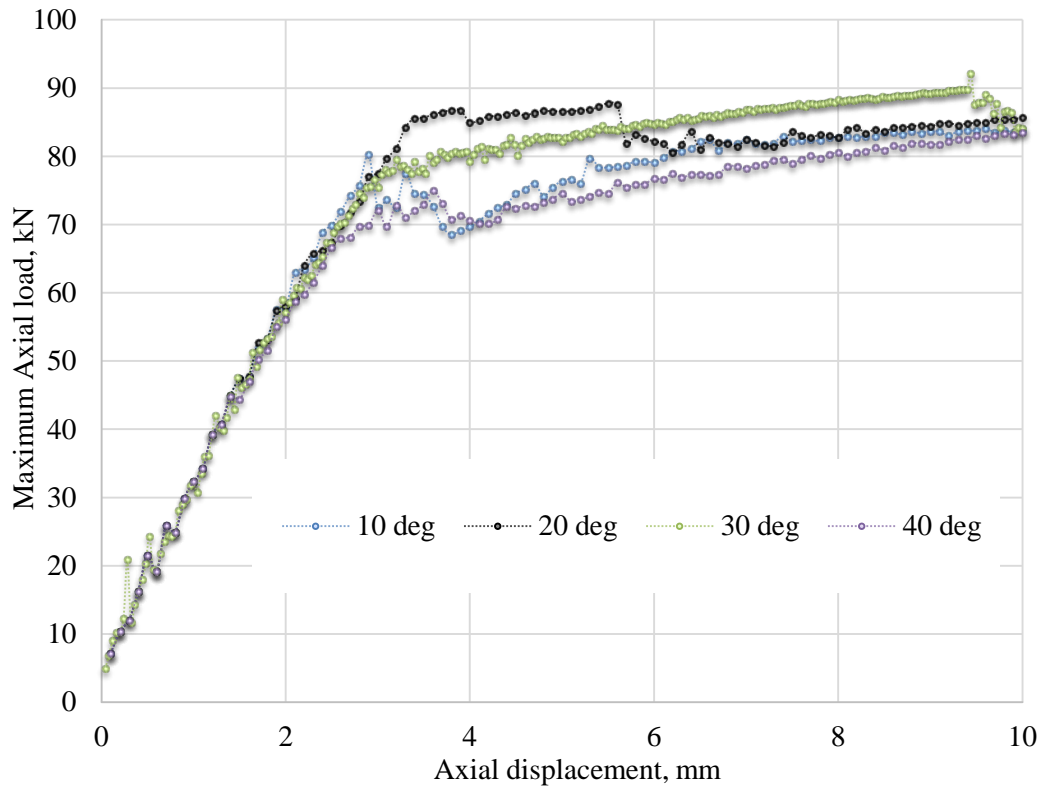


Figure 60 Variation of the Angle of Internal Friction for silty soil

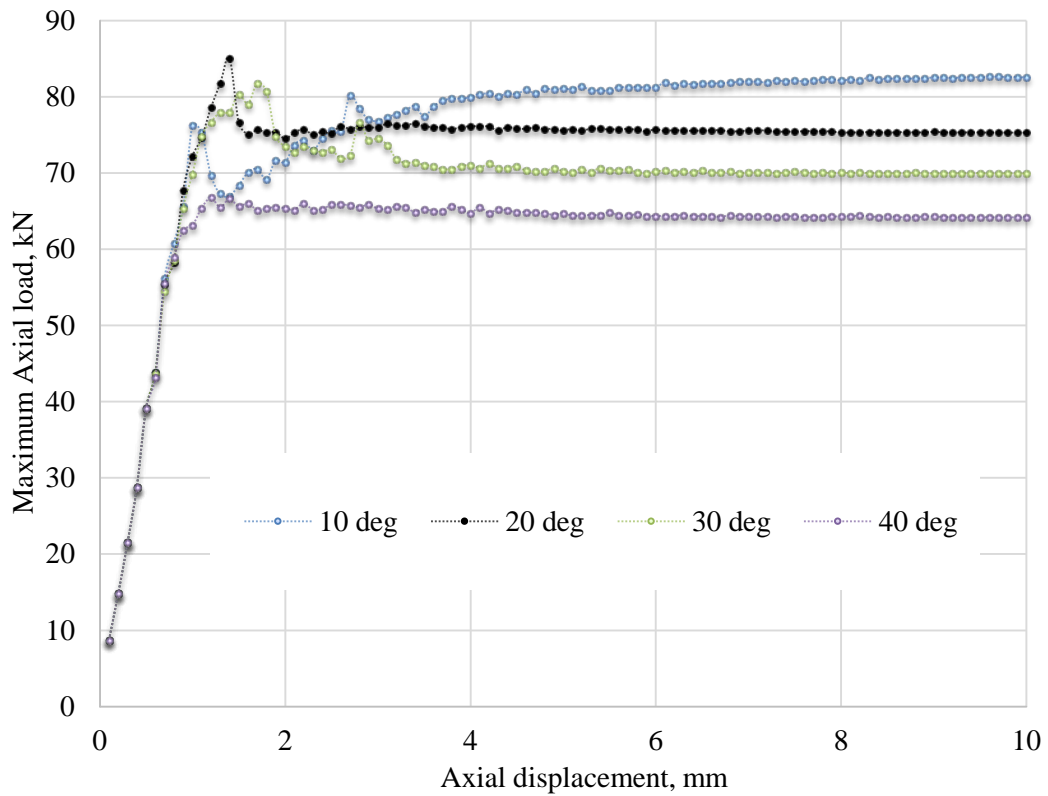


Figure 61 Variation of the Angle of Internal Friction for clayey soil

The plot shows a curvilinear relationship with maximum values recorded at the 20° angle in internal friction. The maximum values of the ultimate axial load obtained are 93.67kN and 85.78kN for dense sand and silty soils respectively. Sandy clay depicted a dramatic reduction in bearing capacity as the angle of internal friction increased to 40° where the ultimate axial load fell to 64.23kN as shown in Figure 62.

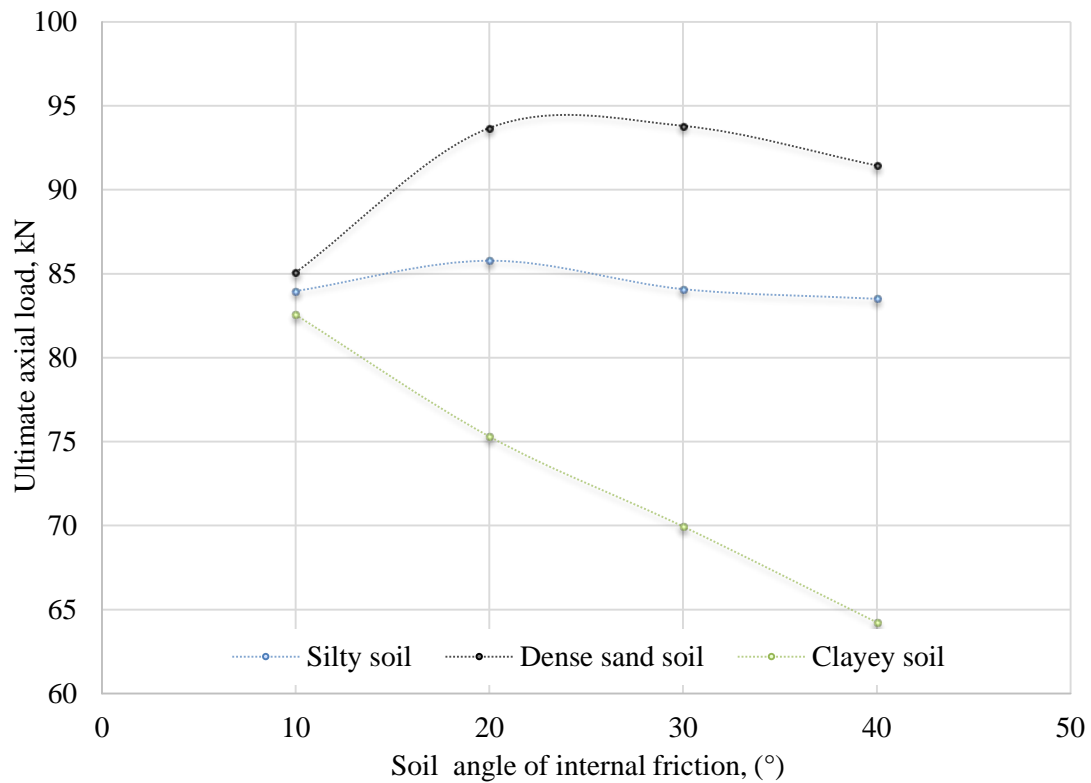


Figure 62 Influence of the angle of internal friction of the soil

6.4.3 Influence of Gap Formation during Loading

In this FLAC2D model, the interaction between the pile element and the grid can be represented by the normal and the shear coupling springs that tend to squeeze the grid/soil medium element on to the pile element. The pressing ensures a continuous wall/ medium contact. During the application of the axial load, this constant contact may be affected in a way that tends to bring in separation called the gap formation. The gap is mainly evident upon the failure of the structure itself from the ultimate load recorded. Figure 63, 64 and 65 shows the load deflection curves for the dense sand, silty soil and clayey soils respectively.

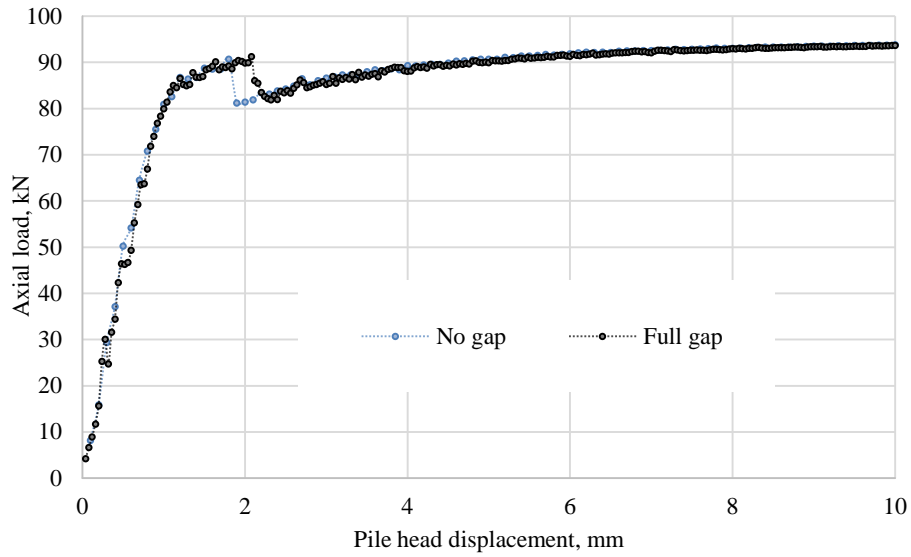


Figure 63 Influence of Gap Formation during Loading for dense sand

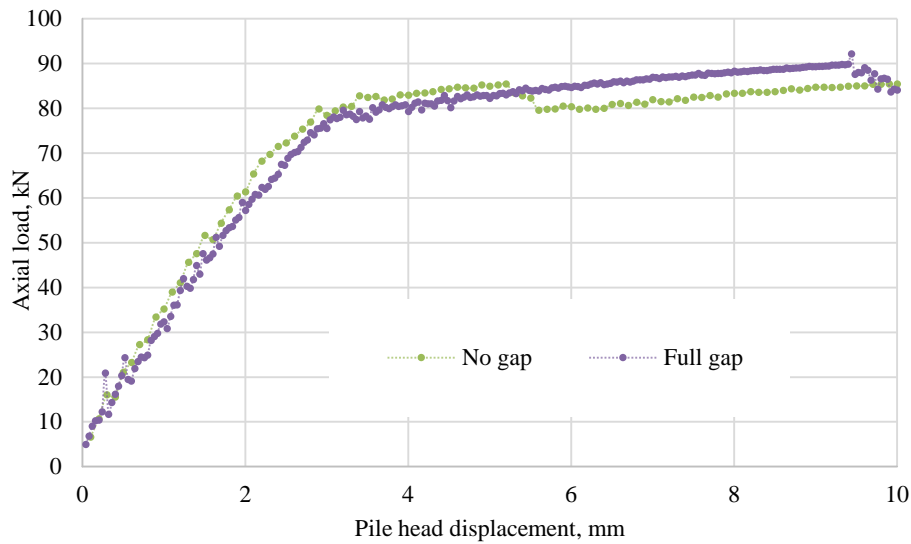


Figure 64 Influence of Gap Formation during Loading for silty soil

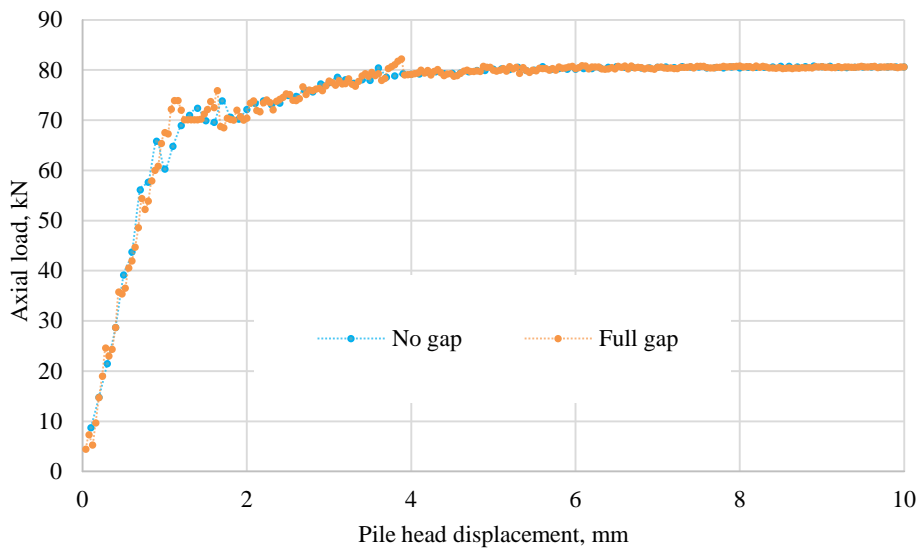


Figure 65 Influence of Gap Formation during Loading for clayey soils

From this experiment, two formulations are taken into account that is, analysis with the expectation of gap formation and the other analysis without the gap formation. From the output, it is recorded that for sandy soil, and clay soil, the creation of gap has minimal effects on the ultimate load recorded and the differences in the pile head displacements. On the other hand, silty soils attain a higher final pressure when no gap formation is occurring than when there is no gap. The model with no gap and full gap predicts an ultimate load of 85kN and 80kN respectively as shown in Figure 64. Figure 66 is a comparison of the major difference attained in accordance to axial capacity. This plot depicts that dense sand have higher axial capacity of up to 90kN the clay soils with an ultimate axial load of 75kN at minimal displacement of 2mm and 1mm respectively. Silty soils have a higher axial capacity of 85kN with no gap than the clay soils but this higher axial load is attained at higher pile head displacements of up to 5mm.

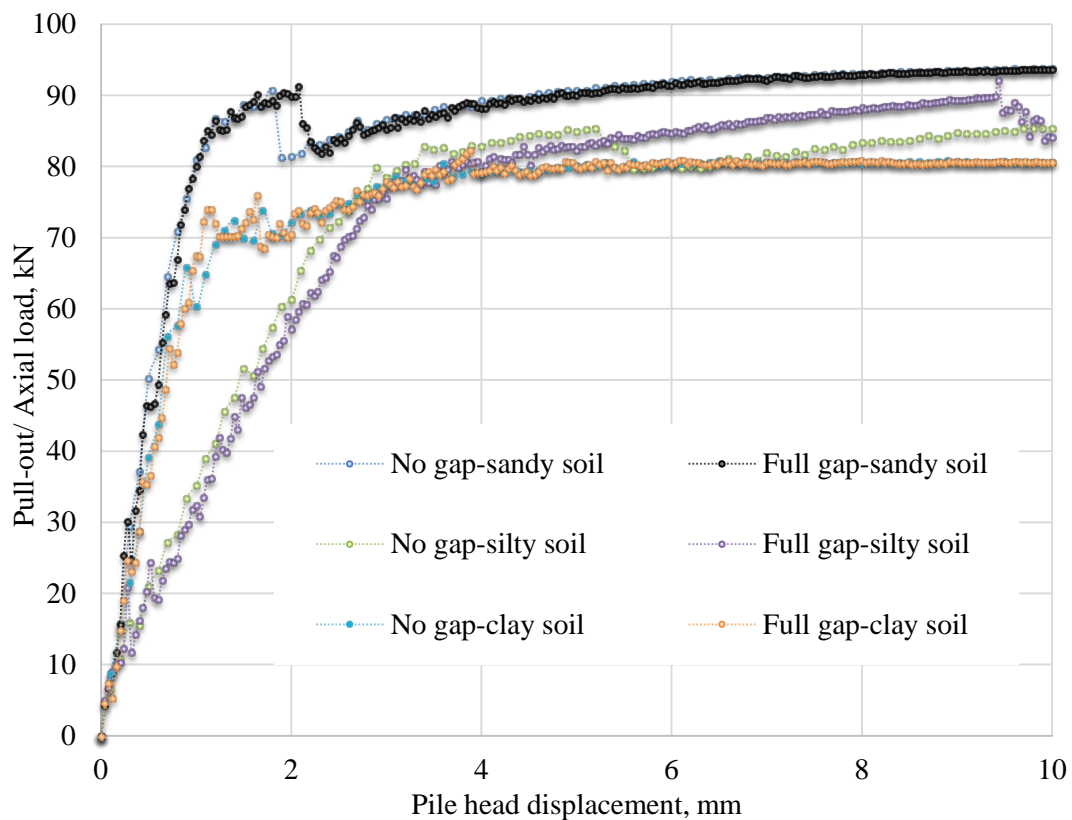


Figure 66 Effects of the gap on the ultimate axial load

6.5 FACTOR OF SAFETY (FoS)

FoS is used for the measurement of the load carrying capacity of a structure beyond the expected or designed loads. It measures how strong the foundation is supposed to be for the intended or design loads thus giving the reliability of a given design. The focus of this research is to determine the foundation behaviour when subjected to lateral loading which as a result will provide a clear reflection on the bearing capacity of the pile. FoS evaluates the strength of the composite pillar foundation in accordance to the loads it will be subjected to once in full operation and the ability to channel all the forces to the ground without the fear of failure. From this relation then the factor of safety can be calculated using the equation (11).

$$FoS = \frac{F_{L \text{ actual}}}{F_{L \text{ design}}}$$

Where $F_{L \text{ actual}}$ is the actual lateral force, the composite foundation can hold during testing, and $F_{L \text{ design}}$ is the design horizontal/lateral load subjected to the composite foundation for equilibrium.

Considering the analysis of the composite single pile foundation for the lateral capacity, the foundation shows a factor of safety of three. This is a good room for redundancy with respect to the fluctuating field loading conditions.

On the other hand, the pull-out capacity study shows a factor of safety of more than three. This is a good sign of strength in the foundation structure design. Strength is a major determinant of the durability of the structure upon complete installation. Up to date, the composite single pile foundation has been able to withstand the strong winds experienced in the two regions i.e. Matsusaka City and Kasugai City with the best test tested during the Typhoon Jebi which has winds up to 40m/s.

CHAPTER 7

CONCLUSIONS

7.0 CONCLUSION

7.1 CONCLUSION BASED ON LATERAL CAPACITY STUDY

The composite foundation portrays good lateral capacity under the specified design loads. With design loads set at 4 kN, the composite foundation can support the ultimate lateral load up to 15 kN which gives a factor safety of greater than 3. The foundation is, therefore, able to withstand the wind loads at 40 m/s inclusive of the solar panels installation design weights without any risks of failure.

Through the introduction of numerical modelling using FLAC2D, more detailed examination of the foundation and soil interaction can be established. Such correlations include soil movements on the surface and also along the depth of the composite foundation. The composite foundation tends to experience varying magnitudes of the applied horizontal load with depth during transmission into the soil component represented by the model grid.

Based on the above study, it is concluded that the design of composite foundation can be achieved using straightforward techniques in the construction industry taking into consideration the economic factors such as minimum cost evaluation and minimum material usage.

7.2 CONCLUSION BASED ON LATERAL PARAMETRIC STUDY

The primary objective of this study was to evaluate the response of the load transfer curve and the displacements produced. This response shows the influence factor of the lateral load under different circumstances depending on the parameter under study. The parametric study, therefore, acts as a model validation process as it shows clearly the influence produced by a given setting concerning the design value at hand. From this study, it is evident that the integration of the stresses in the grid element around the pile element is an obvious way of understanding the p-y curve characteristics in the soil.

Additionally, the variation of the parameters such as pile stiffness, loading velocity, and eccentricity have shown that clayey soils have the highest ultimate load bearing capacities of between 15.5kN to 15.8kN at minimal pile displacements of below 5mm.

It is also valid that FLAC2D as a numerical technique in the modelling field is a vital tool for investigating the realistic soil behavior under different conditions and is helpful in simulating all construction sequences concerning the provided design parameters.

7.3 CONCLUSION BASED ON PULL-OUT CAPACITY STUDY

This study focused on the analysis of the pile structural element for strength and the ability to resist the axial loads subjected to it. Axial loads are the forces that tend to pull the structure of the soil medium. Such effects are due to earthquakes or winds depending on the area of the basic installation. The approach used in this paper is the numerical simulation approach using FLAC2D which employed the use of finite difference method embedded within the program to determine the shear capacity of the pile during loading. The results are a clear indication of good strength with permissible loads shooting up to slightly above 90kN. The load can withstand external forces that may be subject to the pile foundation. In this study, the pile foundation is focused on supporting the solar panels at a cheaper cost than the existing structures.

The aim is also based on the economics with more emphasis on the material costs for the realization of green energy in the developing countries. The parametric study further portrays an indication of the pile foundation flexibility for use in a variety of soil mediums with a minimum fluctuation of the strength properties. The result is vital in giving design engineers an in-depth understanding of the new foundation approach for proposed structural developments. Further research is necessary to determine the effects of the variable shape of the piles on the ultimate bearing capacity considering the structure to be constructed.

8.0 SUMMARY

- ❖ From this study, it is evident that the integration of the stresses in the grid element around the pile element is an obvious way of understanding the p-y curve characteristics in the soil.
- ❖ Clay soils gives better lateral capacity than the silty soils with maximum loads of up to 14kN and 12kN respectively.
- ❖ The p-y curves further show that during design the soil parameters have a major influence on the projected strength and durability of the foundation.
- ❖ Additionally, the variation of the parameters such as pile stiffness, loading velocity, and eccentricity have shown that clayey soils have the highest ultimate load bearing capacities of between 15.5kN to 15.8kN at minimal pile displacements of below 5mm.
- ❖ Pile stiffness and the eccentricity play a major role in the determination of the foundation depth hence, should be considered with high precision depending in the load subjected to the foundation.
- ❖ With the numerical models in place, experimental simulations can be done with lots of accuracy and at a lower cost compared to the procedures involved in the full scale experimental tests in the field.
- ❖ The results are a clear indication of good strength with permissible loads shooting up to slightly above 90kN.
- ❖ The load can withstand external forces that may be subject to the pile foundation (Wind/Typhoon case study, 40m/s)
- ❖ The composite single pile foundation is focused on supporting the solar panels at a cheaper cost than the existing structures. The aim is also based on the economics with more

emphasis on the material costs for the realization of green energy in the developing countries.

- ❖ The parametric study further portrays an indication of the pile foundation flexibility for use in a variety of soil mediums with a minimum fluctuation of the strength properties.
- ❖ The result is vital in giving design engineers an in-depth understanding of the new foundation approach for proposed structural developments.

REFERENCES

Owino, A, Hossain, Z and Shiau, J 2018, "Parametric Study on the Response of Composite Single Piles to Lateral Load by Numerical Simulation (FDM)", *European Journal of Engineering Research and Science*, 3(10), pp. 16-20. doi: 10.24018/ejers.2018.3.10.899.

Owino, A, Hossain, Z and Shiau, J 2018, "Pull-out Resistance of Single Piles and Parametric Study using the Finite Difference Method (FDM)." *American Journal of Civil Engineering and Architecture*, vol. 6, no. 5, pp. 193-198. DOI: 10.12691/ajcea-6-5-4

Akins, R & Cermak, J 1975, "Wind pressure on buildings-Technical report CER7677REA-JEC15, Fluid dynamics and diffusion lab", Colorado state university, Fort Collins, Colorado.

Aihara, T, Asami Y, Nishimura, H, Takamori, K, Asami, R & Somekawa, D 2008, 'An area correct factor for the wind pressure coefficient for cladding of hip roof — The case of square plan hip roof with a roof pitch of 20 degrees', *The 22nd Wind Engineering Symposium*, pp.339-344.

Engel, M 2012, "Evaluation of Barnes' Method and Kriging for estimating the Low-Level Wind", 1st ed.: Biblioscholar.

Broms, B 1964, 'Lateral Resistance of Piles in Cohesive Soils', *Proceedings of the American Society of Civil Engineers, Journal of the Soil Mechanics and Foundations Division*, Vol. 90, SM2.

Cundall, P, C. Carranza-Torres and Hart, R 2003, "A New Constitutive Model Based on the Hoek-Brown Criterion," in *FLAC and Numerical Modeling in Geomechanics (Proceedings of the 3rd International FLAC Symposium, Sudbury, Ontario, Canada, October 2003)*, pp. 17-25. R. Brummer, et al., Eds. Lisse: Balkema.

Amadei, B 1982, “The influence of rock anisotropy on measurement of stresses in situ”, Berkely, California, [The Author].

Lekhnitskii, SG 1981, “Theory of Elasticity of an Anisotropic Body”, Moscow, Mir Publishers.

Britto, AM, and Gunn, MJ 1987, Critical State Soil Mechanics via Finite Elements, Chichester U.K, Ellis Horwood Ltd.

Roscoe, KH, and Burland, JB 1968, “On the Generalised Stress-Strain Behavior of ‘Wet Clay’,” in Engineering Plasticity, J. Heyman and F. A. Leckie, Eds. Cambridge, Cambridge University Press, pp. 535-609.

Somekawa, D, Koizumi, T, Taniguchi, T & Taniike, Y 2012, ‘Wind loads acting on the photovoltaic panels arrayed near ground’, The 22nd Wind Engineering Symposium, pp.157-160

Klepikov, S 1965, “Calculation of beams on an elastic foundation with a variable modulus of subgrade reaction. Soil Mechanics and Foundation Engineering, 2(5), pp.296-299.

Caseiro, C 1986, “Behavior of Elastomeric Materials Under Dynamic Loads IV”, The Shock and Vibration Digest, 18(1), pp.3-6.

Reese, L & Matlock, H 1971, ‘The Analysis of Piles Under Lateral Loading’, Proceedings, Symposium on the Interaction of Structure and Foundation, Midland Soil Mechanics and Foundation Engineering Society, University of Birmingham, England.

Architectural Institute Japan 2004, “Recommendations for Loads on Buildings”, Architectural Institute of Japan, Tokyo

Okahara, M, Nakatani, S & Matsui, K 1991a, 'A study on vertical and horizontal bearing characteristics of piles', JSCE Journal of Structural Engineering, Vol. 37, pp. 1453-1466, Japan. In Japanese.

Okahara, M, Takagi, S, Nakatani, S & Kimura, Y 1991b, 'A study on the bearing capacity of single piles and design method of column-shaped foundations', Technical Memorandum of PWRI (2919), Public Works Research Institute, Japan. In Japanese.

JIS C8955: Japanese Industrial Standards 2004, "Design guide on structures for the photovoltaic array", Standard Japan, https://www.techstreet.com/standards/jis89552017?product_id=1984692

JIS C8917: Japanese Industrial Standards 2005, "Environmental, and endurance test methods for crystalline solar PV modules", Standard Japan, <https://www.techstreet.com/standards/jis-c-8955-2017?product_id=1984692>.

Poulos, HG 1971, "The behaviour of laterally loaded piles: I- single piles", Journal of Solid Mechanics, Foundation Division, ASCE, 97, pp. 711-731.

Brown, DA, Shie, C & Kumar, M 1989, "P-y curves for laterally loaded piles derived from three-dimensional finite element model", Numerical Models in Geomechanics, NUMOG III, pp. 683-690 Elsevier Applied Science.

Cox, W & Reese, L 1978, "Pullout Tests of Grouted Piles in Stiff Clay", Journal of Petroleum Technology, 30(03), pp. 349-356.

Duncan, JM, Jr. Evans, LT & P. S. K.Ooi 1994, "Lateral Load Analysis of Single Piles and Drilled Shafts", Journal of Geotechnical Engineering ASCE, Vol. 120, No. 5, pp.1018- 33.

Broms, B 1964, “The lateral resistance of piles in cohesionless soils”, J Soil Mech Found Div, ASCE 90(SM3), pp. 123–156

Billiaux, D, Barla, G & Barla, M 2001, ‘FLAC and Numerical Modeling in Geomechanics’, Proceedings of the 2nd International FLAC Conference, Lyon, France, Rotterdam, Balkema.

Cernica, JN 1995, “Geotechnical Engineering: Foundation Design”, John Wiley & Sons Publishers, New York.

Energy and the challenge of sustainability 2000, United Nations Development Programme and World Energy Council. September 2000. Retrieved 17 January 2017.

Hamada, M, Doboku, G & Takeshi K 2015, “Critical Urban Infrastructure Handbook”, 1st ed, CRC Press, Boca Raton, Florida.

IEA Bioenergy Update 2014, Biomass and Bioenergy, 61, p.I-VII.

Reese, L, Cooley, L & Radhakrishnan, N 1984, “Laterally Loaded Piles and Computer Program COM624G”, Defense Technical Information Center, Ft. Belvoir Virginia.

Begemann, HK 1965, “The Maximum Pulling Force on a Single Tension Pile Calculated on the Basis of Results of the Adhesion Jacket Cone”, Proc. 7th International Conference on SMFE

Downs, DL and Chieurzzi, R 1966, “Transmission Tower Foundations”, Journal of Power Division, ASCE. Vol.92, No.2, pp. 91-114

Sowa, VA, 1970, “Pulling Capacity of Concrete Cast-In-Situ Bored Piles”, Canadian Geotechnical Journal, Vol.7, pp. 482-493

Meyerhof, GG 1973, “Uplift Resistance of Inclined Anchors and Piles”, Proceedings 8th International Conference on SMFE, Moscow. Vol.2, pp. 167-173

McClelland, B 1974, "Design of Deep Penetration Piles for Ocean Structures", Journal of GTE Division, ASCE, Vol.100, pp.709-745

Sharma, BVR 1988, "Uplift Capacity of Anchor Piles in sand Under Axial Pulling Loads", M. Tech Thesis, Kharagpur, India

Poorooshasb, HB and Paramesw VR 1982, "Uplift of Rigid Piles in Frozen Sand", Soils and Foundations, Vol.22, No.2, pp. 82-88

Kulhawy, FH, Kozera, DW, and Withium, JL 1979, "Uplift Testing of Model Drilled shafts in Sand", Journal of GTE Division, ASCE. Vol. 105, pp. 31-47

Kulhawy, FH 1985, "Drained Uplift Capacity of Drilled Shafts", 11th International Conference on SMFE, San Francisco. Vol. 3, pp. 1549-1551

Turner, JP, and Kulhawy, FH 1990, "Drained Uplift Capacity of Drilled Shafts Under Repeated Loading", Journal of GTE Division, Vol.116, pp. 470- 491

Patra, NR and Pise, PJ 2001, "Ultimate Lateral Resistance of Pile Groups in Sand", Journal of Geotechnical and Geo-Environmental Engineering Division, ASCE, Vol. 127, pp. 481-487

Das, BK and Pise, PJ 2003, "Effect of Compressive Load on Uplift Capacity of Model Piles", Journal of Geotechnical and Geo-Environmental Engineering Division, ASCE, Paper No.023132

Lysmer, J 1970, 'Limit analysis of plane problems in soil mechanics', ASCE Journal of the Soil Mechanics and Foundations Division, vol. 96, pp. 1311-34

Sharma, BV and Pise, PJ 1994, "Uplift Capacity of Anchor Piles in Sand Under Axial-Pulling Loads", IGJ, Vo1. 24, pp. 181-203

Geddes, JD 1969, "Boussinesq-Based Approximations to the Vertical Stresses Caused by Pile-Type Subsurface Loadings", *Geotechnique* 19(4), pp. 509-514

Banerjee, PK, and Davis, TG 1978, "The behaviour of axially and laterally loaded single piles embedded in non-homogeneous soils", *Geotechnique*, 28, No. 3, pp. 309-326.

Trochanis, AM, Bielak, J & Christiano, P 1991, "Three-dimensional nonlinear study of piles", *Journal of Geotechnical Engineering, ASCE*, 117, pp. 429-447.

O'Neill, MW, Blaney, GG & Muster, GL 1982, "Behavior of Single Pile and Pile Group in Overconsolidated Clay Under Relatively Low-Frequency Loading", Fugro-Gulf, Inc., and Univ. of Houston-University Park.

Cundall, PA 1976, "Explicit Finite Difference Methods in Geomechanics", in *Numerical Methods in Engineering, Proceedings of the EF Conference on Numerical Methods in Geomechanics*, Blacksburg, Virginia, Vol. 1, pp. 132-150.

Britto, AM, & Gunn, MJ 1987, "Critical State Soil Mechanics via Finite Elements", Chichester U.K, Ellis Horwood Ltd